School of Doctoral Studies in Biological Sciences
University of South Bohemia in České Budějovice
Faculty of Science

Light-harvesting like domain of the cyanobacterial ferrochelatase

Ph.D. Thesis

Mgr. Marek Pazderník

Supervisor: Doc. Roman Sobotka, Ph.D.

Institute of Microbiology, Academy of Sciences of the Czech Republic

University of South Bohemia, Faculty of Science, České Budějovice

České Budějovice 2019

This thesis should be cited as:
Pazderník M., 2019: Light-harvesting like domain of the cyanobacterial ferrochelatase, Ph.D. Thesis. University of South Bohemia, Faculty of Science, School of Doctoral Studies in Biological Sciences, České Budějovice, Czech Republic, 102 pp.

Annotation

This thesis is focused on elucidating the function of the C-terminal transmembrane light-harvesting complex like (LHC) domain of the cyanobacterial ferrochelatase (FeCh). Using the model cyanobacterium *Synechocystis* PCC 6803, I show that the FeCh LHC domain can bind chlorophyll (Chl) and carotenoids; however, this pigment binding occurs only when the biosynthesis of heme and Chl in the cell is misbalanced. Further, I found that point mutation, which prevents the pigment binding to FeCh LHC domain results in a misregulated ratio between heme and Chl during stress conditions due to low heme accumulation. My data also show that the FeCh LHC domain interacts with CurT protein most likely to localize the FeCh into a specialized membrane domain, where the synthesis of photosystem II is proposed to occur. Based on my data I propose that the role of the FeCh LHC domain is to monitor the availability of Chl during photosystem biogenesis and to coordinate Chl availability with the synthesis of heme.

Declaration [in Czech]
Prohlašuji, že svoji disertační práci jsem vypracoval samostatně pouze s použitím pramenů a literatury uvedených v seznamu citované literatury.

Prohlašuji, že v souladu s § 47b zákona č. 111/1998 Sb. v platném znění souhlasím se zveřejněním své disertační práce, a to v úpravě vzniklé vypuštěním vyznačených částí archivovaných Přírodovědeckou fakultou elektronickou cestou ve veřejně přístupné části databáze STAG provozované Jihočeskou univerzitou v Českých Budějovicích na jejích internetových stránkách, a to se zachováním mého autorského práva k odevzdanému textu této kvalifikační práce. Souhlasím dále s tím, aby toutéž elektronickou cestou byly v souladu s uvedeným ustanovením zákona č. 111/1998 Sb. zveřejněny posudky školitele a oponentů práce i záznam o průběhu a výsledku obhajoby kvalifikační práce. Rovněž souhlasím s porovnáním textu mé kvalifikační práce s databází kvalifikačních prací Theses.cz provozovanou Národním registrem vysokoškolských kvalifikačních prací a systémem na odhalování plagiátů.

České Budějovice, 05.11.2019 .....

Marek Pazderník

This thesis originated from a partnership of Faculty of Science, University of South Bohemia, and Institute of Microbiology, Academy of Sciences of the Czech Republic, supporting doctoral studies in the Molecular and Cell Biology and Genetics study program

Přírodovědecká
fakulta
Faculty
of Science

Funding

This work was supported by the Grant agency of the University of South Bohemia (04-026/2017), by the Czech Science Foundation (17-08755S) and by the Czech Ministry of Education (project LO1416).

Acknowledgments

I want to thank my Ph.D. supervisor Roman Sobotka for his patience and willingness to discuss. I also want to thank the scientific staff at Algatech, namely Vendula Krynická, Lenka Bučinská, Petra Skotnicová, Éva Kiss, Martina Bečková, Jana Knoppová, Grzegorz Konert, Josef Komenda and Martin tichý for frequent discussions. I want to thank the technical staff at Algatech, namely Jan Pilný, Lenka Moravcová, Barbora Zdvihalová and Jiří Šetlík for help with experiments. I want to thank Juergen Tomasch from the Helmholz Institute for Infection Research and Marc Nowaczyk and Jan Lambertz from the University of Bochum for hosting me at their institutions during my Ph.D. study.

Published results and the author's contribution

Pazderník, M., Mares, J., Pilny, J., and Sobotka, R. (2019) The antenna-like domain of the cyanobacterial ferrochelatase can bind chlorophyll and carotenoids in an energy-dissipative configuration. *Journal of Biological Chemistry* 294, 11131-11143, IF(2018) = 4.106

Apart from the phylogenetic analysis, M.P. performed all experiments and interpreted obtained data. M.P. also participated in the design of the whole study and in writing of the manuscript. The study was co-funded by a GAJU project obtained by M.P.

Roman Sobotka, the corresponding author of the listed publication approves the contribution of Marek Pazderník as described above:

…….

Doc. Roman Sobotka, PhD

Table of contents

Acronyms:

ALAD - ALA dehydratase
BN – blue native
CLH – chlorophyllase
CN – clear native
Chl - chlorophyll
CBB - coomassie brilliant blue
Copro III - coproporphyrinogen III
DDM – n-dodecyl-β-D maltoside
DNA – deoxyribonucleic acid
DVR - divinyl protochlorophyllide reductase
DTT - dithiothreitol
ELIP – early light-inducible protein
f.FeCh – 3xFlag-Ferrochelatase
FeCh – ferrochelatase
GGR – geranylgeranyl reductase.
GluRS - glutamyl-tRNA synthetase
GluTR - glutamyl-tRNA reductase
GSAT - glutamate-1-semialdehyde aminotransferase
HB - hydroxymethylbilane
HemeOx – heme oxygenase
Hlip – high light-inducible protein
ChlG – chlorophyll synthase
LHC – light-harvesting complex
Lil – light-harvesting like
MgCh – Mg-chelatase
MME – monomethyl ester
MTF - Mg protoporphyrin IX methyltransferase
OHP – one helix protein
PAGE – polyacrylamide gel electrophoresis
POR - NADPH-protochlorophyllide oxidoreductase
PPIX – protoporphyrin IX
PPOX - protoporphyrinogen IX oxidase
PSI – photosystem I
PSII – photosystem II
RC – reaction center
SEC – size exclusion chromatography
SEP – stress enhance protein
Synechocystis sp. PCC 6803 – *Synechocystis*
TM - transmembrane
Uro III - uroporphyrinogen III
WT – wild type

1. Introduction

1.1 General context

All life is an orchestra of molecules. Inorganic molecules readily available in the environment are taken up by organisms and transformed, based on the information encoded within organisms, into biomolecules. Biomolecules are responsible for most of the features of life as we know it today. Even the information on how to create all biomolecules is encoded within biomolecules themselves, which raises a lot of questions about the origin of life. During the continuous attempt to understand life, scientists divided biomolecules into several groups, based on their composition and properties. Proteins, one of these groups, are made of at least 20 building blocks called amino acids that are connected one after another like wagons of a train. Each amino acid has different chemical properties, thus the sequence, in which they are connected, dictates the properties of the protein. Based on their structural similarity and common evolutionary history, proteins are grouped together into so-called protein families. Proteins can be viewed as molecules of change; catalysis, movement, and regulation are all functions of proteins. In other words, if something changes within an organism, a protein is likely involved in the process.

Sequences and therefore functions of all proteins are encoded within deoxyribonucleic acids (DNAs), long linear or circular molecules. DNA consists of a repetition of four building blocks connected in a sequence, similar to proteins. Information on how to synthesize all biomolecules is encoded within the DNA sequence. Techniques, developed in the last 30 years, allow researchers to effectively determine DNA sequence and thereby roughly predict how many different proteins are produced by each organism. The variance in proteins ranges from thousands to tens of thousands depending on the complexity of the organism. At this time, the role of about one-third of protein-coding genes is unknown (Price et al., 2018). To obtain the ability to manipulate life in a way that will be beneficial to human society, e.g. being able to repair genetic diseases inherited in families or to alter desired properties or skills of people, it is necessary to understand what all proteins do and how they do it.

All biomolecules contain carbon. Primary producers, organisms that are able to use the energy of sunlight to transform inorganic carbon dioxide and water into biomolecules and oxygen, form the basis of life as it exists today on Earth. This process of transformation is called oxygenic photosynthesis (photosynthesis), a unique metabolic strategy, which evolved in cyanobacteria. Other life forms (algae and plants) acquired the photosynthetic ability by forming a symbiotic relationship with a cyanobacterium.

With the emergence of photosynthetic organisms, carbon dioxide started to be depleted from the atmosphere, and a large amount of oxygen and biomass was produced. Organisms, which consume the primary producers and transform the carbon from biomolecules back into CO_2, are called aerobic hetero-organotrophs, because of their strict dependence on the consumption of organic matter. All animals including humans belong to the hetero-organotrophic group.

In my opinion, with the current scientific understanding, the amount of hetero-organotrophs living on our planet can never exceed the relative amount of photosynthetic organisms available for consumption. This limitation has dire implications for human populations in the form of famine. In the last two centuries, scientific progress in the form of synthetic fertilizers, pesticides and herbicides along with the usage of random mutagenesis enabled a large increase in the growth rate, yield, and resistance of consumable plants. Along with the progress in medicine, the increased food supply resulted in a drastic increase in the human population (7 times). Further improvement of crop production and their resistance to adverse conditions is theoretically possible by changing the way plants work via precise DNA manipulations. To be efficient and confident in this process, a detailed understanding of plant physiology and photosynthesis is required. This thesis is a part of the on-going strive to gain a complete understanding of photosynthesis.

In theory, it is possible to lower our strict dependence on primary producers by adding the photosynthetic ability to humans, perhaps in a similar way it was acquired by the ancestors of plants, by creating a symbiosis between human skin cells and cyanobacteria. Such a mixotrophic human could supplement his diet with the energy of light, either sunlight or artificial light. Even if the hypothetical photosynthetic skin tissue was engineered to be efficient enough to fuel most of the energy needs of the human body, it would not completely eliminate the need to eat, as food contains other essential nutrients, not created by photosynthesis. The first milestone in such an endeavor would be the creation of human photosynthetic skin tissue *in vitro*, starting from stem cells. The creation of such tissue would require a deep understanding of skin tissue and photosynthesis and not yet developed technologies allowing extremely precise and large scale genetic manipulation of human cells. The further step would be a successful graft of such tissue on a skin, similar to the grafts used to heal severely burnt victims. In such a case, it may be difficult to convince the body to accept the tissue. The ultimate step of altering embryonal stem cells, to develop a photosynthetic skin tissue after human birth, is rather unthinkable (and currently illegal). However, alteration of DNA in human germline has already started, by genetic manipulation of two children, whose parents are

HIV-positive. The researcher tried to make the children more HIV resistant, using the CRISPR-Cas method. A negative reception by the respective government followed (Normile and Cohen, 2019). On the photosynthetic side of things, the addition of photosynthetic ability into a heterotrophic organism has already begun with a successful implementation of the chlorophyll biosynthesis pathway into *E. coli* (Chen et al., 2018).

1.2 Biosynthesis of chlorophyll and heme

Biomolecules whose structure is not directly coded in DNA, are produced by a specific group of proteins called enzymes, in a sequence of chemical reactions. These sequences of reactions are called metabolic pathways. It is rather arbitrarily decided where one pathway ends and another begins, didactic and historical reasons play a large role in defining these pathways. For the purpose of this thesis, the tetrapyrrole pathway represents the synthesis of tetrapyrrolic precursors of heme and chlorophyll from Glutamyl-tRNA (Czarnecki and Grimm, 2012; Brzezowski et al., 2015) (Figure 1); note that this pathway can also lead to synthesis of other tetrapyrroles, such as bacteriochlorophyll, siroheme, vitamin B12 or bilins (not shown). Chlorophyll itself occurs in several different forms (Chl *a* – Chl *f*). Various mixtures of Chl forms can be found in different species. In this thesis, Chl denotes chlorophyll *a*, which is ubiquitous in oxygenic phototrophs (cyanobacteria, algae and plants) and is an essential cofactor of their photosynthetic apparatus. Heme also occurs in several forms and, for this thesis, heme denotes heme *b* (protoheme) unless stated otherwise.

Chl consists of two distinct parts, a "ring" and a "tail", each synthesized in a separate pathway and joined together in a final step catalyzed by Chl synthase (ChlG; Figure 1). The Chl "ring"; (containing the Mg atom; Figure 2) is built in the tetrapyrrole pathway from glutamate (Brzezowski et al., 2015) (Figure 1). The "tail" originates from the terpenoid pathway and thus shares a precursor (geranylgeranyl-pyrophosphate; Figure 1) with carotenoids and tocopherols. Chlorophillide *a* and Phytyl-PP, the two last precursors of Chl, can both originate from their respective metabolic pathways to produce a *de-novo* Chl (green arrow; Figure 1). However, one or both of Chl parts can also be "recycled" from a degraded Chl (red arrows; Figure 1); this process of Chl recycling has been demonstrated in cyanobacteria (Vavilin and Vermaas, 2007).

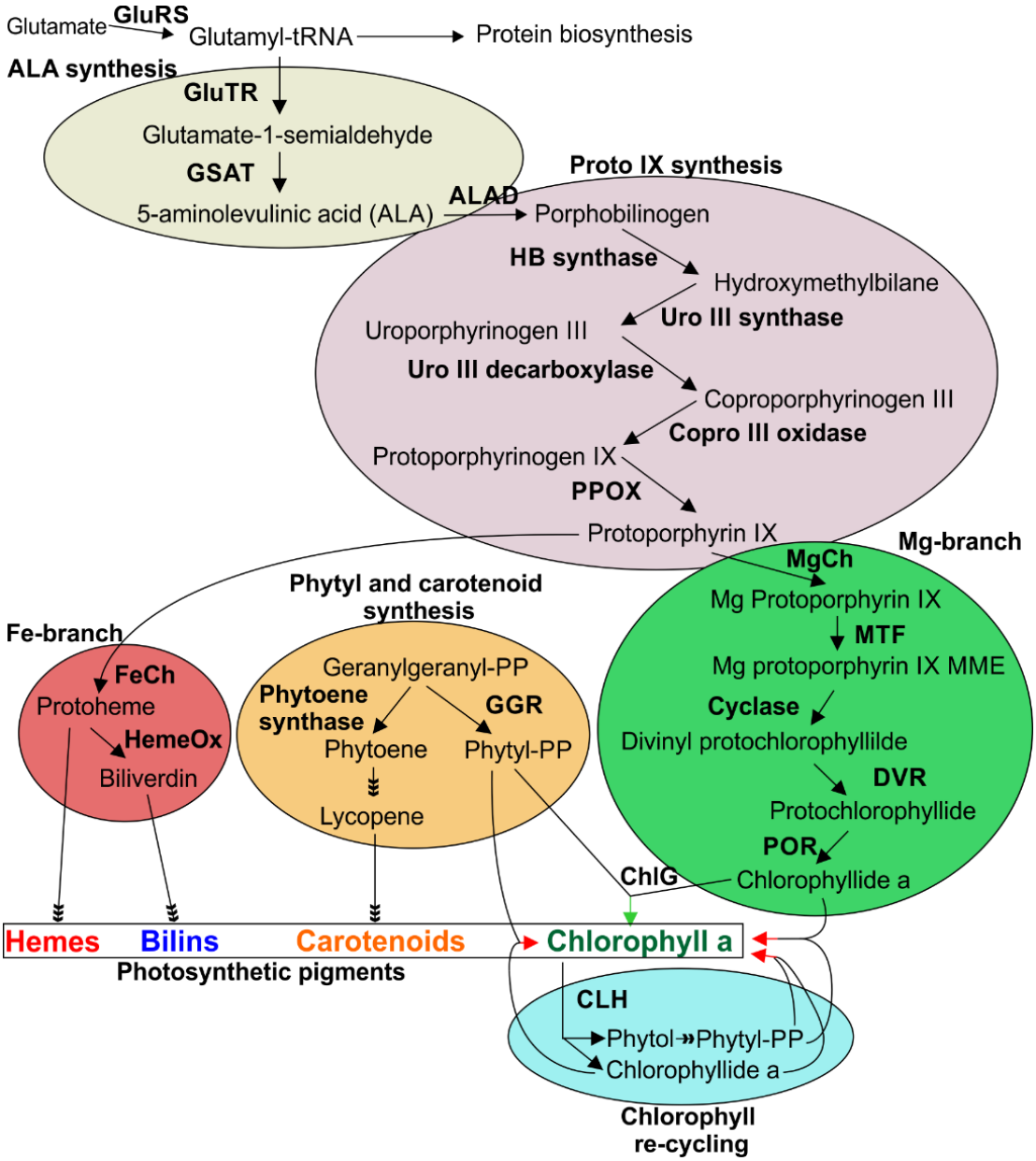

Figure 1. **Schematic representation of the biosynthesis of photosynthetic pigments in cyanobacteria with emphasis on the synthesis of Chl and heme.** The green arrow denotes the synthesis of de-novo Chl. Red arrow denotes synthesis of re-cycled or partially re-cycled Chl. Multiple arrowheads indicate more than one enzymatic step. GluRS - glutamyl-tRNA synthetase; GluTR - glutamyl-tRNA reductase; GSAT - glutamate-1-semialdehyde aminotransferase; ALAD - ALA dehydratase; HB - hydroxymethylbilane; Uro III - uroporphyrinogen III; Copro III - coproporphyrinogen III; PPOX - protoporphyrinogen IX oxidase; MgCh – Mg-chelatase; MTF - Mg protoporphyrin IX methyltransferase; MME - monomethylester; DVR, divinyl protochlorophyllide reductase; POR - NADPH-protochlorophyllide oxidoreductase; ChlG – Chlorophyll synthase; CLH – Chlorophyllase; FeCh - Ferrochelatase; HemeOx – Heme oxygenase; GGR – Geranylgeranyl reductase.

Heme biosynthesis shares several steps with Chl biosynthesis (Figure 1). The last step in Heme synthesis is the formation of two covalent and two coordination bonds between an iron atom and protoporphyrin IX (PPIX). This step is catalyzed by ferrochelatase (FeCh, protoheme ferro-lyase, EC 4.99.1.1). Heme, the product of FeCh, is a ubiquitous metabolite, performing a variety of functions in all organisms.

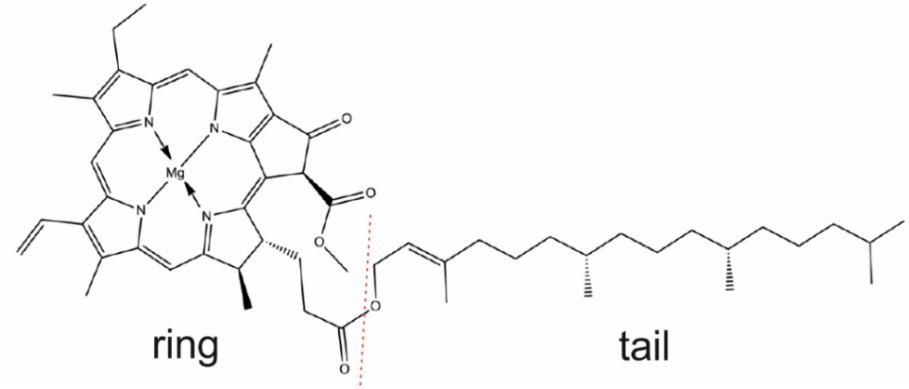

Figure 2. **Structure of Chl.** Red dashed line indicates structural parts produced in tetrapyrrole (left) and terpenoid (right) pathways.

The metabolite flux through every metabolic pathway needs to be regulated from both directions. Both too high and too low synthesis of a metabolic product will impair the fitness of the organism. In general, the regulation of any metabolic pathway can be divided into a transcriptional and (post)translational. The rate at which genes coding for enzymes are transcribed regulates to some extent enzyme levels in the cell and thus modulates how likely they convert their substrate(s) into products. The post-translational regulation of enzymes further determines the enzyme levels by influencing the rate of their degradation. The enzyme activities can be further controlled by a myriad of post-translational modifications, metabolite feedbacks or by the formation of protein complexes.

It is reasonable to expect that the first committed step of any metabolic pathway will be subject to strong regulation. Glutamate-1-semialdehyde, the product of Glutamyl-tRNA reductase (GluTR), is the initial metabolite committed to becoming a tetrapyrrole, thus if any enzymatic step after GluTR had a lower catalytic rate compared to the GluTR, it would result in accumulation of function-less intermediates. In *Salmonella typhimurium* the degradation of GluTR is induced by binding of heme to GluTR N-terminus (Wang et al., 1999), thus creating an elegant feedback loop preventing long-term over and under-synthesis of heme. Higher plants contain two GluTR isoforms. GluTR1, dominantly expressed in green tissue, does not seem to bind heme directly, but a GluTR binding protein (GBP) (Czarnecki et al., 2011) binds to the N-terminal part of

GluTR1 (Zhao et al., 2014; Fang et al., 2016). Importantly, binding of heme to the GBP was recently shown to disconnect GBP from GluTR and this event probably triggers the degradation of GluTR (Richter et al., 2019).

Post-translational regulation can directly influence the catalytic properties of enzymes, via modification of their amino acid residues. The cysteine residues of plant GluTR were proposed to be redox-regulated by NADPH-dependent thioredoxin reductase C, based on the observed interaction between this protein and GluTR (Richter et al., 2013). In general, enzymes of the tetrapyrrole pathway seem to be often regulated by the redox state of the chloroplast in plants(Richter and Grimm, 2013). No research has been so far published on the regulation of cyanobacterial GluTR.

PPIX is the last common precursor of heme and Chl (Figure 1). When one metabolite is distributed towards multiple products, such a position in a metabolic pathway is called a metabolic branch-point. If the products behind a metabolic branch point are required at different quantities, and even more so if the required ratio of these products is variable during the life of the organism, regulation has to operate to ensure correct metabolite distribution into all metabolic branches. Impaired activity of FeCh leads to a massive accumulation of PPIX both in plants and cyanobacteria (Papenbrock et al., 2001; Sobotka et al., 2008). On the contrary, low activity of magnesium chelatase (MgCh, Figure 1), leads to the downregulation of the whole tetrapyrrole pathway (Papenbrock et al., 2000). These results are in line with the proposed feedback inhibition of GluTR by heme (Richter et al., 2019).

I did not find any study directly addressing the distribution of PPIX between FeCh and MgCh. Also, virtually nothing is known about potential posttranslational regulation of FeCh in plants or cyanobacteria; however, MgCh, which is made of three subunits (ChlH, ChlI, and ChlD), appears to be a strictly regulated enzyme. The ChlI subunit seems to be regulated by the redox state of chloroplast (Jensen et al., 2000; Luo et al., 2012; Da et al., 2017), the activity of ChlD subunit was recently reported to be increased after phosphorylated (Sawicki et al., 2017). The MgCh activity is strongly enhanced by the Gun4 protein that physically binds to the catalytic ChlH subunit (Larkin et al., 2003). Gun4 was shown to bind both the substrate (PPIX) and the product (Mg-PPIX) of MgCh in cyanobacteria (Verdecia et al., 2005) as well as in plants (Adhikari et al., 2011) and the binding of porphyrins somehow strengthens the interaction between Gun4 and ChlH (Adhikari et al., 2011; Kopecna et al., 2015). Recently, Gun4 was proposed to reflect the availability and flux of PPIX via increased generation of singlet oxygen upon PPIX binding (Tabrizi et al., 2016). Thus, so far it seems that the distribution of PPIX between MgCh and FeCh is mainly modulated by the strongly regulated activity of MgCh.

1.3 Chl-binding proteins

Chl performs two functions in photosynthesis. Firstly, Chl acts as a redox cofactor in the reaction centers of photosystem I (PSI) and photosystem II (PSII). Photosystems are light powered enzymes (oxidoreductases). Apart from Chls which perform redox photochemistry in the reaction centers, photosystems contain many more Chl molecules, which capture (harvest) the energy of light and transfer the energy into the reaction centers. However, these useful abilities of Chl have a negative, so-called phototoxic, side. The energized (excited) Chl molecules can convert to a so-called triplet state, which can transfer its excitation energy to oxygen. Resulting oxygen radicals cause (oxidative) damage to other molecules (Rinalducci et al., 2004) potentially resulting in the death of the organism. To reduce the amount of the oxidative damage, light-harvesting Chl molecules are positioned in proximity of carotenoids, which can quickly absorb (quench) the energy of Chl triplet state and dissipate it as heat (Ballottari et al., 2013) reducing the oxygen-mediated damage.

The so-called Chl-binding proteins (Chl-proteins) provide a scaffold (a frame) which holds Chls and carotenoids together and positions them into beneficial orientations so that they can transfer energy between themselves efficiently. PSII contains four Chl-proteins: D1, D2, CP43, and CP47, whereas PSI contains two main Chl-proteins: PsaA and PsaB. An excess of energy in the PSII reaction center quickly leads to its photo-inhibition, thus an elaborate repair and protective mechanism evolved to maintain PSII functional under high-light (high energy) conditions (Komenda et al., 2012; Jarvi et al., 2015; Lu, 2016).

One of the mechanisms that protect PSII from photoinhibition under high energy conditions is a diversion of the excess energy away from the reaction center. In plants and algae, Light-harvesting complexes (LHCs) are Chl and carotenoid binding proteins acting as an external "antenna" for PSII and PSI. During low light (low energy) conditions, LHCs increase the energy available to the reaction centers. However, under high light conditions they instead divert the excess energy away from the reaction centers by a mechanism called non-photochemical quenching (Ruban, 2016).

LHC proteins are characterized by the presence of two transmembrane helices containing a conserved sequence (ExxN/HxR) called LHC motif; LHC proteins consist of three transmembrane helices, two of which contain the LHC motif. Two LHC motifs bound to each other are forming a structure capable of binding four Chl molecules (Eggink and Hoober, 2000; Standfuss et al., 2005; Wei et al., 2016). Particularly, each sidechain of glutamate (E) and asparagine (N) directly coordinates Chl molecule (Figure

3a, 3b). The arginine (R) forms an ionic bond with the Chl-coordinating glutamate from the second LHC motif, stabilizing the LHC structure (Figure 3a, 3b).

1.4 Light-Harvesting Complex like (Lil) proteins

There is a large number of proteins containing the LHC motif, but having a different structure or function than the LHC proteins, these proteins are called Light-harvesting complex like (Lil) proteins (forming a subgroup of a large LHC protein superfamily). Lil proteins are often expressed during stress conditions, suggesting a regulatory or photo-protective role; however not a light-harvesting role (Engelken et al., 2010; Engelken et al., 2012; Heddad et al., 2012). Lil proteins are easy to identify in the genome sequences of organisms due to the conserved LHC motif. Historically, two organisms were preferentially used to investigate the function of Lil proteins, the plant *A. thaliana*, and the cyanobacterium *Synechocystis* sp. PCC 6803 (*Synechocystis*). Lil proteins of *A. thaliana* can be divided into three groups, based on the number of transmembrane (TM) helices and the number of TM LHC motif-containing helices (LHC-helices). One helix proteins (OHP) have one LHC-helix. Stress-enhanced proteins (SEP) have one TM-helix and one LHC-helix. Early light-inducible proteins (ELIPs) have one TM-helix and two LHC-helices (similarly to LHC proteins).

The occurrence of Lil proteins in cyanobacteria seems to be limited to High-light inducible proteins (Hlips) sometimes also called Small Chlorophyll-*a*/*b*-binding proteins (SCPs) depending on the author. Hlips contain one LHC-helix and are thus homologous to the OHPs of *A.thaliana*. Hlips were first discovered in 1995 (Dolganov et al., 1995) and are thought to be the progenitors of the whole LHC family (Engelken et al., 2010). None so-far sequenced cyanobacteria have been reported to contain SEP or ELIP-like genes. It should be noted that the LHC-helix of LHC and Lil proteins is in some literature called Chl-*a*/*b*-binding domain (CAB domain).

1.5 Binding of Chl and carotenoids on the Lil proteins

So far, several studies showed that Lil proteins bind Chl *in vivo* and *in vitro*. In 1999, an ELIP protein was shown to bind Chl and lutein *in vivo* during plastid development (Adamska et al., 1999; Adamska et al., 2001). In 2008, a Lil3 (a SEP protein) was reported to assemble in a Chl-binding complex *in vivo*, also during plastid development (Reisinger et al., 2008). In the same year, the interaction between Chl and Hlips was observed using fluorescence resonance energy transfer (FRET) *in vitro* (Storm et al., 2008). Later, Lil3 was shown to bind Chl *in vitro* (Mork-Jansson et al., 2015) and

in the same year, Hlips were shown to bind Chl and β-carotene *in vivo* (Staleva et al., 2015). In summary, the Chl-binding ability of Lil proteins is well proven.

However, the purpose of the Chl binding on Lil proteins is an open question. The Hlips were shown to have a photoprotective role (similar to LHC proteins) but Hlips and their plant homologs OHPs, seem to bind only assembly intermediates of PSII (Komenda and Sobotka, 2016; Hey and Grimm, 2018) contrary to LHC proteins, which associate with fully functional photosystems (Wei et al., 2016). No published study so far addressed the purpose of Chl binding on Hlips by removing their Chl binding ability while preserving the protein. However, one could speculate that they bind Chl to be able to channel excess energy away from PSII, while its undergoing repair or assembly under high-light conditions. But SEPs do not seem to have a photoprotective role. The Lil3 (SEP) was found to bind the two pre-terminal enzymes of Chl synthesis in *A. thaliana* (POR and GGR; Figure 1)(Tanaka et al., 2010; Hey et al., 2017; Zhou et al., 2017). The reported interaction between Lil3, POR and GGR strongly suggests a regulatory role of Lil3 in the final steps of Chl synthesis, perhaps ensuring a proper localization of the synthesis of both Chlorophillide *a* and phytol/geranylgeranyl to the same membrane domain, thus making Chl synthesis more efficient. I was able to find only one study which addressed the *in vivo* role of the Chl binding on SEPs or ELIPs. Interruption of the Chl-binding amino-acids on Lil3 resulted in an aberrant assembly of Lil3 with GGR (Takahashi et al., 2014); however, expression of Lil3 with another transmembrane domain, which cannot bind Chl, instead of the LHC-helix, eliminated the phenotype of Lil3 deletion (Takahashi et al., 2014). The physiological role of the Lil3 LHC motif and its ability to bind pigments thus remains unclear.

1.6 Ferrochelatase LHC domain

With the onset of the whole-genome sequencing in the mid-90s, *Synechocystis* was among the first organisms with fully sequenced DNA available (Kaneko and Tabata, 1997). Shortly after the genome sequence was made public, it was noticed that the FeCh in *Synechocystis* contains an LHC-helix on its C-terminus. As it was already known that the LHC motif is required for Chl binding, the discovery of the C-terminal FeCh LHC motif implied a possible role of Chl in the regulation of FeCh activity, thus perhaps also in the distribution of PPIX between FeCh and MgCh.

After the first fully sequenced plant genome became available (*Arabidopsis thaliana*; (Kaul et al., 2000), it was reported that the LHC domain is also part of the plant FeCh (Jansson, 1999). The author hypothesized that either the LHC protein family

originated from FeCh or FeCh had to fuse with an Hlip early in the evolution of cyanobacteria before the ancestor of plastids separated. It was argued that the FeCh LHC domain must have an important function to be conserved throughout the evolution. It should be noted that plants contain two FeCh isoforms (Chow et al., 1998). Type I FeCh does not contain the LHC domain whereas type II (plastid-type FeCh) does. Since 2000, the LHC motif was found on the C-terminus of FeChs also in green algae and mosses (Figure 3); this feature seems to be conserved in the whole green lineage of oxygenic phototrophs. Technically speaking, the plastid-type FeCh, due to the LHC motif, can be placed in the Lil protein family, and currently, the FeCh is the only known enzyme containing the LHC motif.

In 1999, a first study investigating the role of the FeCh LHC-helix was published (Funk and Vermaas, 1999). *Synechocystis* FeCh was truncated before the LHC domain by the insertion of an antibiotic resistance cassette into the *hemH* gene coding for FeCh. The authors did not observe any discernible phenotype in the mutant strain. However, when the interrupted *hemH* gene was combined with the lack of PSI, the authors reported an increased tolerance of the mutant to high light.

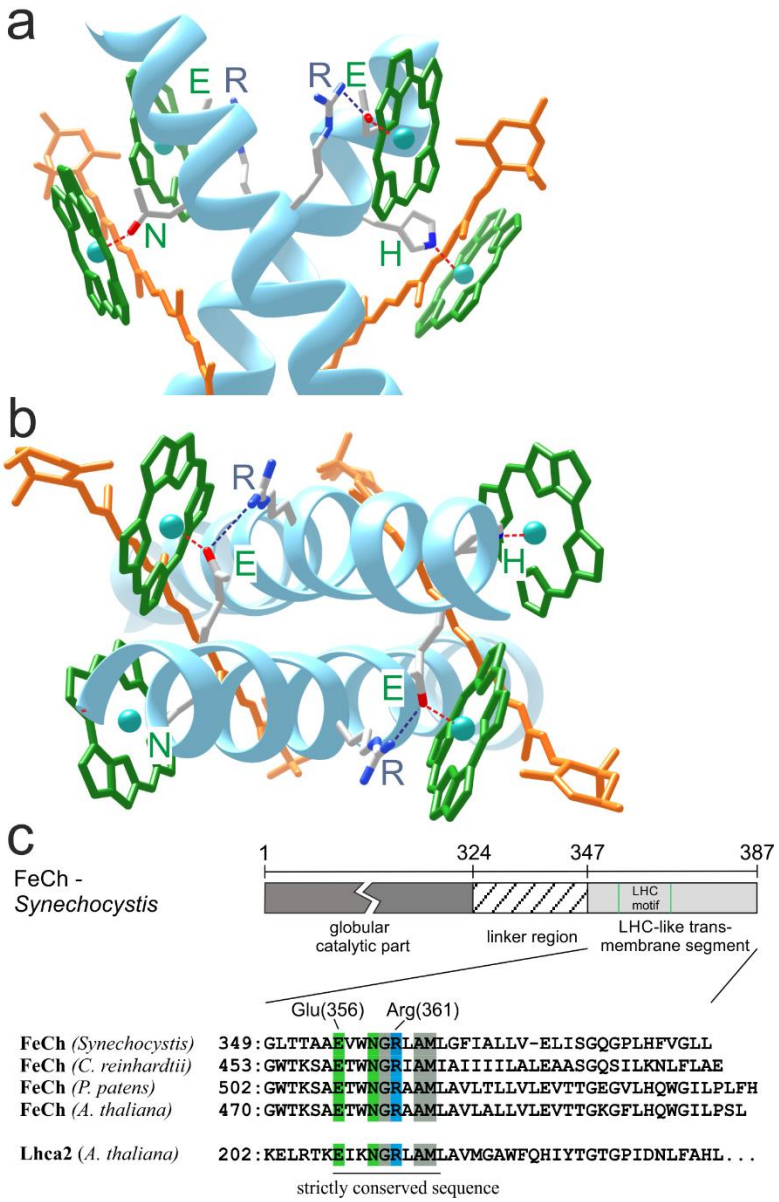

Figure 3. **Structural model of the LHC motif and its conservation in FeCh of photosynthetic model organisms. a**) Side (membrane) view of the crystal structure of LHC-helices of plant LHCII antenna protein (Standfuss et al., 2005) with bound Chl and carotenoids. The conserved amino acids of the LHC motif coordinating Chl and forming ionic bonds are displayed. The red dashed line denotes the donor-acceptor bond between amino-acids and Chl. The purple dashed line denotes an ionic bond. **b**) Top (stromal) view of the same structure displayed in (a). **c**) Alignment of the FeCh LHC-helix from photosynthetic model organisms. Conserved amino-acid residues coordinating Chl in LHC proteins are in green, a charged arginine residue is in blue. Grey color denotes conserved residues with non-polar side-chains. *Synechocystis* (BAA10523.1); *Chlamydomonas reinhardtii* (AAK16728.1); *Physcomitrella patens* (XP_024401127.1); *Arabidopsis thaliana* (CAA73614.1) and LHCa2 protein from *Arabidopsis thaliana* (OAP01790.1).

In our laboratory, the research on FeCh in *Synechocystis* was initiated by the investigation of the CP47 (PSII subunit) combinatorial mutant with an aberrant photoautotrophic growth. It was found that the photoautotrophic growth of this mutant can be almost fully restored by a secondary mutation in FeCh (Tichy and Vermaas, 2000). It was speculated that these secondary FeCh mutations resulted in a lowered FeCh activity and that the decreased synthesis of heme or increased synthesis of Chl restored the photoautotrophic growth. A few years later, a more detailed analysis confirmed a decrease in FeCh activity in pseudo-revertants of the original CP47 mutant (Sobotka et al., 2005). This study also showed that the mutations in CP47 increased the cellular FeCh activity above WT levels in an *in vitro* assay. Furthermore, the level of Chl precursors was found to react inversely to FeCh activity, therefore it was proposed that the FeCh activity regulates the level of tetrapyrroles in cyanobacteria, which was in line with the same observation in plants (Papenbrock et al., 2001).

The following study focused on the role of the C-terminal domain of photosynthetic FeCh. A *Synechocystis* FeCh-Δ324 mutant, missing both linker region and LHC motif (see Figure 3c and Figure 4), contained only about 5% of FeCh level compared to WT, probably due to intensive degradation of the protein or its RNA (Sobotka et al., 2008). The FeCh-Δ324 strain had massively increased levels of PPIX and elevated levels of Chl precursors, supporting the idea that the properly tuned FeCh activity is required for the regulation of tetrapyrrole biosynthesis. Furthermore, the FeCh-Δ324 protein was still a membrane protein clarifying that the association with the membrane is not the function of the FeCh LHC domain.

In the following study (Sobotka et al., 2011), the focus was on dissecting the role of the FeCh LHC-helix. A FeCh-Δ347 strain preserving the linker but lacking the LHC-helix and another strain expressing the LHC-helix and the linker as a separate small protein (His-C-tn) were constructed (Figure 4). Using these strains it was shown that the C-terminal LHC-helix is required for the dimerization of FeCh. It was also reported that the FeCh-Δ347 strain has slightly higher FeCh activity in an *in vitro* assay and that it does not grow under increased light intensity (300 μE). However, this particular phenotype was later not reproduced perhaps because of a change in cultivation conditions (Pazderník, unpublished data).

The final study on the role of the FeCh transmembrane segment, before I started working on it, was performed by (Storm et al., 2013). These authors produced a recombinant FeCh and FeCh-Δ347 in *E. coli*. Removal of the C-terminal-helix led to an increased catalytic turnover number of FeCh *in vitro*. Upon addition of pigments, extracted from *Synechocystis* cells to the refolded FeCh, the authors did not observe any

interaction of Chl with the FeCh LHC domain using FRET. To my knowledge, the FeCh LHC motif was so far not investigated in other organisms than *Synechocystis*.

1.7 State of knowledge

The FeCh LHC motif is conserved among the whole green lineage from cyanobacteria to higher plants, which suggests an important function in the cell/chloroplast and makes it worth investigating. In summary, two things are known about the FeCh LHC-helix: a) FeCh LHC-helix is required for the dimerization of FeCh b) FeCh is still a membrane protein after the removal of the LHC-helix. At this point, it is unknown whether the FeCh LHC motif binds Chl, similarly to a few characterized Lil proteins, or whether it evolved to serve a different function. The physiological function of the FeCh LHC motif is unknown. It is also not known whether it plays a role in other protein-protein interactions apart from FeCh dimerization. In the experimental part of my thesis, I addressed these unknowns.

2. Objectives

1) Investigate the ability of the FeCh LHC domain to bind pigments
2) Investigate the role of the LHC domain in the interactome/localization of FeCh
3) Investigate the physiological role of the FeCh LHC domain

3. Methods

3.1 Previously constructed strains and growth conditions

These mutants of the glucose-tolerant *Synechocystis* strain were used in the thesis (see Figure 4). i) *f.hemH*/Δ*hemH* strain producing Flag-tagged FeCh from the *psbAII* promoter, the native *hemH* gene is interrupted by an erythromycin resistance cassette (Sobotka et al., 2011); ii) *hemH-*Δ*347* strain possessing only a truncated FeCh lacking the LHC-helix (Sobotka et al., 2011); iii) *f.hemH-*Δ*347* strain producing Flag-tagged truncated FeCh-Δ347 (Sobotka et al., 2011); iv) *His-C-tn* strain harboring an artificial gene placed under the *psbAII* promoter, which produces His-tagged C-terminal part of the *Synechocystis* FeCh (Sobotka et al., 2011).

All strains were grown in BG-11 medium; solid media contained in addition 10 mM TES/NaOH, pH 8.2, 1.5% agar and 0.3% sodium thiosulphate. Liquid cultures were grown either in 250 ml conical flasks (50 ml culture) or in 1 L cylinders (800 mL culture)

and were shaken/stirred at 29 °C. Unless stated otherwise the surface irradiance was 40 μmol photons $m^{-2} s^{-1}$ of white light. Cultures were harvested by centrifugation (5000 RCF for 5 min) in the exponential phase at a cell density of ~10^8 /mL corresponding to an optical density at 750 nm in range of 0.8–1.0. FeCh inhibitor N-methyl mesoporphyrin IX (Shipovskov et al., 2005) (Frontier Scientific, USA) was added (where applicable) from a concentrated stock (10 mM) dissolved in DMSO to a final concentration of 275 nM.

3.2 DNA isolation, amplification and transformation

To isolate chromosomal DNA from *Synechocystis*, cells were resuspended in Tris-EDTA buffer (pH=8), mixed with phenol in 1:1 ratio and centrifugated (6700 RCF, 2 min, 4 °C). The obtained supernatant was mixed with chloroform in a 1:1 ratio and centrifugated again (6700 RCF, 2 min). The supernatant was mixed with 1/10 of the volume of 3 M sodium acetate (pH=5.3) and 2.5x volume of 96 % ethanol. Samples were incubated at -70 °C for one hour followed by centrifugation (14 100 RCF; 15 min, 4 °C); the supernatant was decanted and the pellet washed by 70% ethanol and centrifugated (14 100 RCF; 15 min, 4 °C). The precipitated DNA was finally air-dried and dissolved in water.

PCR amplification was performed with Q5 DNA polymerase (BioLabs) or with DreamTag polymerase (ThermoFisher) and, if needed, PCR products were purified using GeneJET PCR purification kit (ThermoFisher). Restriction enzymes and T4 DNA ligase were purchased from ThermoFisher. Plasmid DNA from *E. coli* was isolated using the GeneJET plasmid miniprep (ThermoFisher) and *E. coli* cells were transformed by electroporation at 1.9 kV and grown in LB medium at 37 °C. *Synechocystis* strains were transformed by incubating a liquid culture with DNA for 1 hour followed by transfer to an antibiotic-free agar plate for 24 hours with subsequent transfer to an antibiotic agar plate for the transformant segregation.

3.3 RNA isolation, RNA sequencing, and processing of transcriptomic data

To isolate RNA from *Synechocystis*, around 20 x 10^8 cells were filtered on hydrophilic polyethersulfone filters (Pall Supor 800 Filter, 0.8 μm). The filter covered with cells was immediately immersed in 1 ml of PGTX (41.4% (v/v) phenol, 6.4% (v/v) glycerol, 480 mM guanidinium hydrochloride, 800 mM guanidine thiocyanate, 90 mM sodium acetate, 20 mM EDTA, 7 mM 8-Hydroxyquinoline) containing glass beads. This

mixture was vortexed 5x15 sec and incubated at 65 °C for 20 min. 0.7 mL chloroform was added and mixed for 10 min followed by centrifugation (12 000 RCF, 3 min, RT). The upper-most supernatant was collected and mixed with isopropanol in 1:1 ratio. This mixture was incubated at -80 °C for 2 hours; the supernatant was collected, mixed with 1 mL of 70% ethanol and centrifuged (12 000 RCF, 5 min, 4 °C). The pellet was air-dried, resuspended in water and the contaminating DNA removed using TURBO DNase (Thermo-fisher) according to the manufacturer's instructions.

Quality assessment of the isolated RNA and RNA sequencing was performed in the Helmholtz-Zentrum (Braunschweig, Germany) on a bioanalyzer (Agilent Technologies 2100, Waldbronn, Germany). The RNA sequencing library was generated from 500 ng total RNA using RiboZero rRNA Removal Kit – Bacteria (Illumina) for rRNA depletion followed by NEBNext Ultra II Directional RNA Library Prep Kit (New England BioLabs) according to manufacturer´s protocols. The libraries were sequenced on Illumina HiSeq 2500 using TruSeq SBS Kit v3 - HS (50 cycles) with an average of 5 $x10^6$ reads per RNA sample. Obtained RNAseq data were processed using CLC genomics workbench 12.0, TPM was used in the calculation of PCA and *p*-values.

3.4 Construction of Synechocystis mutant strains

In order to prepare a *Synechocystis* strain producing 3xFlag-tagged *A. thaliana* FeCh2, a synthetic gene coding for this enzyme (AKOO22639.1) without its first 83 codons (predicted chloroplast targeting sequence) and with optimized codon usage was purchased from Genescript (NJ, USA). The synthetic *ara-hemH* gene, cloned into plasmid pUC57-mini, was amplified with Ara1 and Ara2 primers containing *NotI* and *Bgl*II restriction sites respectively (all primers used are listed in Appendix 8.1). The amplified product was inserted into the pSK9 plasmid described in (Kuchmina et al., 2012), which contains upstream and downstream homologous fragments (which put the inserted gene into a neutral site between *slr1597* and *sll1514*), copper-controlled *petJ* promoter followed by 3xFlag tag and a chloramphenicol resistance cassette. The resulting pSK9-*ara-hemH* plasmid was electroporated into *E. coli* DH5α cells. Subsequently, the *Synechocystis* WT-P substrain (Tichy et al., 2016) was transformed using this plasmid and segregated on increasing concentrations of chloramphenicol (10-50 $mg.L^{-1}$). Full segregation was confirmed by PCR (Figure 5a) using Ara3 and Ara4 primers (Appendix 8.1). The correct sequence of Flag-*ara-hemH* was confirmed by sequencing; the resulting sequence is in Appendix 8.3.

The *f.hemH*-Δ347 strain is expressing FeCh enzyme truncated at the amino-acid 347 (lacking the LHC-helix) from the *psbAII* promoter (Sobotka et al., 2011). To interrupt the native *hemH* gene in this strain, the *f.hemH*-Δ347 cells were transformed using a chromosomal DNA isolated from Δ*hemH* strain and segregated on increasing concentrations of erythromycin (10-50 $mg.L^{-1}$). Full segregation was confirmed by PCR (Figure 5b) using HemH1 and HemH2 primers.

To construct *Synechocystis* strain producing a Citrine-FeCh fusion protein, the pUC57-Cit-Km plasmid containing genes for the Citrine fluorescence protein (Rizzo et al., 2004) and kanamycin resistance, surrounded by 300 bp upstream and downstream of *Synechocystis hemH* gene, was purchased from Genescript (NJ, USA). *Synechocystis hemH* gene (without the start codon) was amplified using cit1 and cit2 primers (Appendix 8.1) containing the *Acc65*I and *Pst*I restriction sites, respectively. The amplified product was inserted behind the *citrine* gene into the pUC57-Cit-Km in frame, and the resulting plasmid electroporated into *E. coli* DH5α cells. The WT-P substrain of *Synechocystis* (Tichy et al., 2016) was transformed using the isolated plasmid and segregated on the increasing concentrations of kanamycin (10-50 $mg.L^{-1}$); full segregation was confirmed again by PCR (Figure 5c) using cit3 and cit4 primers. The correct sequence of the fused *cit-hemH* gene (see Appendix 8.3) in *Synechocysits* was confirmed by sequencing.

The *Synechocystis hemH*-ΔChl strain, which has the Chl-binding Glu(356) and Asn(359) residues in the FeCh LHC domain replaced with Ala and Gly, was prepared by Monika Žuberová during her MSc project (Žuberová 2006). However, as I used this mutant strain in my thesis, albeit in the different WT-P background (Tichy et al., 2016), I describe its construction here. The mutant was constructed in several steps. First, a zeocin resistance cassette was placed immediately behind the FeCh gene by PCR-mediated insertion (Lee et al., 2004). In the second step, the DNA from the resulting WT_{zeo} strain (where WT stays for wild type) was isolated and used as the template for site-directed mutagenesis based on the PCR megaprimer method (Ke and Madison, 1997). The resulting PCR product contained the *hemH* gene with point mutations in two residues coordinating Chl molecules in LHC proteins (356Glu GAA -> Ala GCG, 359Asn AAT -> Gly GGT), the zeocin cassette, and corresponding upstream and downstream regions. This PCR product was directly used to transform the *WT* to prepare the *hemH*-ΔChl. *Synechocystis* transformants were selected on a BG-11 medium with an increasing concentration of zeocin (3 to 24 $mg.L^{-1}$).

His-C-tn/hemH-ΔChl strain was prepared by the transformation of *His-C-tn* using chromosomal DNA isolated from *hemH-ΔChl* and selected on increasing concentrations

of zeocine (5 to 30 mg.L^{-1}). Full segregation was confirmed by PCR (Figure 5d) using Zeo1 and Zeo2 primers (Appendix 8.1) and the presence of mutated codons in *His-C-tn*/*hemH*-ΔChl strain was verified by sequencing.

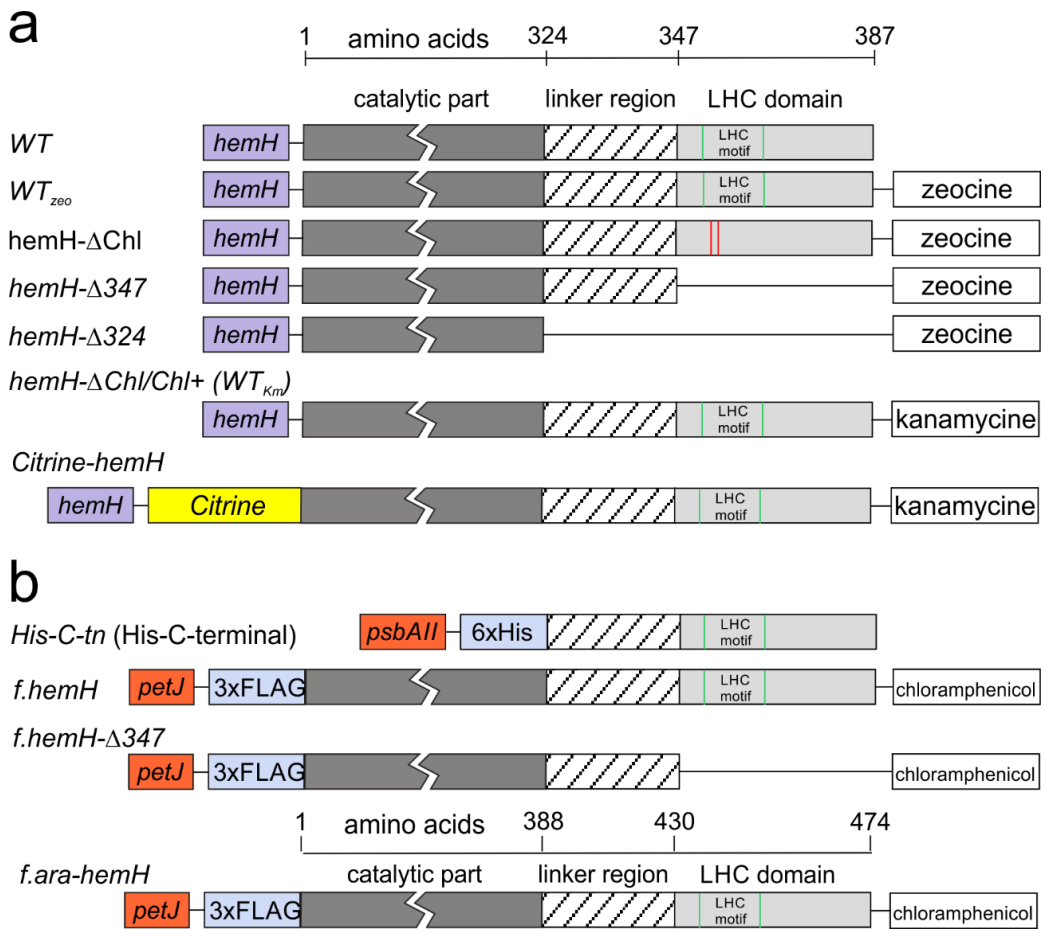

Figure 4. **A scheme of *Synechocystis* FeCh mutant strains used in this thesis**. **a**) Modified *hemH* genes expressed from the native *hemH* promoter (in purple). LHC motif – conserved amino-acids required for Chl binding. FeCh-ΔChl protein has the Chl binding residues Glu(356) and Asn(359) replaced by Ala and Gly respectively. Citrine is a fluorescent protein (a derivative of GFP), a synthetic Citrine-coding sequence is fused with the *hemH* gene. **b**) *PsbAII* is a native strong consecutive promoter; *petJ* promoter is induced by a lack of copper. *f.ara-hemH* is a gene coding for the 3xFlag-tagged FeCh2 enzyme from *A. thaliana* and it is expressed in *Synechocystis*.

In order to confirm that the observed phenotype of the *hemH*-ΔChl strain is not due to a secondary mutation in the genome, I replaced the two mutated amino acids Ala(356) and Gly(359) with the original Glu(356) and Asn(359), thus restoring the LHC motif in FeCh (*hemH-ΔChl/Chl*$^{+}$ strain). To make this complementation the whole *hemH* gene from *Synechocystis* WT cells was amplified using Chl3 and Chl4 primers (Appendix 8.1) containing *NdeI* and *PstI* restriction sites, respectively. The obtained PCR product

was inserted into the pUC57-Cit-Km plasmid described above (see the construction of *citrine-hemH* strain) in a way that the sequence for *citrine* was eliminated. The resulting construct contained the full-length *hemH* gene followed by a kanamycin resistance cassette. The *hemH*-Δ*Chl* strain was transformed by this plasmid and segregated on increasing concentrations of kanamycin (10-50 $mg.L^{-1}$). Full segregation was confirmed by PCR (Figure 5e) using Chl5 and Chl6 primers (Appendix 8.1). Replacement of the *hemH*-ΔChl allele by WT *hemH* was verified by sequencing. A control WT_{Km} strain containing just the kanamycin cassette downstream of *hemH* gene was constructed and verified identically to *hemH*-Δ*Chl/Chl*$^{+}$ (Figure 5f); however, in this case, the WT cells were transformed instead of *hemH*-Δ*Chl* cells.

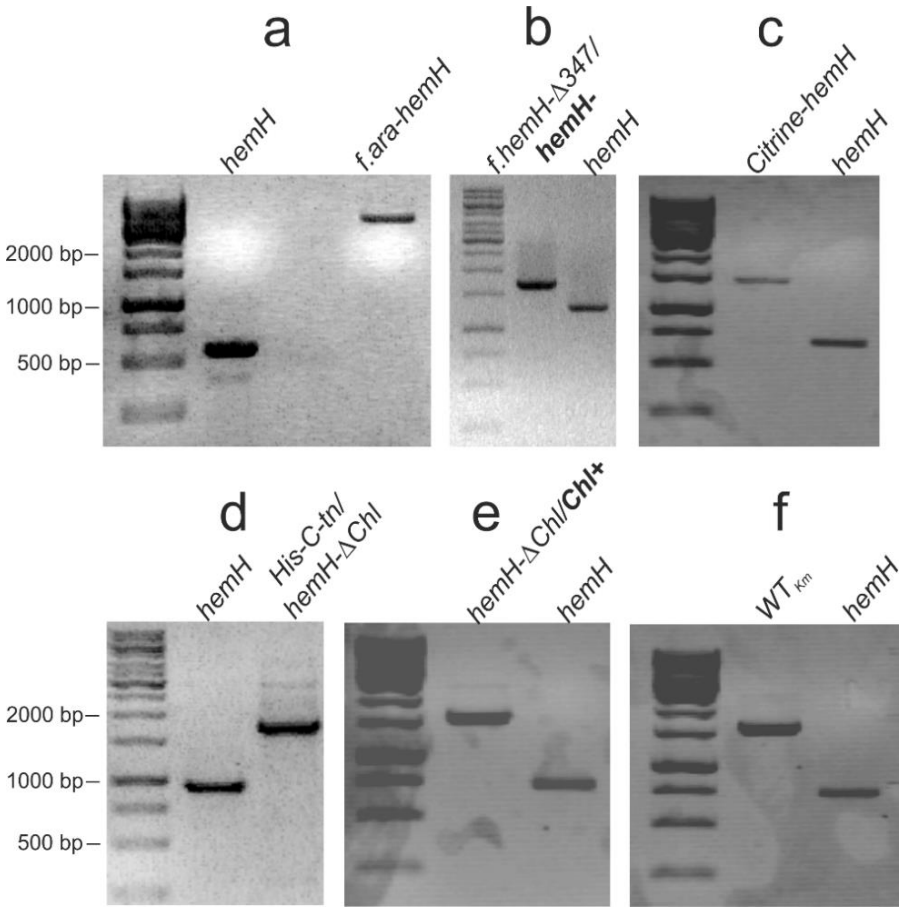

Figure 5. Segregation control of *Synechocystis* strains mutated in the *hemH* gene. Following primers (displayed in Appendix 8.1) were used to amplify WT *hemH* and mutated loci: a) Ara3, Ara4; b) HemH1, HemH2; c) Cit3, Cit4 d) Zeo1, Zeo2; e+f) Chl5, Chl6. Full segregation was judged by the absence of the WT-sized signal in the mutant strains. In multiple mutants, the mutation which was being screened is written in bold.

3.5 Isolation of membranes from Synechocystis cells

For chromatographic preparations, pelleted cells were resuspended in an isolation buffer (20 mM MES, pH=6.5, 150 mM NaCl, complete protease inhibitor cocktail; Roche), mixed with glass beads of 100-200 in μM diameter in 1:1 ratio (1 volume of dense cell solution with 1 volume of glass beads). This suspension was vortexed 6 x 10 seconds with 1 minute on ice in between each cycle. After vortexing, the glass beads were washed 4x with isolation buffer, obtained supernatants were pooled and centrifuged using 40,000 RCF for 15 min. After centrifugation, the pellet (membrane fraction) was resuspended in isolation buffer and frozen (-80 °C) for further use. For electrophoretic separations the isolation buffer was was 25 mM MES, pH=6.5, 10 mM $MgCl_2$, 10 mM $CaCl_2$, 25% (w/v) glycerol, complete protease inhibitor cocktail; Roche. Cells were broken using Mini-Beadbeater-16 (Biospec) instead of the vortex.

3.6 BN-PAGE, CN-PAGE, SDS-PAGE and protein immunodetection

To separate membrane proteins using blue-native electrophoresis (BN-PAGE), isolated membranes (400 μg Chl/mL) were solubilized using 1 % (w/v) n-dodecyl-β-D maltoside (β-DDM) or 1 % digitonin (Sigma-Aldrich) for 5 minutes on ice. Unsolubilized material was removed by centrifugation (20 000 RFC, 10 min). Supernatant corresponding to 4 μg of Chl was mixed with 1/10 volume of a sample buffer containing 750 mM aminocaproic acid and 5 % (w/v) coomassie brilliant blue G-250 (CBB-G). The sample was then separated at 4°C on 8-16 %, or alternatively 4-12 % gradient polyacrylamide gel, containing 500 mM aminocaproic acid and 50 mM Bis-Tris/HCl, pH=7.6 according to (Schagger and Vonjagow, 1991). The starting blue cathode buffer (50 mM tricine, 50 mM Bis-Tris/HCl, pH=7.0, 0.2 % (w/v) CBB-G) was exchanged after 1/3rd of the run for clear cathode buffer (50 mM tricine, 50 mM Bis-Tris/HCl, pH=7.0). 50 mM Bis-Tris/HCl, pH=7.0 was used as anode buffer. For clear-native electrophoresis (CN-PAGE), the sample was not mixed with any sample buffer prior to loading and only clear cathode buffer was used with the addition of 0.05 % (w/v) sodium deoxycholate and 0.02 % (w/v) n-dodecyl-β-D-maltoside. Fluorescence of Chl molecules in CN gels was detected using LAS-4000 (Fuji) after illumination with blue light.

Unless stated otherwise the denaturing 16-20 % SDS-PAGE contained 7 M urea and 650 mM Tris/HCl, pH=8.6 and was prepared according to (Dobakova et al., 2009). Complete lanes from the native gel were excised and incubated for 30 min in 25 mM Tris/HCl, pH 7.5, containing 1 % SDS (w/v) and 2 % dithiothreitol (DTT; w/v). Subsequently, excised lines were placed on the top of the denaturing gel; two lanes were

analyzed in a single denaturing gel. 25 mM Tris, 192 mM Glycine, 0.2 % SDS (w/v) was used as cathode buffer and 25 mM Tris/HCl, pH=8.3 was used as anode buffer. For all gels, the 1:60 ratio of acrylamide to bis-acrylamide was used. To stain separated proteins with CBB-G, gels were first incubated in fixing solution (25 % methanol, 10 % acetic acid) for 30 min, further in the staining solution containing 0.1 % (w/v) CBB-G in 45 % methanol and 10 % acetic acid for 60 min. Gels were destained in 7 % acetic acid. For protein staining with SYPRO Orange (Thermo Fisher), the gel was incubated for 50 min in a solution containing 5000x diluted SYPRO Orange in 10 mM Tris/HCl, pH=7.6, 150 mM NaCl, 10 % (v/v) methanol. SYPRO Orange fluorescence was detected by LAS-4000 (Fuji). MS identification of proteins excised from SDS-PAGE gels was done as described previously (Janouskovec et al., 2013). For the immunodetection the proteins were first transferred from an SDS-gel onto Immobilon-P membrane (0.45 μm, millipore) in a carbonate buffer (Na_2CO_3 3.18 g/L, $NaHCO_3$ 8.4 g/L) using 3 mA/cm^2 applied for 3 h. After electrotransfer, the membrane was blocked for 30 min with 0.05% (w/v) Tween-20 in 10 mM Tris/HCl, pH=7.6, 150 mM NaCl. Subsequently, the blocked membrane was incubated with a primary antibody followed by a secondary antibody-horse-radish peroxidase conjugate (Sigma-Aldrich). Peroxidase activity was visualized by incubating the membrane in a substrate for 20 seconds (LuminataTM Crescendo Western HRP) and detected using LAS-4000 (Fuji).

Primary antibodies used in this thesis were as follows: i) a polyclonal anti-FeCh antibody raised against a recombinant FeCh (Sobotka et al., 2011); ii) a rabbit polyclonal antiserum raised against residues 325 to 353 of precursor D1 from *Pisum sativum* (Komenda et al., 2002); iii) a polyclonal purified anti-PsaA antibody against residues 2 to 18 of PsaA from *Synechocystis*; iv) a polyclonal purified anti-C-tn antibody raised against the synthetic peptide VPHPKKNMKMYPQER (FeCh linker region). v) monoclonal anti-Flag antibody (Sigma).

3.7 Radiolabelling of Chl and proteins, quantification of tetrapyrrole metabolites and pigments.

In order to assess the rate of Chl formation by pulse-labeling, cells (50 mg of Chl) in an exponential growth phase at cell density ~ 50 million/mL (OD_{750} = 0.5) were harvested by centrifugation (2700 RCF, 3 min). Cells were resuspended in a fresh BG-11 medium containing 20 mM TES pH 8.0 to a final volume of 540 uL. The cell suspension was shaken in 10-mL glass tubes for 30 min at 29 °C with a surface irradiance of 40 μmol photons m^{-2} s^{-1}. After this preincubation, 60 μL of [^{14}C]Glu with specific activity 248 mCi/mmol (Moravek Biochemicals) was added and the incubation continued

for another hour. After this time period, cells were harvested (10 000 RCF, 2 min) and frozen in liquid nitrogen. Pelleted cells were washed, resuspended in 50 μL of water and Chl was extracted by 1 mL methanol; the extract was cleared by centrifugation (10 000 RCF, 4 min). The obtained pigment extract was injected into Agilent-1260 HPLC system coupled with a diode-array detector and a flow-scintillation detector (Radiomatic 150TR; Perkin Elmer). Separation was carried out on a reverse-phase column (Kinetex C8, 2.6 μm particle size, 3.9 × 150 mm; Phenomenex) with 35 % methanol and 15 % acetonitrile in 0.25 M pyridine (solvent A) and 20 % methanol, 20 % acetone in acetonitrile as solvent B. Pigments were eluted with a linear gradient of solvent B (30–95 % in 25 min) followed by 95% of solvent B at a flow rate of 0.8 mL min^{-1} at 40 °C.

For *in vivo* radiolabelling of proteins, cells corresponding to 75 μg Chl were harvested (3000 RCF, 3 min) and resuspended in 0.5 mL BG-11. The cell solution was mixed with [^{35}S]Cys+Met (specific activity 400 mCi/mmol) and incubated under 600 μE for 30 minutes. Labeled cells were harvested and membrane fraction prepared essentially as described above for unlabeled cells. Labeled proteins were separated by SDS-PAGE and blotted as described above. The obtained western blots were exposed to a phosphorimager plate and detected using Storm860 (Molecular Dynamics).

Tetrapyrrole metabolites were quantified as described in (Pilný et al., 2015). To identify pigments bound on the purified Flag-FeCh and His-C-tn proteins, collected elutions were concentrated on 10-kDa cut-off micro-concentrators (AmiconR Ultra 0.5mL; Sigma-Aldrich). The obtained concentrated solution (25 μL) was extracted with 90 % methanol and the extract analyzed by Agilent-1260 HPLC. The separation was carried out as already described for the [^{14}C] radiolabeled samples. Pigment stoichiometries were calculated from calibration curves prepared using authentic standards. Extraction and quantification of heme were done essentially as described previously (Koreny et al., 2012).

3.8 Affinity, size-exclusion and anion-exchange chromatography

His- and Flag-tagged proteins were purified from the solubilized membrane fraction in isolation buffer (20 mM MES, pH=6.5, 150 mM NaCl, complete protease inhibitor cocktail; Roche) according to manufacturer's instructions using Protino Ni-NTA Agarose (Macherey-Nagel) and anti-Flag M2 affinity gel (Sigma-Aldrich) respectively using 10 mL column. Prior to ion-exchange/size exclusion chromatography samples were 5-times concentrated using a 10 kDa cutoff micro-concentrators (AmiconR Ultra 0.5 mL; Sigma-Aldrich).

The Flag-FeCh eluate was injected onto an Agilent-1200 HPLC machine and separated on Yarra SEC-3000 column (Phenomenex) using mobile phase containing 20 mM MES pH=6.5, 100 mM NaCl and 0.06 % (w/v) n-dodecyl-β-D maltoside at a flow rate of 0.25 ml.min^{-1} at 15 °C. Eluted proteins and complexes were detected by a diode-array detector and a fluorescence detector set to 440 nm/680 nm (excitation/emission wavelengths). Membranes solubilized by 1% (w/v) n-dodecyl-β-D maltoside were separated identically to the Flag-FeCh eluate.

The His-C-tn eluate was injected onto an Agilent-1200 HPLC machine and separated on MonoQ 4.6/100 PE (GE Healthcare) using mobile phase composed of buffer A1 (20 mM HEPES pH=8.1, 5 mM $MgCl_2$, 0.06 % β-DDM; w/v) and buffer B1, which was the same as the buffer A1 but contained 1 M NaCl. The linear gradient was run as follows: 0 to 10 min – 0 % B, 10 to 15 min – linear increase from 0% to 20% B, 15 to 45 min – linear increase from 20 to 55% B, 45 to 47 min – linear increase from 55 to 100% B; all steps at a flow rate of 0.8 mL.min^{-1} and at 15 °C. Eluted proteins and complexes were detected by a diode-array detector (190 – 750 nm) and a fluorescence detector set to 440/680 nm (excitation/emission wavelengths).

3.9 Chl fluorescence yield

The quenching of Chl fluorescence was estimated from the fluorescence yield measured using the ratio of fluorescence/absorbance of the Chl bound to the FeCh LHC domain in comparison with the Chl in β-DDM micelles at their respective maxima. Similar extinction coefficients and fluorescence constants were assumed for both Chl populations.

3.10 Crosslinking and mass spectrometry

Flag-FeCh pulldown (600 ug protein/mL) was incubated with 5 mM BS3-H12/D12 cross-linker – a 1:1 mixture of BS3-H12 and deuterated version BS3-D12 (Creative Molecules Inc.) dissolved in a buffer containing 20 mM MES/NaOH, pH 6.5, 10 mM $CaCl_2$ and 0.03% (w/v) digitonin. After 30-min incubation on ice, 100 mM NH_4HCO_3 was added and the reaction mixture was incubated for 15 min at room temperature to terminate the cross-linking reaction. Tryptic digestion and sample preparation were performed after protein precipitation by the addition of cold acetone according to(Cormann et al., 2016). Tryptic peptides were desalted with ZipTips (Millipore) and resuspended in buffer A2 (0.1 % (v/v) formic acid in water). Samples were applied to a UPLC Symmetry C_{18} trapping column (5 μm, 180 μm × 20 mm; Waters,

Milford, MA, USA) and subsequently transferred to a UPLC BEH C_{18} column (1.7 µm, 75 µm × 150 mm; Waters, Milford, MA, USA). Both columns were driven by the nanoACQUITY gradient UPLC pump system (Waters) coupled to an Orbitrap Elite Velos Pro Hybrid FTMS mass spectrometer (Thermo Fisher Scientific Inc., Waltham, MA, USA) via a PicoTip Emitter (SilicaTip, 30 µm, New Objective, Woburn, MA, USA). The column was heated on 45 °C and the spray voltage was set to 1.5–1.8 kV. Peptides were eluted with a multistep gradient of buffer A2 to buffer B2 (0.1 % formic acid in acetonitrile) at a flow rate of 0.4 µl/min (0–5 min: 1 % buffer B; 5–10 min: 5 % buffer B; 10–175 min: 40 % buffer B; 175–200 min: 99 % buffer B; 200–210 min: 1 % buffer B). The linear ion trap and orbitrap were operated in parallel, i.e., during a full MS scan on the orbitrap in the range of 300–2000 m/z at a resolution of 240,000. Tandem MS (MS/MS) spectra of the 20 most intense precursors were detected in the ion trap. The desolvation capillary was heated on 200 °C and the relative collision energy for collision-induced dissociation was set to 35 %. Dynamic exclusion was enabled, with a repeat count of one and a 1-min exclusion duration window. Singly or doubly charged ions, as well as ions with an unassigned charge state, were rejected from MS/MS. StavroX v. 3.6.6.6 was used for the interpretation of MS/MS data (Gotze et al., 2012) with the following settings: Protease cleavage sites: K and R; missed cleavages: K:1 and R:1, semi-random digest; cross-linker: BS3-H12/D12; cross-linked amino acids: 1. K, N-term.; 2. K, S, T, Y, N-term; precursor precision: 5.0 ppm; fragment ion precision: 0.8 Da; lower mass limit: 200 Da; upper mass limit: 6000 Da; S/N ratio: 2.0; ion types: *b*- and *y*-ions; neutral loss: only of identified fragments.

3.11 Confocal microscopy

Images were acquired using Zeiss LSM 880 confocal microscope with Plan-Apochromat 63x/1.4 Oil DIC M27 objective and GaAsP photomultiplier. *Synechocystis* cell expressing Citrine-FeCh were excited with 514 nm laser (MBS 458/514) and emissions were detected at indicated wavelengths. Images were taken with 8-bit mode, 5x zoom, 512 x 512 pixels, pixel size 0.053 µm; pixel dwell time 65.9 µs.

4. Results and discussion

4.1 The connection between FeCh activity and the pigment binding on the FeCh LHC-helix

Potential binding of Chl on FeCh is discussed since the discovery of the conserved FeCh LHC-helix in cyanobacteria and plants (Jansson, 1999). The obvious hypothesis states that binding of Chl on FeCh may regulate FeCh activity and thus, via a heme feedback loop (Richter et al., 2019), Chl molecules could regulate their own synthesis. However, if this hypothesis was valid, the activity of FeCh should control the rate of Chl biosynthesis. Previously published data show that the impairment of FeCh results in the upregulation of the tetrapyrrole pathway (Papenbrock et al., 2001; Sobotka et al., 2005). However, as a part of the Chl molecule (phytyl chain) is synthesized by the terpenoid pathway (Figure 1), the upregulated synthesis of tetrapyrroles does not necessarily have to result in increased Chl synthesis.

4.1.1 Low FeCh activity accelerates the synthesis of de-novo Chl and leads to Chl accumulation in membranes

To test whether FeCh activity can influence the rate of Chl synthesis, first I partially inhibited FeCh using the specific FeCh inhibitor N-methyl mesoporphyrine IX (MPP) (Shipovskov et al., 2005) and, after 3 h of the MPP treatment, I supplemented *Synechocystis* cells with a labeled tetrapyrrole precursor [^{14}C]Glutamate. After a 1 hour pulse, I extracted total Chl, separated it by HPLC and compared Chl absorbance with radio-emission from Chl molecules. In theory, if a cell produces more Chls during the pulse, the amount of Chl emission per its absorbance should increase, because a larger pool of the total Chl will be radio-labeled. A growth assay (Figure 1a) showed that the MPP in the 275 nM concentration slowed down the growth rate of *Synechocystis* by 6 % in 24 hours at our standard laboratory conditions. Even though the MPP-treated cells grew slower, the addition of MPP accelerated the synthesis of Chl by over 20 % (Figure 6b). From this experiment, I concluded that the activity of FeCh is likely inversely reflected in the rate of *de-novo* Chl synthesis and that the *Synechocystis* cell has no other regulatory mechanism which could prevent over-synthesis of Chl if the activity FeCh is not high enough, at least under our standard conditions.

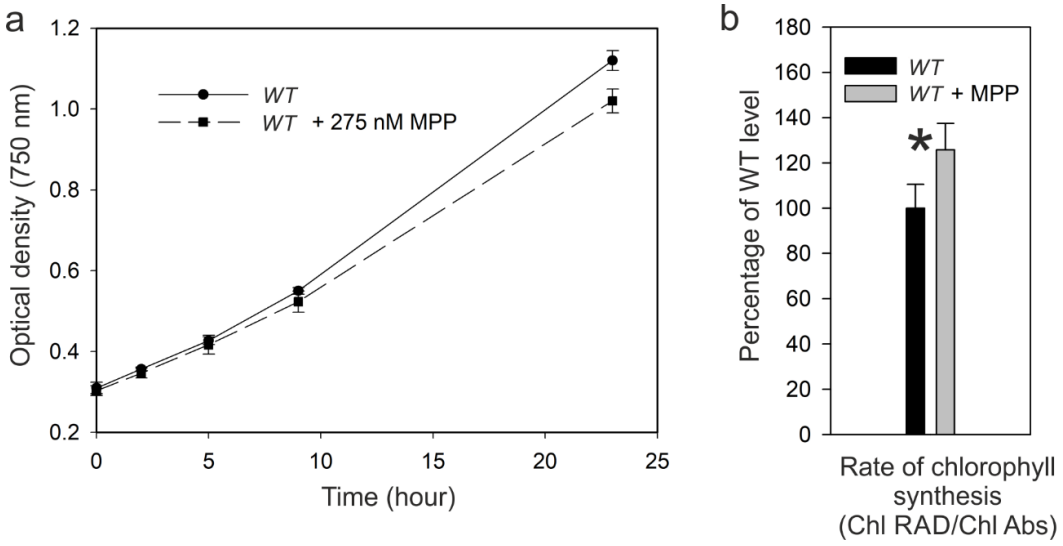

Figure 6. Partial inhibition of FeCh results in an increased rate of *de-novo* Chl synthesis. **a**) The effect of 275 nM MPP on the growth rate of *Synechocystis* cells, measured as an increase in the optical density of the culture. **b**) *WT* and *WT* pre-treated with MPP (inhibitor of FeCh) for 3.5 hours were supplemented with radiolabeled ^{14}C Glutamate for 1 hour prior to harvest. Total pigments were extracted and separated on HPLC coupled with absorbance and scintillation detectors. The rate of Chl synthesis was estimated from the ratio of Chl emission/absorbance. Error bars give s.d., n = 4 independent experiments. *****P = 0.029; Student's t-test.

To get insight into what happens with the excess of over-synthesized Chl (Figure 6b) produced during MPP treatment, I separated the Chl containing fraction (membrane fraction) using CN gel. Cells treated with MPP, after 4 hours, had more than double the amount of free or loosely bound Chl in their membranes (Figure 7). Based on this experiment I suggest that the inhibition of FeCh causes Chl accumulation in the thylakoid membranes. However, even after 24 hours, the MPP-treated culture did not have more total Chl compared to the control (Figure 8, note the similar Chl absorbance peak at 680 nm). This experiment led to two conclusions: Firstly, the amount of unbound Chl in *Synechocystis* is very small when compared to the total Chl, therefore its increase is not detectable using the absorbance of the whole cells. Secondly, in 24 hours, *Synechocystis* divides about twice under our standard conditions (Figure 6a), in the experiment described in Figure 8 the cells were likely living for two generations with increased synthesis of Chl but did not accumulate more Chl-proteins. Therefore, I expect that Chl degradation also increased after FeCh inhibition. In conclusion, the above-normal synthesis of Chl resulted in increased concentration of free Chl in the membranes but did not translate into an increased amount of photosystems in *Synechocystis*. This is in

agreement with a report performed on *A. thaliana*, that the rate of translation of Chl-proteins is not influenced by Chl availability (Zoschke et al., 2017).

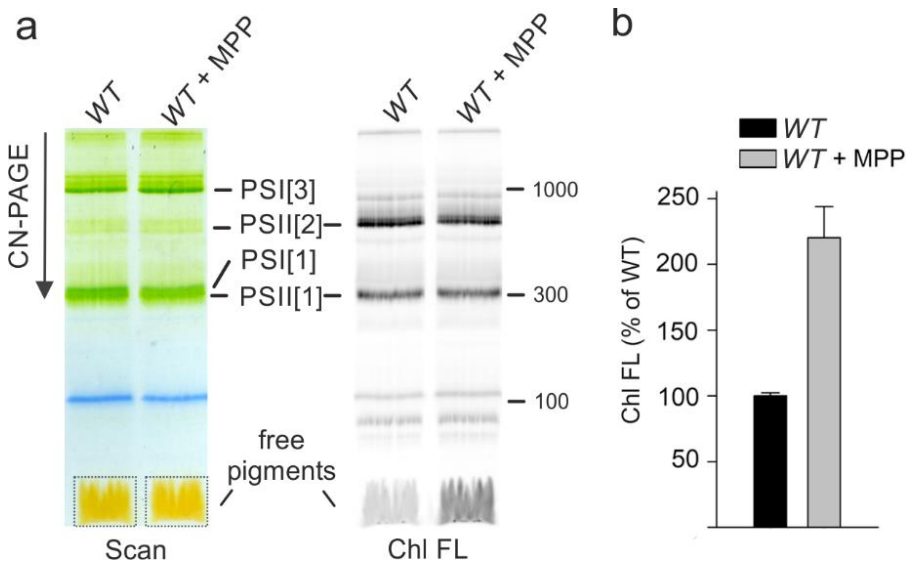

Figure 7. Accumulation of 'free' Chl in MPP-treated *Synechocystis* cells. a) Membrane fractions isolated from *WT* and *WT* treated with MPP (FeCh inhibitor) were solubilized using β-DDM and separated on a 4-12 % CN-PAGE. Separated complexes were scanned (left) and Chl fluorescence was recorded (right). Note the marked increase of Chl fluorescence in the free pigment area after MPP treatment. **b**) Quantification of Chl fluorescence from the free pigment area (dotted) from A. Error bars give S.D. n=3 biological replicates.

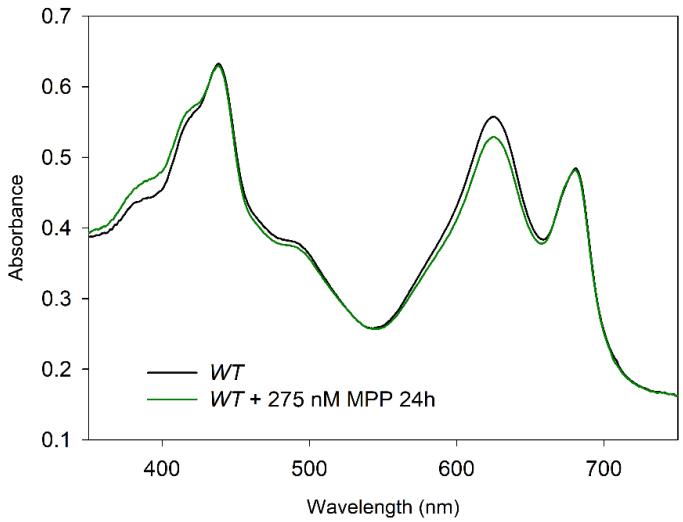

Figure 8. A long-term (24 h) treatment with MMP does not result in a detectable increase in the total cellular level of Chl. Absorbance was recorded for *WT* and *WT* treated with 275 nM MPP for 24 hours. Spectra were normalized to optical density (750 nm). Note the similar absorbance of Chl at 680 nm.

4.1.2 FeCh binds Chl and carotenoids when its activity is low

I knew that f.FeCh, when purified from *Synechocystis*, does not bind Chl or any other pigments, based on the previously published results (Sobotka et al., 2011). However, it was possible that under certain conditions the plastid-type FeCh binds pigments because several LHC-like proteins with the LHC motif do (Standfuss et al., 2005; Mork-Jansson et al., 2015; Staleva et al., 2015). Albeit these proteins are probably not enzymes, when the amino acid sequence is conserved, in protein-pigment interactions it should not matter whether a protein is an enzyme or not.

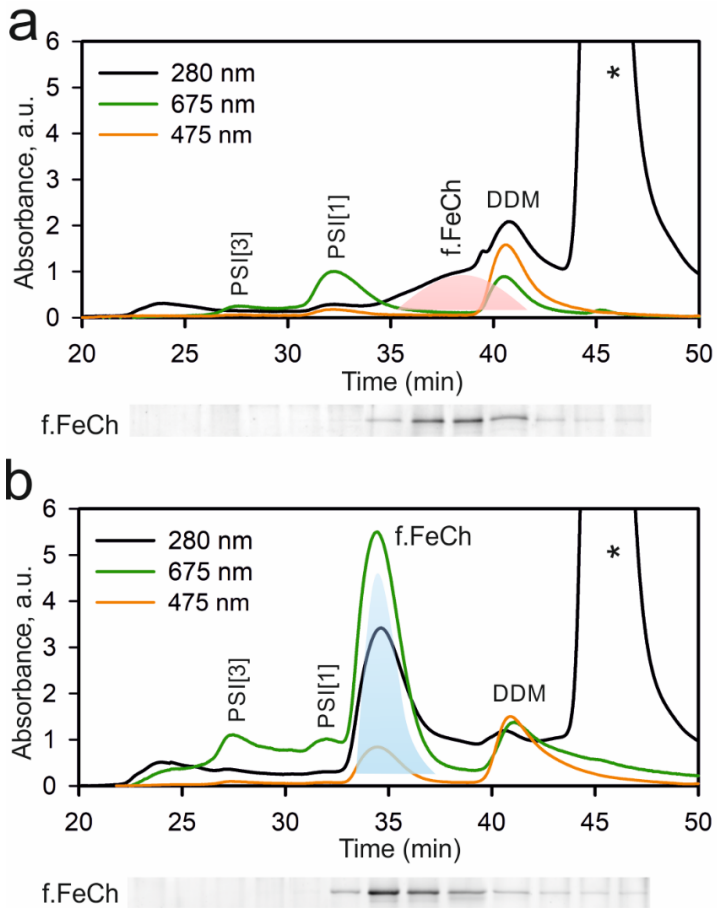

Figure 9. **MPP treatment induces binding of Chl and carotenoids on the *Synechocystis* f.FeCh. a**) f.FeCh was purified from the solubilized membrane fraction using an anti-Flag gel. The obtained eluate was further separated on a size-exclusion column. Minute fractions were collected and subsequently separated on SDS-PAGE stained with SYPRO Orange (below the chromatogram figure). The red peak denotes the elution profile of f.FeCh. **b**) Cells expressing the f.FeCh were incubated with 275 nM MPP (FeCh inhibitor) for 4 hours prior to harvest. The isolation of f.FeCh was identical to (a). The blue peak indicates the shift in the retention time of the purified f.FeCh after MPP treatment. A new Chl peak (675 nm) as well as the absorption of carotenoids (475 nm) co-migrated with f.FeCh after MPP treatment. The asterisk denotes absorbance of the 3xFlag-peptide used to elute f.FeCh from the affinity resin.

I hypothesized that the FeCh LHC motif is a Chl sensor monitoring the Chl abundance in the cell, and therefore will bind Chl only when Chl is present in excess. Based on the observation that FeCh inhibition leads to aberrant accumulation of free Chl (Figure 7a), I tested whether this situation will result in the binding of Chl on the FeCh. I isolated f.FeCh by a combination of affinity and size exclusion chromatographies from the cells treated by 275 nM MPP and from untreated control. Importantly, the f.FeCh, purified from the cells grown in the presence of MPP, co-migrated during size-exclusion chromatography (SEC) with Chl and carotenoids, which contrasted the 'colorless' f.FeCh purified from untreated cells (Figure 9).

The absorption spectrum and pigment analysis of the eluted f.FeCh-pigment complex confirmed the presence of Chl and carotenoids (Figure 10a,b). Based on these data, I conclude that the cyanobacterial FeCh binds Chl and carotenoids *in vivo*, similarly to other Lil proteins (Adamska et al., 1999; Reisinger et al., 2008; Shukla et al., 2018); however this binding is linked to a surplus of free Chl that can be induced by lowering FeCh activity.

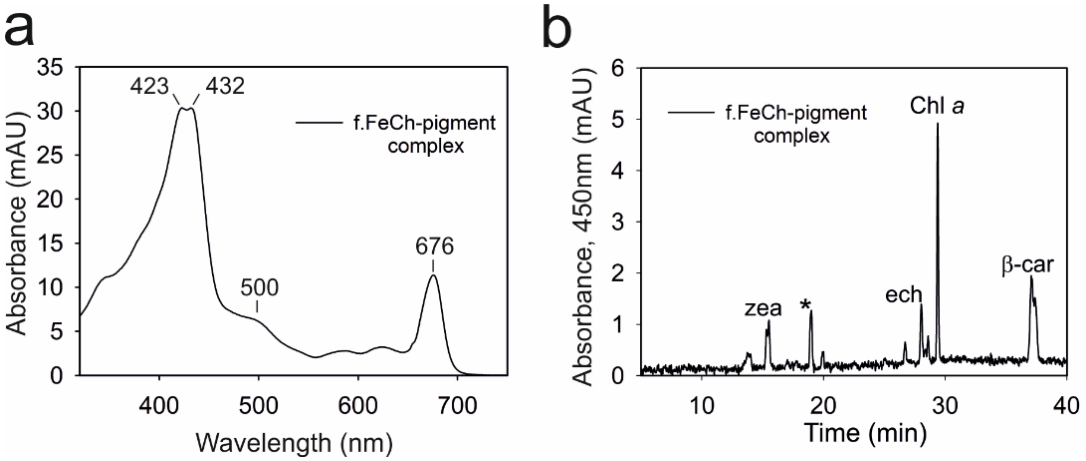

Figure 10. **The isolated f.FeCh is associated with Chl, β-carotene, zeaxanthin, echinenone, and an unknown carotenoid species. a)** Absorbance spectrum of the f.FeCh-pigment complex isolated using pulldown and SEC (Figure 9b). **b**) Pigments bound on the f.FeCh (a) were extracted using methanol and separated on a C18 column by HPLC. Pigments were identified based on their retention time and absorption spectra. Zea - zeaxanthin, ech – echinenone, β-car – β-carotene. The asterisk indicates an unknown carotenoid species.

4.1.3 Partial inhibition of FeCh induces its dimerization

The purified f.FeCh-pigment complex (Figure 9b), eluted much earlier (3 min) from the size-exclusion chromatography (SEC) column compared to the pigment-less FeCh (Figure 9a). According to the calibration of the SEC column (Figure 11), the

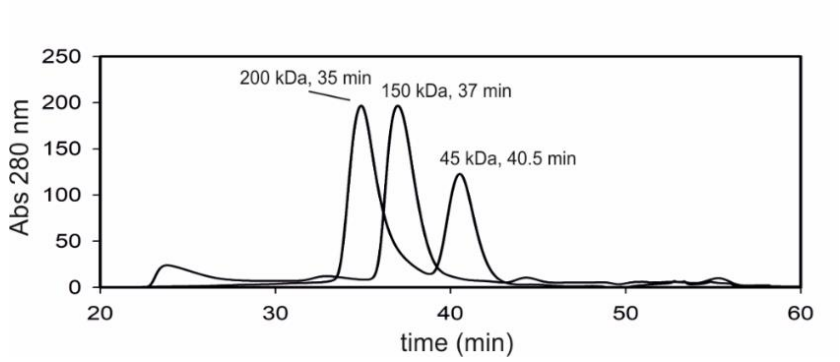

Figure 11. **Calibration of the SEC column used in this thesis;** 200 kDa β-amylase, 150 kDa alcohol dehydrogenase, 45 kDa albumin.

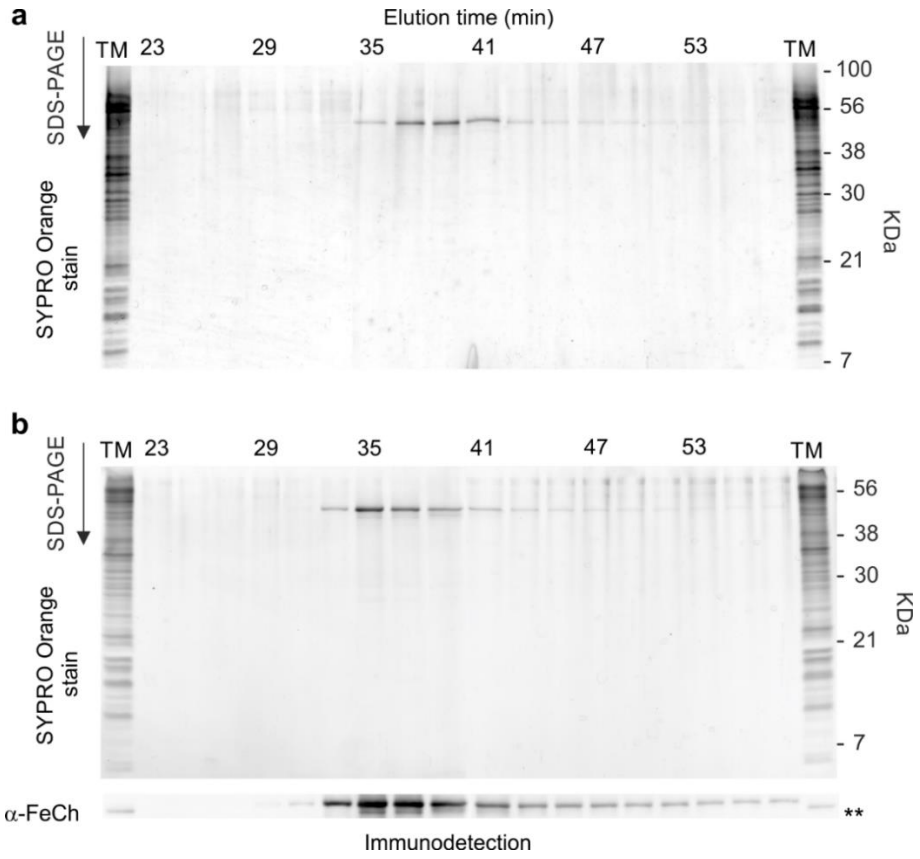

Figure 12. **f.FeCh migrates notably slower on a SEC column after MPP treatment** **a**) Minute fractions collected during the SEC separation of f.FeCh eluate were further separated by SDS-electrophoresis and strained by SYPRO Orange. Values on the top of the gel indicate the elution time from the column. **b**) The identical analysis described in (a) but for the f.FeCh eluate pulled down from cells treated with MPP (FeCh inhibitor). In this case, the stained gel was blotted and the f.FeCh protein immunodetected. TM denotes solubilized membrane fraction loaded as a positive control. Asterisks denote the native FeCh present in wild-type membranes migrating slightly faster than the f.FeCh.

f.FeCh-pigment complex eluted at the apparent size of around 210 kDa, which corresponds to the mass of about 4-5 FeCh (43 kDa) proteins. The pigment-less f.FeCh also eluted at an unexpected size corresponding to 120 kDa. In theory, association with several pigments should not make such a shift in the elution time. Also, both pigmented and pigment-free f.FeCh purifications did not contain any other proteins (potential interaction partners) visible on a stained gel (Figure 12). Therefore, 210 kDa retention time of f.FeCh after MPP treatment would suggest a formation of FeCh tetramer. This is however not consistent with the separation of WT solubilized membranes by SEC followed by immunodetection of the (native) FeCh. The retention time of the native FeCh corresponded to a mass of 40 kDa (Figure 13). The MPP treatment also induced a shift in the elution time of the native FeCh to about 90 kDa (Figure 13), which corresponds to FeCh dimer. Therefore, I conclude that the presence of 3xFlag-tag significantly increases the retention time of FeCh in the SEC column, most likely due to the charged amino-acids of the Flag-tag, and the MPP treatment induces dimerization of both f.FeCh and the native FeCh apart from pigment binding.

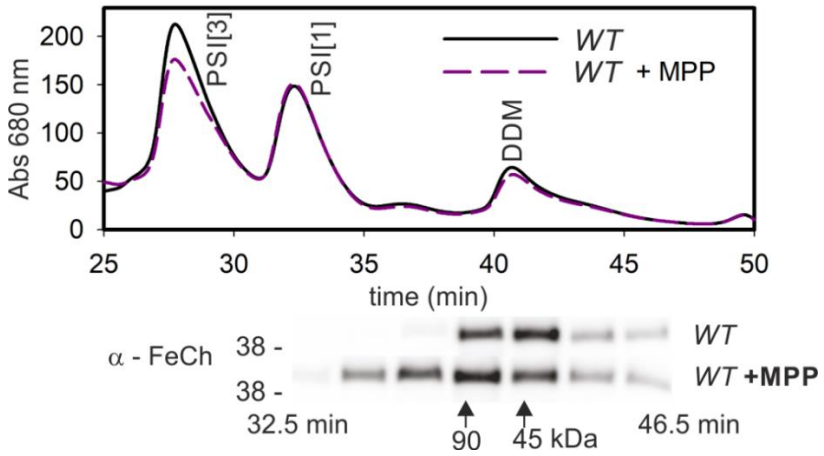

Figure 13. **MPP treatment causes a shift in the retention time of the non-tagged FeCh during SEC corresponding to FeCh dimerization.** Solubilized membrane fractions of *WT* and *WT* treated with 275 nM MPP for 4 hours were separated using size exclusion chromatography. Minute fractions were collected, separated on SDS-PAGE, blotted and probed with the anti-FeCh antibody.

To further confirm that the MPP-treatment induces dimerization, I separated the treated *WT* cells using 2D BN/SDS-PAGE followed by immunodetection. Using this method, I observed a clear shift in the FeCh migration in MPP-treated cells corresponding to the size of dimeric FeCh (Figure 14). Furthermore, using the *hemH-*Δ*347* mutant that lacks the LHC-helix, I showed that the FeCh LHC-domain is required for the MPP-

induced dimerization (Figure 14), which agrees with the previous observation that the FeCh lacking LHC-helix cannot dimerize (Sobotka et al., 2011).

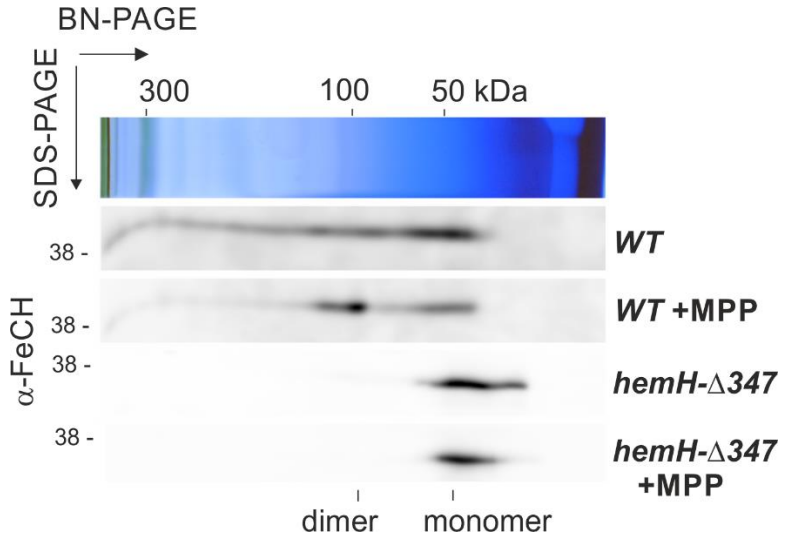

Figure 14. **The LHC domain is required for the MPP induced dimerization.** Solubilized membrane fractions from the indicated strains were separated by 2D BN-PAGE, blotted and the FeCh was immunodetected. Only slices of the blot with the signal of FeCh are shown. The position of monomeric and dimeric FeCh is indicated.

Regarding the observed FeCh dimerization, it cannot be fully excluded that most of FeCh *in vivo* is dimeric. In such a case, the reason for the detection of monomeric FeCh could be a preferential dissociation of the pigment-less dimers upon membrane solubilization. In other words, the FeCh dimer associated with pigments could be more stable towards detergent treatment. However, even after solubilization with a very mild detergent digitonin (Figure 21), I detected practically no FeCh signal with a mobility corresponding to FeCh dimer. I, therefore, find this unlikely.

4.1.4 Expression of FeCh2 from Arabidopsis thaliana in Synechocystis

The rationale behind the expression of *A. thaliana* FeCh in *Synechocystis* was to see whether it will also dimerize upon MPP treatment, especially since there are no published studies dealing with the FeCh LHC-helix in eukaryotes. *A. thaliana* contains two *hemH* genes coding for FeCh. The FeCh2 isozyme called type II (plastidic type) contains the C-terminal LHC-helix (Ac. Nr. KOO22639.1); however, the second FeCh (type I) does not have the LHC motif. I constructed a *Synechocystis f.ara-hemH* mutant expressing a 3xFlag tagged variant of the type II *Arabidopsis* FeCh (f.Ara-FeCh, see strain construction). 2D BN/SDS-PAGE analysis revealed that, after the incubation with MPP, the f.Ara-FeCh2 protein did shift towards a higher mass complex, however not as

clearly as the native *Synechocystis* FeCh did in the same sample. Also, the higher-mass form of f.Ara-FeCh was smaller than what it would be expected for a dimer (Figure 15). This could mean that the f.Ara-FeCh is binding some other protein and not itself after MPP treatment.

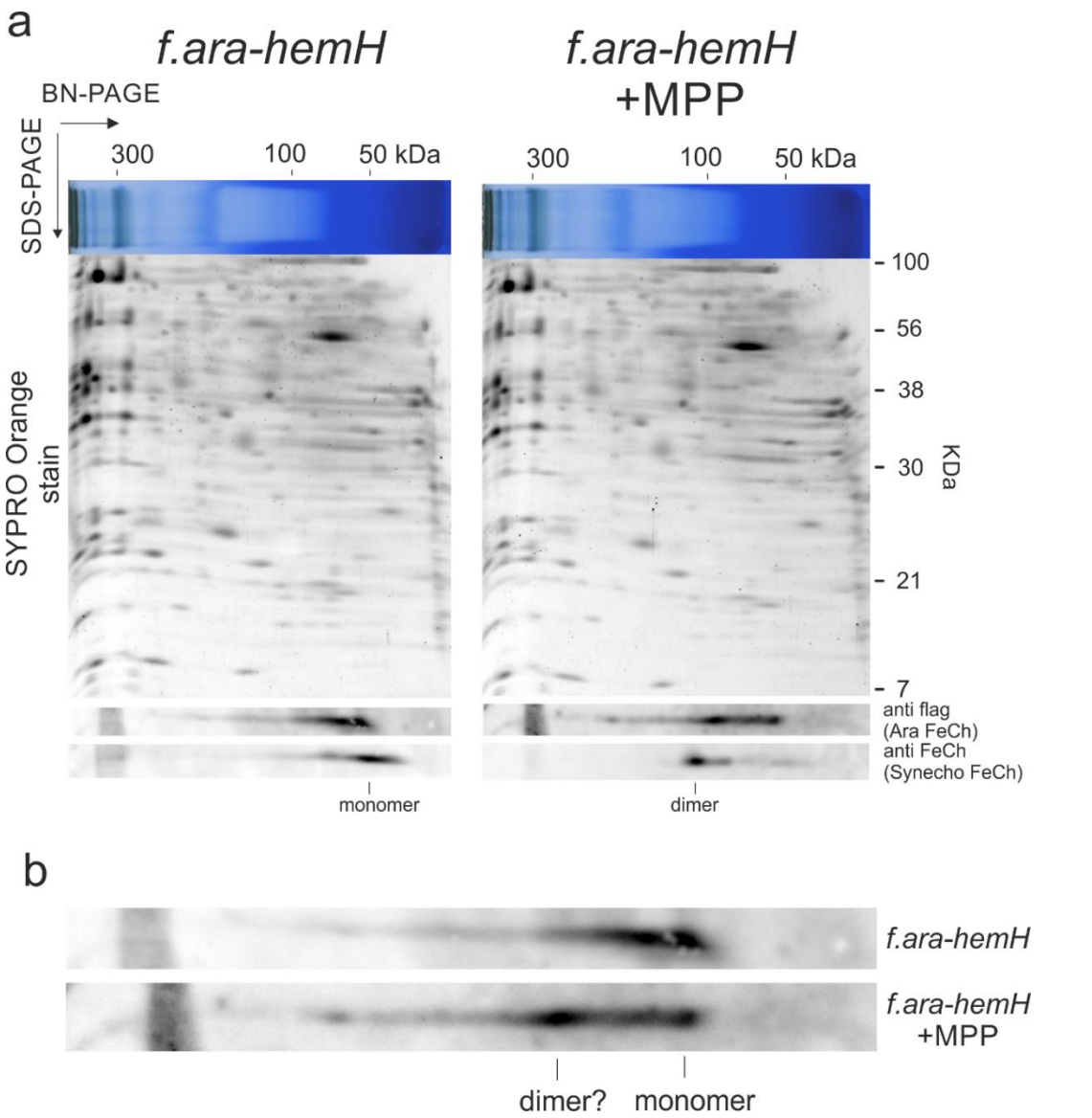

Figure 15. **The *Arabidopsis* FeCh expressed in *Synechocystis* also responds to MPP treatment by a shift in the gel mobility. a**) Membrane fractions from *Synechocystis* expressing the FeCh2 isoform from *Arabidopsis thaliana* (*f.ara-hemH*) and from *f.ara-hemH* cells treated with MPP (FeCh inhibitor) were solubilized and separated by BN/SDS-PAGE, blotted and probed with anti-Flag and anti-(*Synechocystis*)FeCh antibodies. **b**) A closer comparison of migration of Ara-FeCh with and without MPP incubation from (a).

4.1.5 Fluorescence of Chl bound on the FeCh LHC domain is quenched

Synechocystis Hlips (proteins made of one LHC-helix) are reported to be very efficient quenchers of Chl fluorescence (Staleva et al., 2015; Hontani et al., 2018). Therefore, after isolating the pigmented f.FeCh using pulldown and SEC (Figure 9b), I investigated whether the fluorescence of Chl bound on FeCh is also quenched. By recording Chl fluorescence during SEC, it was apparent that the Chl molecules bound to FeCh show much weaker fluorescence when compared to 'free' Chl in detergent micelles (Chl-DDM; Figure 16). I calculated the ratios of fluorescence/absorbance of Chl-FeCh and Chl-DDM at their respective maxima (Table 1). For this calculation, I assumed an identical extinction coefficient and fluorescence constant for both Chl populations. FeCh bound Chl was emitting 85.5% fewer photons upon illumination compared to Chl in DDM micelles. Based on these data, I conclude that the fluorescence of Chl bound to FeCh is quenched, most likely by energy transfer to the nearby-bound carotenoids similarly to the situation in Hlips (Staleva et al., 2015).

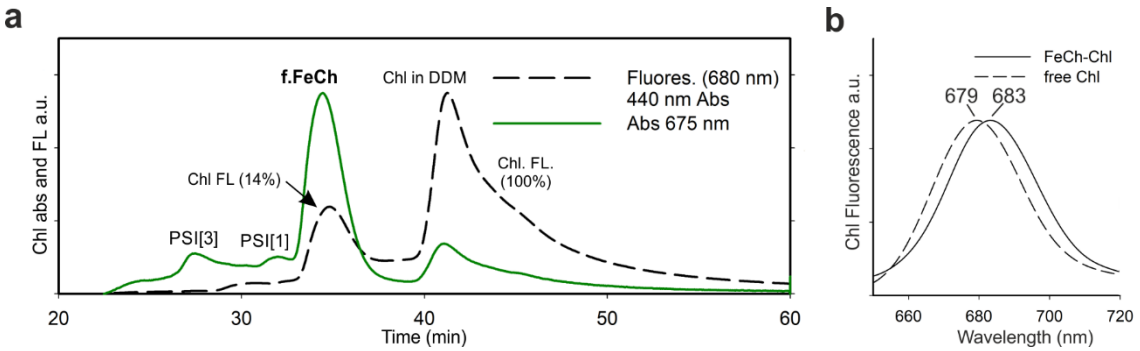

Figure 16. **Chl fluorescence is quenched in the FeCh-pigment complex. a**) SEC separation of f.FeCh purified from Synechocystis cells treated for 4 hours with MPP. Chl absorption and fluorescence were recorded by diode-array and fluorescent detectors respectively. PSI[3] and PSI[1] indicate Chl bound to traces of trimeric and monomeric PSI respectively. Numbers in parenthesis indicate Chl fluorescence yield. The efficiency of quenching was calculated from the ratio of fluorescence/absorbance at their respective maxima for Chls bound to FeCh and for Chl molecules in detergent micelles. The same extinction coefficient was assumed for both Chl populations. **b**) Fluorescence maxima of the f.FeCh-pigment complex and 'free' Chl molecules in β-DDM micelles recorded during SEC chromatography by a fluorescence detector after excitation at 440 nm.

Table 1. Calculation of relative fluorescence of Chl bound to FeCh and of Chl in DDM micelles.

	maximum	area	Chl FL/Abs	
f.FeCh-Chl complex	Chl Abs (676 nm)	1948	6.42	14.48%
	Chl FL (683 nm)	12515		
Free Chl in micelles	Chl Abs (670 nm)	789	44.33	100%
	Chl FL (679 nm)	34977		

4.1.6 Catalytic domain of the Synechocystis FeCh does not play a structural role in pigment binding

It is very likely that the pigments co-purified with f.FeCh (Figure 9b) were associated mostly with the LHC-helix, similarly to plant LHC antenna proteins (Liu et al., 2004). However, the inhibitor (bound in the active site) could have an allosteric effect on the protein inducing the binding of pigments. To exclude an allosteric effect of the FeCh inhibitor and to investigate whether the catalytic domain plays any structural role in the pigment binding, I used a previously constructed strain expressing the FeCh LHC-helix as a small separate protein (*His-C-tn*,(Sobotka et al., 2011)) placed under a strong constitutive *psbAII* promoter (Figure 4). The His-C-tn protein was expressed in the *hemH-*Δ*324* background lacking the FeCh LHC-helix and the linker domain. The *hemH-*Δ*324* mutation mimics the effect of MPP on the amount of free Chl because of the very low cellular level of the FeCh-Δ324 enzym, probably due to its proteolytic instability (Sobotka et al., 2008). Also, the FeCh-Δ324 protein cannot dimerize with the His-C-tn protein, due to the absence of the LHC-helix, thus will not ‘contaminate‘ the His-C-tn purification with the catalytic part of FeCh.

I managed to purify the His-C-tn with a combination of affinity and strong anion exchange chromatographies and observed a Chl-absorbance peak comigrating with the His-C-tn protein. Immunoblot analysis excluded that this Chl peak would originate from Chl-rich photosystems (Figure 17a). From the absorption spectrum of the purified His-C-tn (Figure 17b) it was apparent that this artificial protein also binds carotenoids, the same species as the full-length FeCh. The pigments bound on His-C-tn were identified to be Chl : β-carotene : zeaxanthin in the ratio 3 : 0.9 : 1 with a small amount of echinenone (Figure 17c). The Chl on His-C-tn was also quenched (compare fluorescence/absorbance of Chls in β-DDM micelles and Chls bound to His-C-tn; Figure 17a), same as in the full-length protein (Figure 16). Based on these data, I conclude that the catalytic domain of FeCh does not play any structural role for the pigment binding.

Figure 18 depicts a model of the observed MPP induced dimerization with Chl and carotenoid binding on the FeCh LHC-domain.

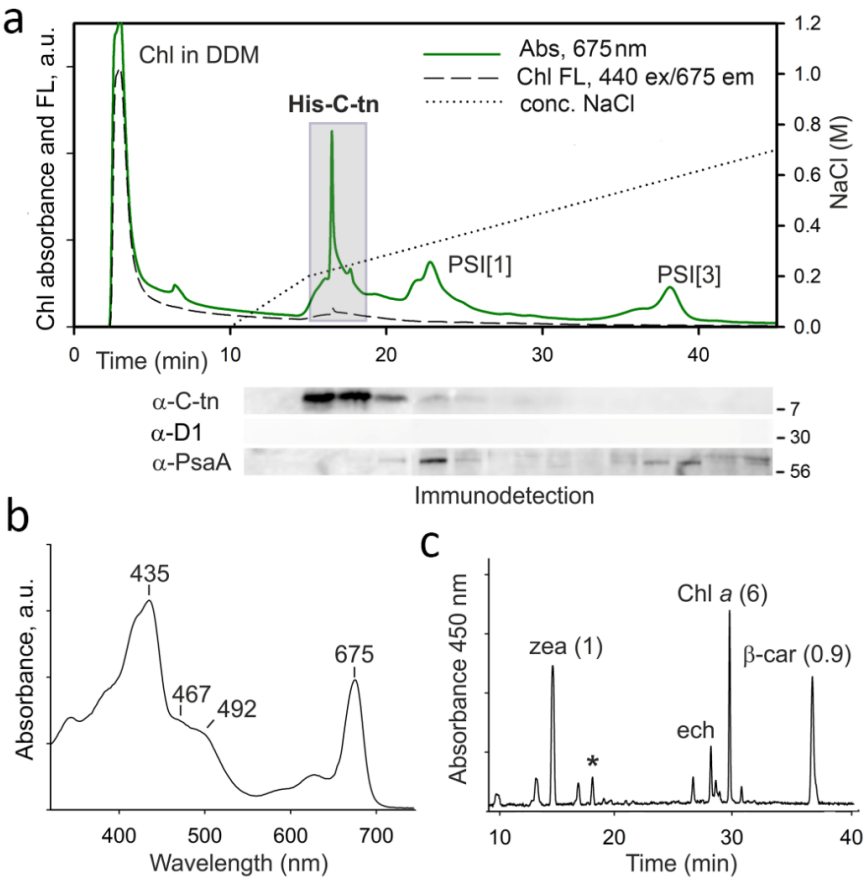

Figure 17. **The C-terminal segment of the *Synechocystis* FeCh lacking the catalytic domain (an artificial His-C-tn protein) binds pigments in a Chl-quenching configuration. a**) The His-C-tn protein expressed in the *Synechocystis hemH-*Δ*324* genetic background was isolated using affinity and anion-exchange chromatographies. Minute fractions were collected, separated by SDS-electrophoresis and the presence of His-C-tn protein was detected by antibodies raised against the FeCh C-terminus. The core PSI and PSII subunits PsaA and D1 were also immunodetected as control of purity. Fractions highlighted by the grey box were pooled and used for the analysis of pigments associated with His-C-tn. **b**) The absorption spectrum of the His-C-tn protein purified by a combination of nickel-affinity and anion-exchange chromatography as described above. **c**) The extracted pigments from the purified His-C-tn protein were separated on a C18 column; the molar stoichiometry of the major constituents is indicated (zea, zeaxanthin; ech, echinenone; β-car, beta-carotene). The unknown carotenoid (see Figure 10b) is marked by an asterisk.

The spectrum and pigment ratio of the His-C-tn-pigment complex (Figure 17 b,c) was very similar to a previously purified HliD (Hlip) from *Synechocystis* (Staleva et al., 2015). However the Hlips, apart from Chl, bound only the less polar β-carotene, FeCh

also bound zeaxanthin and other polar carotenoids (Figure 10b, 17c). Based on these data I conclude that one carotenoid binding site on the FeCh LHC-domain is preferentially occupied with a more polar carotenoid. Since Hlips were never purified completely pigment-less, and only with β-carotene, the presence of a binding site for a polar carotenoid on FeCh may explain the lower affinity to pigments compared to Hlips.

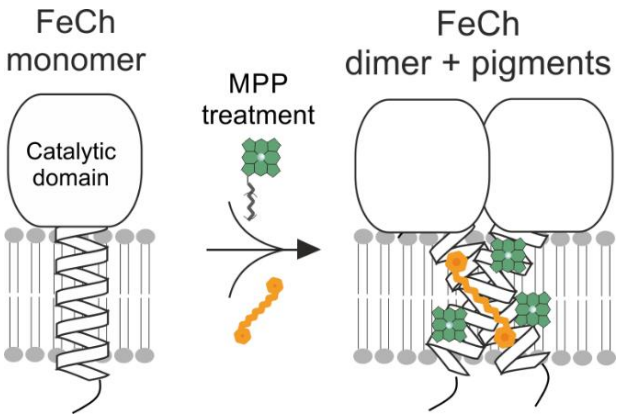

Figure 18. **Model of the observed FeCh dimerization and pigment binding**. Upon a partial FeCh inhibition by MPP, the FeCh forms a dimeric structure via its LHC-domain and binds Chl (green) and carotenoids (yellow).

4.1.7 An increased amount of free Chl in membranes results in the accumulation of His-C-tn protein

When the His-C-tn protein (C-terminal part of FeCh) was expressed in the *hemH-Δ324* background, the following pulldown resulted in a much greater yield of the co-eluted pigments (yet with the almost identical absorption spectrum) compared to the His-C-tn pulldown in *WT* background (Figure 19a). Based on my previous observation that the FeCh LHC domain binds pigments only when the membranes contain an excessive amount of free Chl (Figure 9), I expected that in the *hemH-Δ324* genetic background the His-C-tn protein binds much more pigments due to more free Chl available (Figure 19b). In analogy to full-length FeCh, most of the His-C-tn will be pigment-less if produced in WT background. To my surprise, I found, that the larger amount of pigments in the pulldown from the *hemH-Δ324* background (figure 19a) was not caused by His-C-tn binding more pigments, but by a strong accumulation of the His-C-tn protein (Figure 19c).

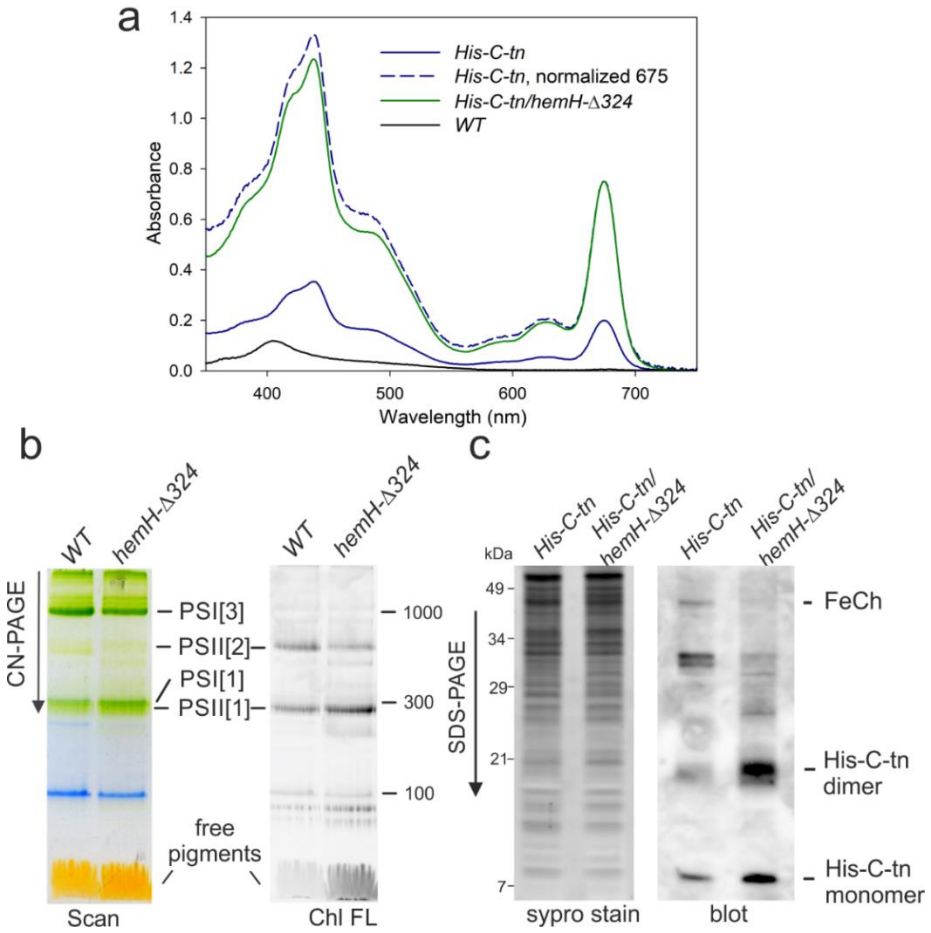

Figure 19. **The C-terminal segment of FeCh lacking the catalytic domain (an artificial His-C-tn protein) accumulates when combined with the *hemH*-Δ*324* mutation (FeCh lacking the C-tn segment)**. **a**) Solubilized membranes from the respective strains corresponding to the same amount of cells were purified on a nickel column. Absorbance spectra of the elutions were recorded. Dashed blue line denotes *His-C-tn* elution normalized to *His-C-tn/hemH-Δ324* elution (the green line) at 675 nm (Chl). **b**) Membrane fractions of the respective strains were solubilized using β-DDM and separated on a 4-12 % CN-PAGE. Separated complexes were scanned (left) and Chl fluorescence was recorded (right). Note the increased Chl FL of free Chl in the *hemH-Δ324* background. **c**) Membrane fractions of the respective strains were solubilized and separated on SDS-PAGE, stained, blotted and immunodetected with the anti-C-tn antibody. Note the larger amount of His-C-tn in the *hemH-Δ324* background.

The observation of the higher level of the His-C-tn protein in the *hemH-Δ324* background could be indeed related to the physiological role of Chl binding on FeCh; the His-C-tn protein can be either more synthesized or less degraded due to a larger amount of free Chl (Figure 19c) or due to the lack of the full-length FeCh. To distinguish between these possibilities, I measured whether the MPP treatment leads to the accumulation of the His-C-tn protein in the WT background. Figure 20a shows that after 48 h incubation

with 275 nM MPP the amount of His-C-tn clearly increased in the cell, suggesting that the low FeCh activity is responsible for the His-C-tn accumulation rather than the truncation of FeCh in the *hemH-Δ324* mutant. In order to assess the rate of His-C-tn synthesis I used protein radiolabeling. After a 30 min pulse with [^{35}S](Cys+Met) it did however not appear that the MPP treatment accelerated the synthesis of His-C-tn (Figure 20b).

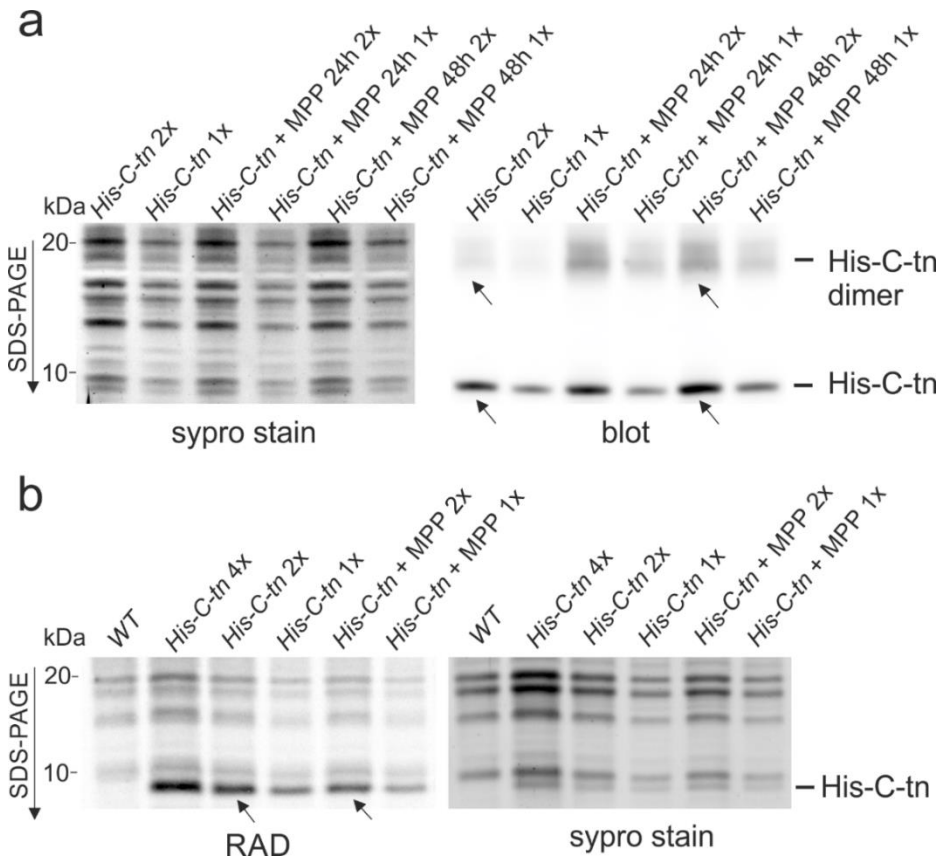

Figure 20. **The C-terminal segment of FeCh lacking the catalytic domain (an artificial His-C-tn protein) accumulates after inhibition of FeCh but its synthesis is not enhanced**. **a**) Membrane fractions from *His-C-tn* and *His-C-tn* cells treated with MPP (FeCh inhibitor) were solubilized, separated by SDS-PAGE, stained, blotted and probed with the anti-C-tn antibody. Note an increase in the His-C-tn amount after the inhibition of FeCh. **b)** WT, *His-C-tn*, and *His-C-tn* treated with MPP for 48 h were pulse-labeled for 30 min [^{35}S](Cys+Met). Isolated membrane fractions were solubilized, separated by SDS-PAGE, blotted and the radio-emission (RAD) was recorded. No significant enhancing of the His-C-tn labeling was detected after FeCh inhibition.

Based on these data, I conclude that the increased amount of free Chl in the membranes leads to the accumulation of His-C-tn, and I speculate that the pigment binding on the His-C-tn protein prolongs its half-life, likely by slowing down its proteolytic degradation.

4.2 The role of FeCh LHC-helix in protein-protein interactions and in localization of FeCh

4.2.1 The LHC domain localizes FeCh to Slr0483(CurT)

The *Synechocytis* FeCh appears to be mostly monomeric, at least during standard growth conditions (Figure 14). The question is whether the FeCh LHC-helix also has a function when the FeCh is monomeric. As long as the FeCh is pigment-less, irrespective of whether monomeric or dimeric, in theory, the amino acid side chains of the LHC-helix, by forming the surface of the helix, should determine the localization of FeCh within the membrane system via interactions with other protein(s).

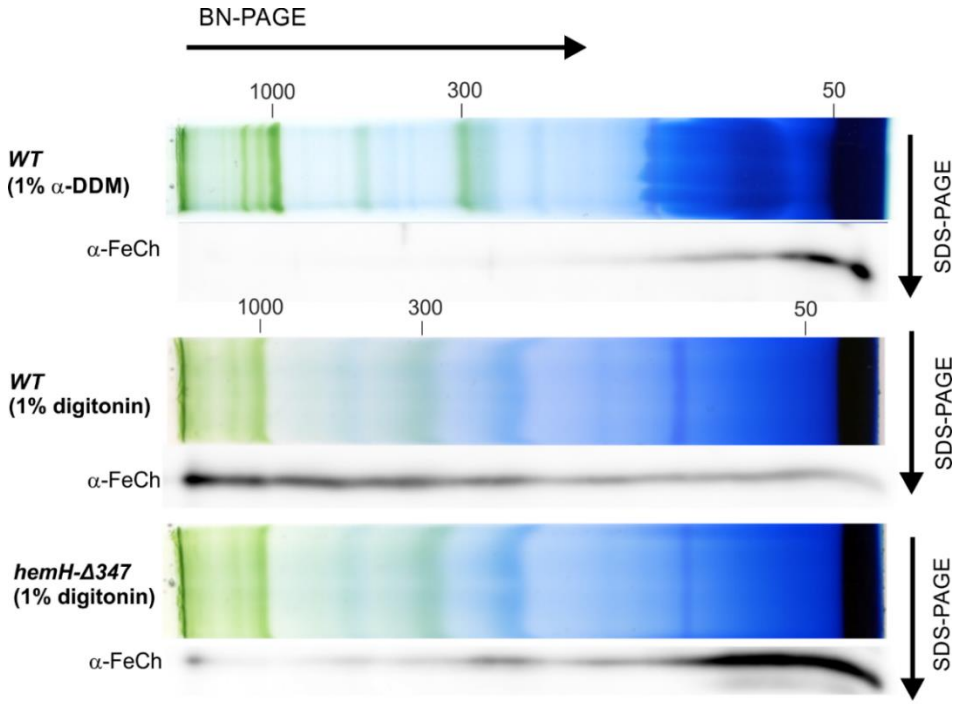

Figure 21. **Solubilization of *Synechocystis* membrane proteins with digitonin preserves the occurrence of FeCh in high mass complexes**. Membrane fractions of *WT* and *hemH-Δ347* were solubilized either with α-DDM or digitonin and resulting complexes separated using 2D BN/SDS-PAGE, blotted and the FeCh immunodetected. Note, that after digitonin solubilization, the full-length FeCh migrates mostly in the upper part of the gel corresponding to large complexes, whereas the truncated FeCh-Δ347 migrates as a low-mass protein.

However, after solubilizing the cell membranes with β-DDM, the f.FeCh is not co-purified with any interaction protein partners that would be detectable on a stained SDS-gel (Figure 12). Therefore, I decided to experiment with two other detergents - n-dodecyl α-D-maltoside (α-DDM) (Pagliano et al., 2012) and digitonin, generally considered as milder than β-DDM. I used 2D BN/SDS-PAGE followed with

immunodetection to judge the "nativeness" of both detergents (Figure 21). The solubilization with α-DDM seemed to have a similar effect on the migration of FeCh as β-DDM. On the other hand, the solubilization with digitonin produced a smeared signal of FeCh, however, it was dominant in the upper part of the gel corresponding larger protein complexes. On contrary, the signal of the FeCh lacking the LHC-helix (FeCh-Δ347) was dominantly in the region of low-mass proteins/small complexes after digitonin solubilization (Figure 21), which suggests a disruption of protein-protein interactions mediated by the FeCh LHC-helix.

In order to obtain more information about FeCh interactions mediated by the LHC-helix, I purified f.FeCh and f.FeCh-Δ347 enzymes from membranes solubilized with digitonin. The f.FeCh elution, apart from the f.FeCh itself, contained three other prominent proteins. MS analysis of these three bands (performed by Peter Koník from our laboratory) revealed them as Slr0483, Sll1106 and the catalytic core of ATP synthase (Figure 22). The f.FeCh-Δ347 elution contained much fewer proteins overall (which corresponds to the BN-PAGE analysis (Figure 21). The catalytic core of ATP synthase was also present in the control, albeit in a much lower amount (Figure 22). Sll1106 is a protein with an unknown function. The Slr0483 protein, which is also called CurT, was shown to induce membrane curvature (Heinz et al., 2016) and is potentially involved in the formation of putative membrane compartments termed thylakoid biogenesis centers. Importantly, the CurT protein seemed to be completely missing in the f.FeCh-Δ347 elution (Figure 22), suggesting that the Slr0483 is specifically interacting with the LHC-helix of FeCh.

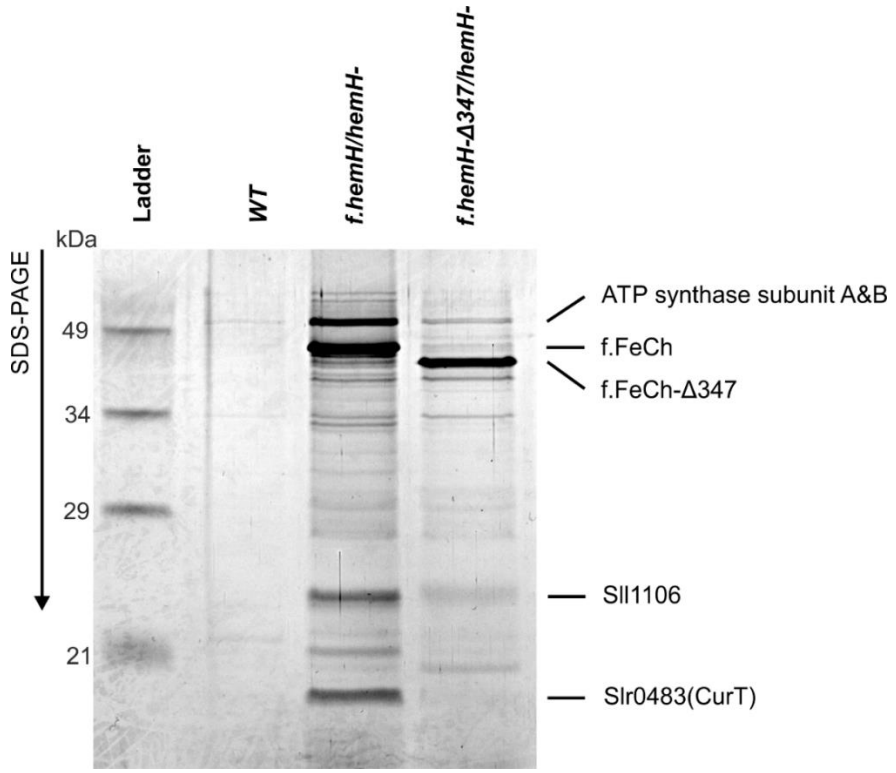

Figure 22. **CurT is co-purified with f.FeCh but not with the truncated f.FeCh-Δ347**. Isolated membranes from *WT*, *f.hemH/hemH-* and *f.hemH-Δ347/hemH-* cells were solubilized with digitonin and the f.FeCh and f.FeCh-Δ347 enzymes purified on an anti-Flag resin. Obtained elutions were separated by SDS-PAGE and stained with CBB. Indicated protein bands were identified using LC-MS.

4.2.2 FeCh LHC-helix is in close proximity of the C-terminal TM helix of CurT in vivo

As the CurT protein was co-purified with f.FeCh but it appeared absent in the f.FeCh-Δ347 pulldown (Figure 22), I further analyzed the f.FeCh-CurT interaction using chemical cross-linking combined with high-resolution MS. For a properly controlled crosslinking study a mixture of a crosslinker with a heavy isotope of itself in a 1:1 ratio is frequently used. The laboratory, where I learned to analyze crosslinks (group of Marc Nowaczyk, Department of Plant Biochemistry, University of Bochum, Germany), is using bis(sulfosuccinimidyl)suberate (BS3) - a 11Å long crosslinker with light and heavy isotope variants differing by 12 Da. I tested BS3 at two different concentrations while keeping the protein concentration at 550 μg/mL (Figure 23). 4 mM concentration of BS3 produced a decent crosslinking signal, while also leaving a large portion of FeCh uncrosslinked with other proteins, thus lowering the chance of producing false positive

crosslinks. I decided to use the 4 mM BS3 concentration for MS2 analysis of the crosslinked sample.

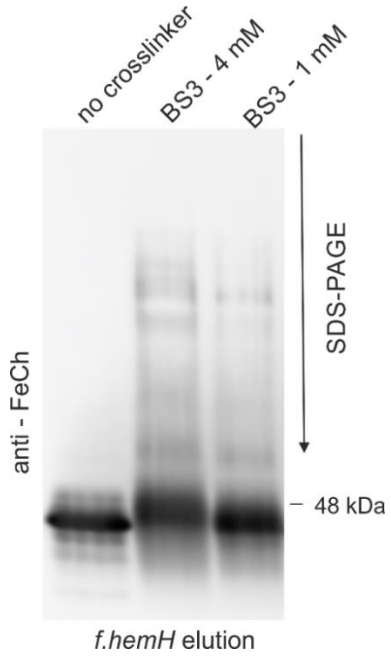

Figure 23. Validation of BS3 crosslinker on the f.FeCh pulldown. Membrane fraction from the *f.hemH/ΔhemH* cells was solubilized with digitonin and the f.FeCh protein purified. The obtained f.FeCh eluate (550 μg protein/mL) was first crosslinked with BS3 and then separated using SDS-PAGE, blotted and the f.FeCh protein was immunodetected. Signals above 48 kDa should result from FeCh crosslinked with itself and/or with other proteins.

Processing and analysis of MS2 data obtained from the f.FeCh pulldown crosslinked with BS3 revealed a crosslink candidate between the FeCh linker above the cytosolic end of the LHC-helix (amino-acids K337-E345) and the cytosolic end of the C-terminal TM helix of Slr0483 (Y125-K131; Figure 24). I processed the MS2 data using the StavroX software (Gotze et al., 2012) and to minimize false-positive crosslink candidates I included these five parameters in the analysis:

1) Identical crosslink with the same charge needs to be observed with both the heavy and light versions of the crosslinker (Figure 24 A – light; B – heavy crosslinker).
2) Candidate spectra of both light and heavy crosslinkers must have fragments containing the crosslinker molecule and these fragments must display correct m/z difference (circled in Figure 24 A, B; uncharged m/z difference between light and heavy BS3 isoforms is 12 Da)
3) Precursor peptides must have a similar retention time (Table 2)

4) The exact same crosslink must be detectable in biological and technical replicates (Table 2, appendix 8.2)
5) Crosslink must be sterically possible (Figure 25e)

Table 2. **Overview of the crosslink candidates between peptide K337-E345 of FeCh and peptide Y125-K131 of Slr0483**. This crosslink was found in biological (BR) and technical (TR) replicates; MS2 spectra of the samples are displayed in Figure 24 (BR-1 TR-1) and appendix 8.2 (other 3 replicates). Deuter = deuterated (heavy) form of BS3. Deviation = difference between the calculated and measured mass of the precursor ion in ppm.

FeCh (337-345)-BS^3-(125-131) Slr0483				
		non-fragmented precursor		
		charge; m/z	retention time (s)	deviation (ppm)
BR-1 TR-1	BS3	3 ; 748.376	9643	-4.61
	BS3 (deuter)	3 ; 752.401	9480	-4.62
BR-1 TR-2	BS3	3 ; 748.377	9721	-3.47
	BS3 (deuter)	3 ; 752.402	9480	-3.73
BR-2 TR-1	BS3	3 ; 748.376	10390	-4.94
	BS3 (deuter)	3 ; 752.401	10462	-4.54
BR-2 TR-2	BS3	3 ; 748.376	10439	-4.29
	BS3 (deuter)	3 ; 752.401	10192	-4.7

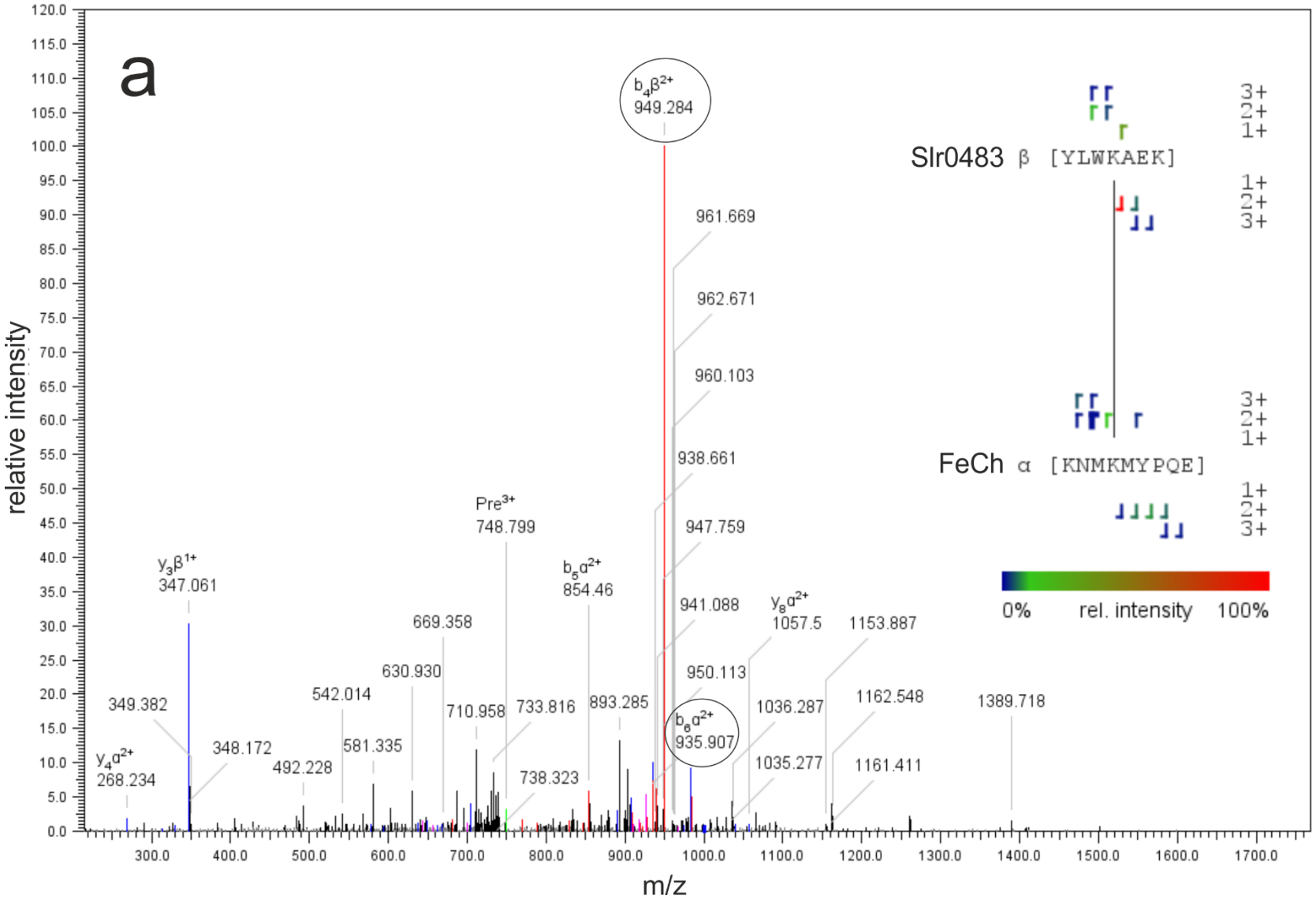
a
relative intensity
m/z
$b_4\beta^{2+}$ 949.284
961.669
962.671
960.103
938.661
947.759
941.088
950.113
$b_8\alpha^{2+}$ 935.907
Pre^{3+} 748.799
$b_5\alpha^{2+}$ 854.46
$y_3\beta^{1+}$ 347.061
$y_8\alpha^{2+}$ 1057.5
1153.887
669.358
630.930
542.014
349.382
710.958
733.816
893.285
1036.287
1162.548
1389.718
348.172
581.335
492.228
$y_4\alpha^{2+}$ 268.234
1035.277
1161.411
738.323
Slr0483 β [YLWKAEK]
FeCh α [KNMKMYPQE]
3+
2+
1+
0%
rel. intensity
100%

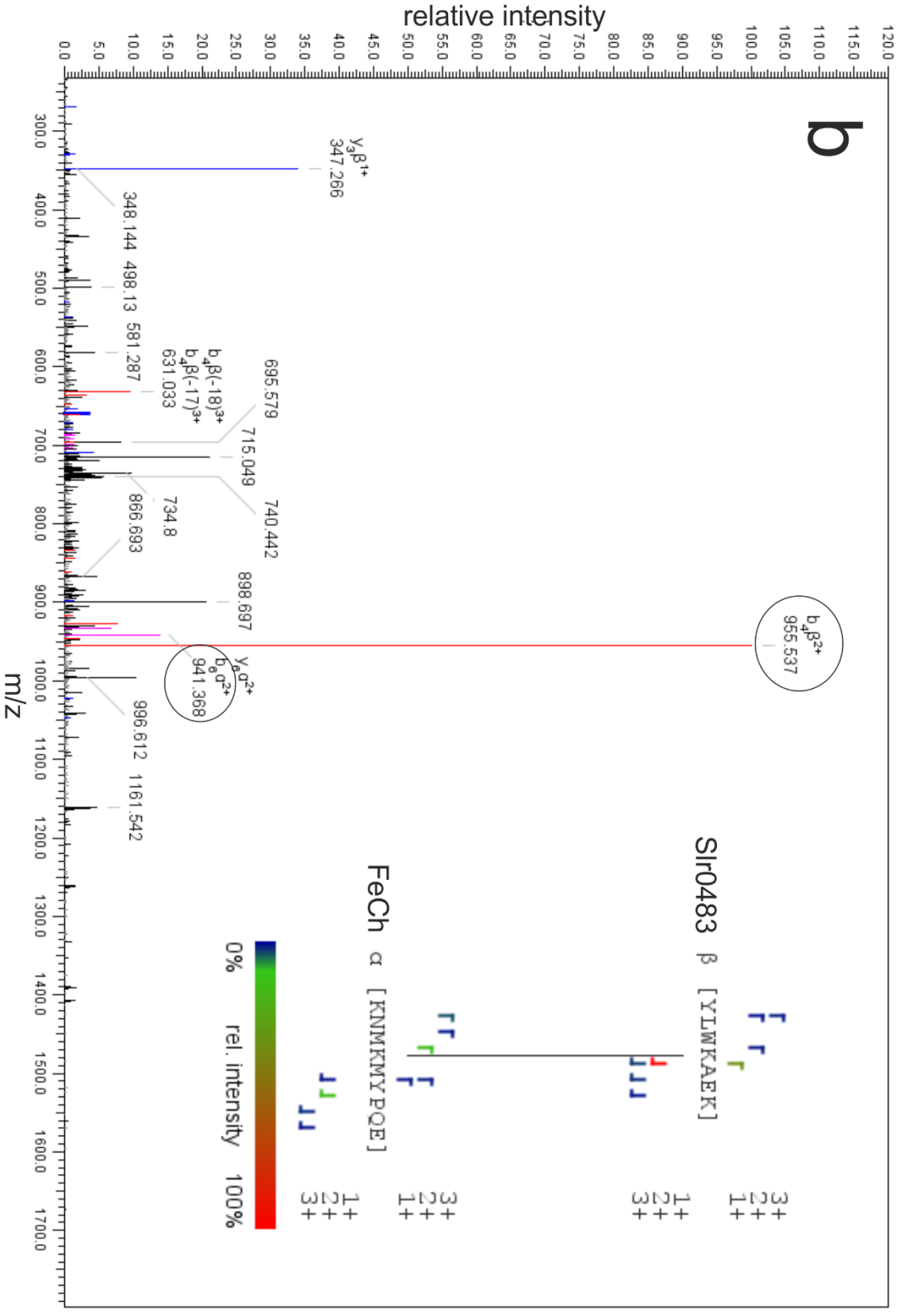

Figure 24. MS2 fragmentation spectra of the FeCh 337-345 - Slr0483 125-131 crosslink candidate (BR-1,TR-1). Membrane fraction from the *f.hemH*/Δ*hemH* cells was solubilized with digitonin and the f.FeCh protein purified by affinity

chromatography. The obtained f.FeCh eluate was crosslinked with isotopically coded BS3, trypsinated and analyzed by MS2. Two major ions ($b_4\beta$ and $b_6\alpha$) containing the crosslinker are circled in both spectra. **a)** MS2 fragmentation pattern containing the light BS3 variant. **b**) MS2 fragmentation pattern containing the heavy BS3 variant.

The FeCh 337-345 region is a part of the linker close to the cytoplasmic side of the LHC-helix (Figure 25e – in blue). Based on a topology analysis of the Slr0483 protein (Figure 25a) the 125-131 region is the cytoplasmic end of the C-terminal TM helix (Figure 25e – in blue). Therefore, this crosslink is sterically not only possible but both cross-linked peptides are close to the cytoplasmic surface of the membrane. Based on the length of the BS3 crosslinker (11 Å), I conclude that the FeCh LHC-helix is localized in the vicinity of the C-terminal TM helix of the Slr0483 protein, possibly the amino acid side chains of the helices are in direct contact.

CurT protein is conserved in cyanobacteria and also in plants and algae (Figure 25c). Interestingly, the C-terminal TM helix of CurT contains a charged arginine that is conserved in both prokaryotic and eukaryotic photosynthetic organisms (Figure 25c), similarly to the charged amino acids in the FeCh LHC-motif. When TM helices of FeCh and Slr0483 are aligned with respect to the membrane (Figure 25e), it is obvious that the observed crosslink is sterically possible. However, it is also apparent that the conserved charged amino acids of both helices are in a correct distance to form an ionic bond (Figure 25e), which could stabilize the interaction between FeCh and Slr0483; similarly to the stabilization of central pair of helices in LHCII (Figure 25d)(Liu et al., 2004).

Slr0483 (CurT) is reported to be essential for the formation of thylakoid convergence zones both in plants and cyanobacteria (Armbruster et al., 2013; Heinz et al., 2016), where the putative PSII biogenesis centers might be located. Based on my data (Figures 22, 24) I propose that the *Synechocystis* FeCh is, due to its LHC-helix, preferentially localized at these putative PSII biogenesis centers; at least when the FeCh is monomeric and thus pigment-free.

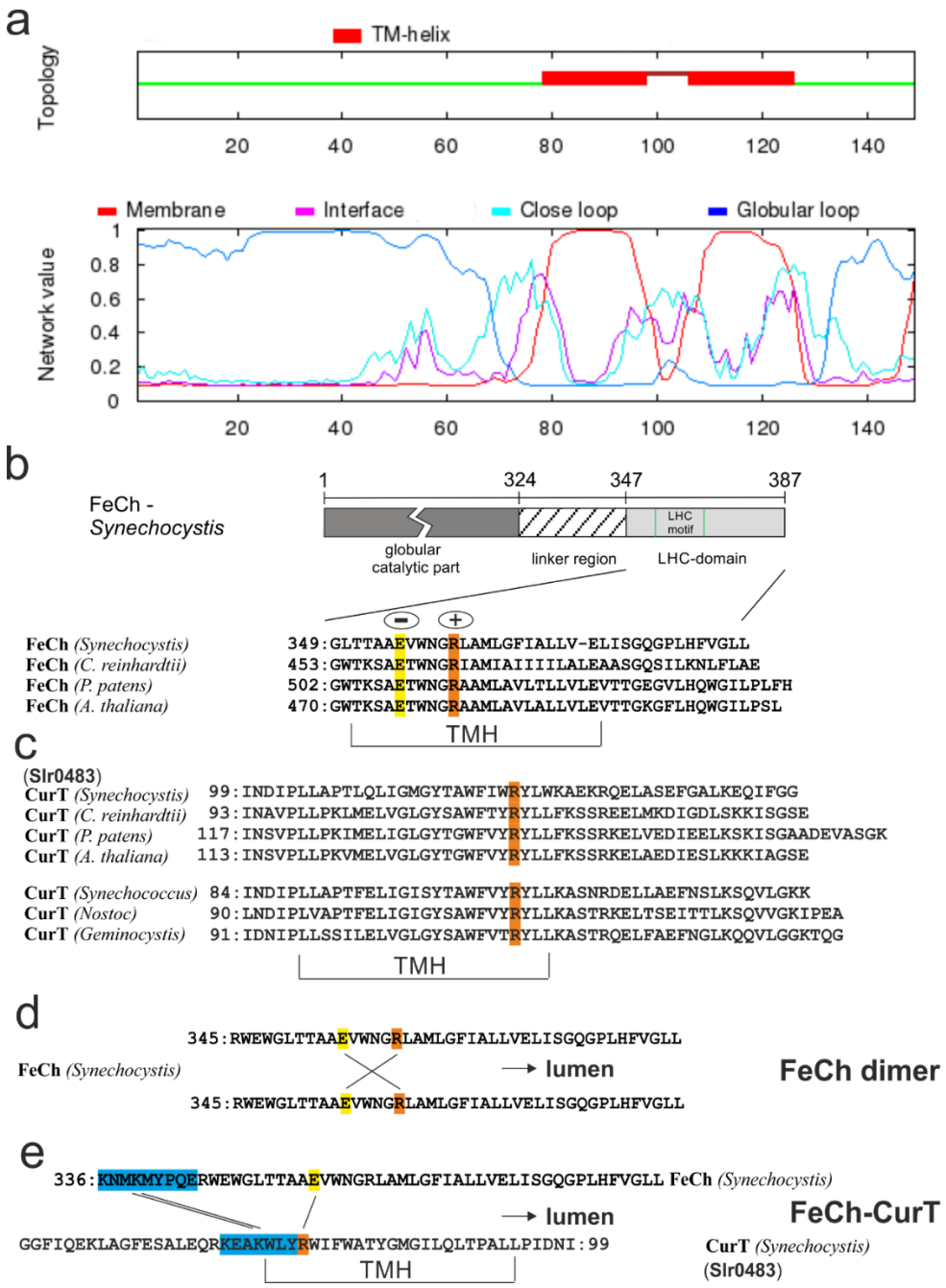

Figure 25. **The interaction between the FeCh LHC-helix and the CurT TM helix may be stabilized by an intramembrane ionic bond. a**) The predicted topology of Slr0483 (CurT) from *Synechocystis* using OCTOPUS (Viklund and Elofsson, 2008) showing two TM helices. **b**) Conservation of the charged amino acids within the LHC-helix of FeCh. **c**) Conservation of the charged amino acid within the C-terminal TM helix of Slr0483 (CurT) from photosynthetic organisms. **d**) Scheme of FeCh LHC-helix dimer based on the crystal structure of LHC antennas (Wei et al., 2016). Intramembrane ionic bonds between Glu and Arg are indicated by the solid line. **e**) Proposed interaction between FeCh LHC-helix and CurT C-terminal TM helix. Blue denotes identified crosslink (see fig. 24). The solid line indicates a possible ionic bond between CurT and FeCh TM helices.

The StavroX crosslinking software (Gotze et al., 2012) uses a decoy analysis that employs reversed FASTA sequences to detect fake candidates (impossible crosslink candidates). By using these decoy candidates a *p*-value for each real crosslink candidate is estimated. It should be noted, that to get crosslink candidates which scored below a 0.05 *p*-value, I had to select a semi-random digest in the data processing because when selecting only tryptic digest, the StavroX software did not report any crosslink candidates with a *p*-value below 0.05. The reported crosslinked peptides between Slr0483 (122-WR|YLWKAEK|RQ) and FeCh (334-PK|KNMKMYPQE|RW; Figure 24) have three tryptic cleavages. However, the cleavage between FeCh 345(E) and 346(R) is on the N-terminus of arginine, which is a non-tryptic cleavage; only the side C-terminal to arginine should be tryptic. According to (Olsen et al., 2004) trypsin cleaves exclusively C-terminus of lysine and arginine; however since then at least two studies argue that the commercially available trypsins are not that specific (Burkhart et al., 2012; Fang et al., 2015). The authors show, that, depending on the concentration of to-be digested proteins, the ratio of protein : trypsin and also on the particular trypsin supplier, nonspecific cleavages can vary from 2 to 30% of all cleavages. Therefore, I conclude that the digestion in my samples was most likely not 100% tryptic.

From the limited time I spent dealing with chemical *in vitro* crosslinking of proteins, I concluded that one can never be very sure that the data measured by the MS and evaluated by the software as crosslink candidates are not false positive due to a possible ambiguous assignment; particularly if the sample contained many different proteins (Cormann et al., 2016). In my opinion, ideally crosslinking should be used on very pure samples and only when one is sure that two proteins interact. Further, it is possible that the interaction I observed between FeCh and CurT is artificially generated only after membrane solubilization by digitonin because the addition of detergent induces the formation of a new lipid-protein interaction equilibrium. A reciprocal purification of FeCh using a Flag-Slr0483 should be performed and the interaction between FeCh and Slr0483 should ideally be confirmed using another method that does not employ digitonin solubilization. However, the presence of a conserved positive charge within the CurT C-terminal TM helix in the binding distance of the negative Glu in the FeCh LHC motif is a positive indication of this interaction. It would also be interesting to know whether the CurT gets purified with f.FeCh if the conserved Arg-124 of the CurT got replaced with a non-polar amino acid.

4.2.3 Localization of Synechocystis FeCh by its fusion with a Citrine fluorescence protein

The rationale behind the visualization of FeCh using a fluorescence protein tag was to confirm whether the FeCh is preferentially localized to a certain (CurT-rich) membrane region(s), as suggested by pulldown (Figure 22) and cross-linking data (Figure 24). Therefore, I constructed a *Synechocystis* mutant (*citrine-hemH*) expressing a fusion protein of Citrine (yellow emission) and FeCh from the original *hemH* locus (see methods). Figure 26a shows that the Citrine-FeCh is synthesized in the mutant and this enzyme is apparently active, otherwise such mutation would be lethal.

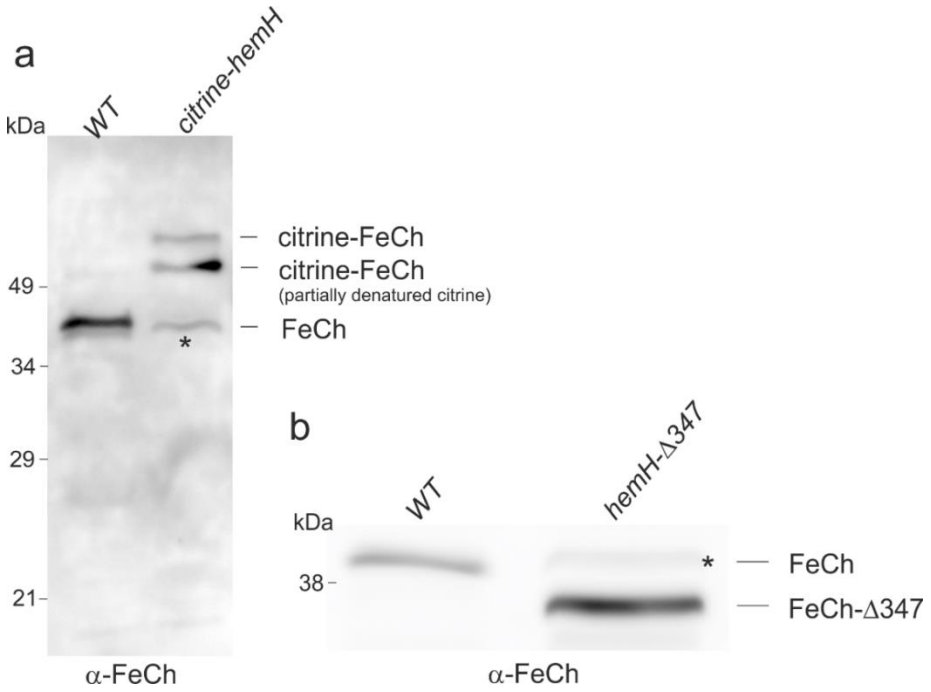

Figure 26. **Validation of the c*itrine-hemH* strain**. **a**) Membrane proteins isolated from *WT* and *citrine-hemH* cells were separated on a 16-20 % SDS-PAGE, blotted, and probed with the anti-FeCh antibody. The asterisk indicates an unspecific cross-reaction with the FeCh antibody. **b**) Membrane proteins from *WT* and *hemH-Δ347* strain were separated on a 16-20 % acrylamide gel, blotted, and probed with the anti-FeCh antibody. The asterisk denotes a cross-reaction of the FeCh antibody with a protein, which has a similar migration rate as FeCh.

I detected also a band close to the size of non-tagged FeCh in the *citrine-hemH* strain (Figure 26a), which would suggest that some of the Citrine is being cleaved of the Citrine-FeCh. However, using the *hemH-Δ347* strain, which completely lacks the full-length FeCh, I demonstrated that the FeCh antibody used weakly cross-reacts with another protein with a similar mass as FeCh (Figure 26b). It is therefore very likely that

the signal with the size of FeCh in the *citrine-hemH* strain (Figure 26a) is an unspecific cross-reaction. The formation of the double band, as observed for Citrine-FeCh (Figure 26a), is typical for fluorescent proteins, which, unless heated, denature only partly due to their stable conformation. A partially denatured Citrine-FeCh migrates faster.

Inspection of the exponentially grown *citrine-hemH* cells by a confocal microscope showed a detectable emission of the Citrine-FeCh protein after excitation with a 514 nm laser. 2D fluorescence scan of *WT* and *citrine-hemH* cells suggests that the Citrine-FeCh is not uniformly distributed throughout the thylakoid membranes but rather preferentially localized to spots or domains (Figure 27). However, although the measured emission has a maximum expected for Citrine (529 nm,(Griesbeck et al., 2001)), the average fluorescence of c*itrine-hemH* cells in this region was only about twice as strong as the background fluorescence of WT, as is apparent from the single-photon counter (detector set at maximum sensitivity; Figure 28). The emission of Citrine-FeCh is very weak compared to around 50 times higher signal detected in *Synechocystis* for some abundant proteins fused with fluorescent tags, *e.g*. PsaF-YFP (Straskova et al., 2018). Therefore, no clear conclusion about the Citrine-FeCh localization can be made with certainty. The presented data from the confocal microscope were recorded and processed by Dr. Grzegorz Konert from the Laboratory of photosynthesis, Institute of Microbiology, Třeboň.

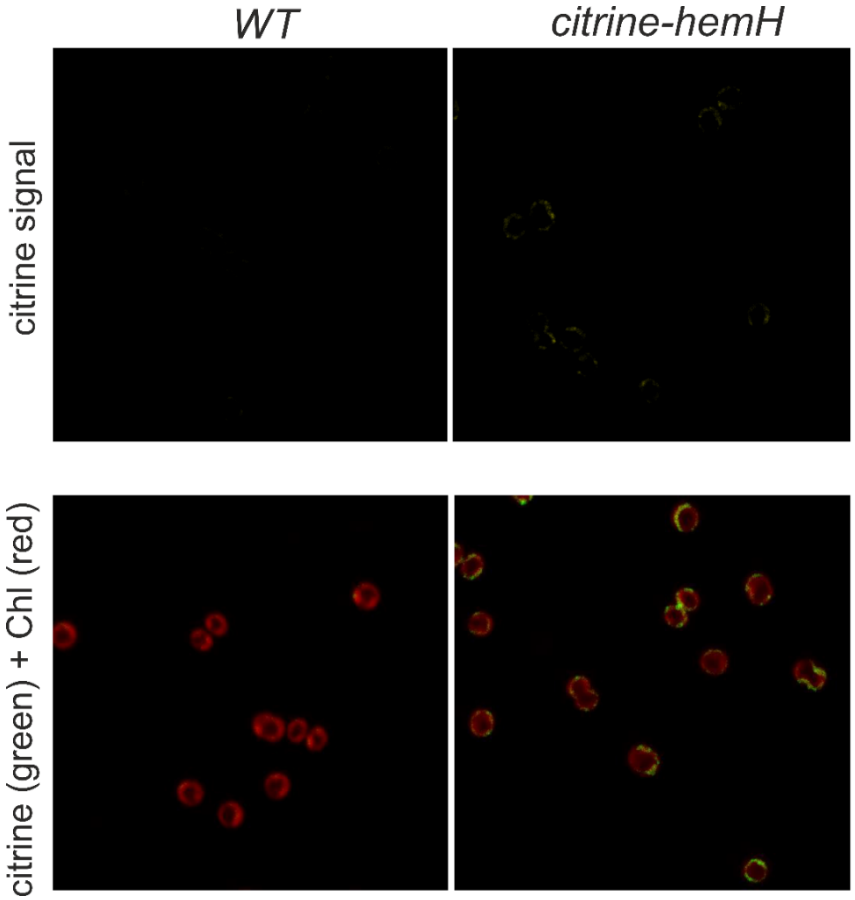

Figure 27. **Citrine-FeCh protein is not uniformly distributed in the thylakoid membranes**. Fluorescence emission of Citrine at 526-562 nm (514 nm exc.) and Chl fluorescence at 695-758 nm (488 exc.) were measured by confocal microscopy in *WT* and *citrine-hemH* cells.

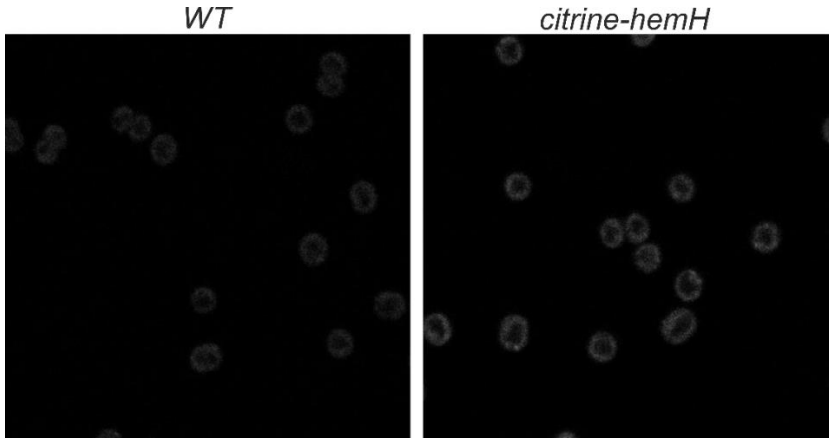

Figure 28.: **Single-photon counter (detector set at maximum sensitivity) at the range of Citrine emission (526-562 nm) of *WT* and c*itrine-hemH* strains.** Cells were excited at 514 nm. The signal in *WT* strain originates from the background fluorescence of the cell.

I also constructed a strain expressing mTFP-FeCh fusion protein; however, the emission of mTFP observed in confocal microscope was even weaker than for the Citrine-FeCh. Furthermore, I tried to determine the localization of FeCh in the cell using fluorescence immunolabeling, employing a variety of primary antibodies against FeCh coupled with fluorescently labeled secondary antibody. However, using this approach I detected no positive signal at all. I conclude that *Synechocystis* FeCh is likely a very low abundant enzyme, thus not well suited for fluorescent localization.

4.3 The physiological role of the FeCh LHC motif

4.3.1 The C-terminal helix of FeCh is essential under cold/light stress

Initially, I tested whether I can reproduce the high-light (300 μE) growth retardation phenotype reported previously for the *hemH*-Δ*347* strain (missing the C-terminal FeCh LHC-helix) (Sobotka et al., 2011). However, the identical mutation in the *Synechocystis* GT-P background, which is now considered to be "genetically healthy" (Tichy et al., 2016), and is now used to investigate mutations in our laboratory, the *hemH*-Δ*347* mutant did not have a growth problem even under very high light (1500 μE) if grown under 28 °C (not shown).

Based on published data, which show that the levels of tetrapyrrole metabolites are dependent on the activity of FeCh both in plants and cyanobacteria (Papenbrock et al., 2001; Sobotka et al., 2008) I hypothesized, that under certain conditions the FeCh LHC-helix modulates the activity of FeCh. If my hypothesis would be valid, a difference in the tetrapyrrole levels should be detectable in the *hemH*-Δ*347* mutant under appropriate conditions because as I described earlier, the FeCh-Δ347 protein cannot bind Chl (Figure 14). However, I tested a lot of different stress conditions (*e.g.* high light, fluctuating light, high/low temperature, nitrogen depletion/repletion, iron depletion, darkness) and every time the tetrapyrrole metabolites adjusted exactly the same way in the mutant as in the control (not shown).

Since the FeCh LHC motif is conserved in the whole green lineage from cyanobacteria to higher plants (Figure 3), it should play an important role in the cell. I, therefore, started thinking that maybe a certain combination of stresses is necessary to observe a phenotype. I designed an experiment where I adjusted one of three parameters every 4 hours (light intensity, temperature and nitrogen availability by changing the growth medium. After three days I noticed a difference in color between *WTzeo* and *hemH*-Δ*347*. I followed by removing the condition variability one by one until I found

that lowered temperature (28 -> 18 °C) followed by increased light (40 -> 600 μE) is enough to practically bleach all Chl in the mutant during the first 20 hours (Figure 29).

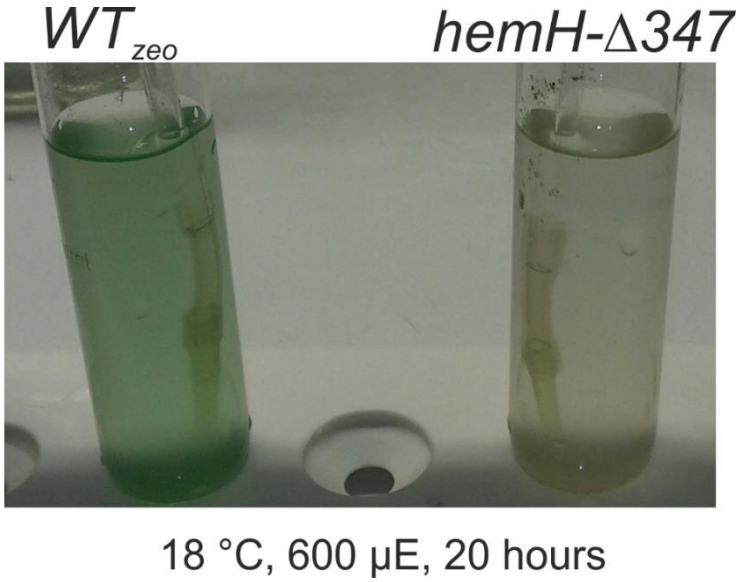

Figure 29. **The FeCh LHC-helix is essential under a combination of cold and light stress**. *WT$_{zeo}$* and *hemH-Δ347* strains were transferred from 28 °C to 18 °C, after one hour the light intensity was increased from 30 to 600 μE. The *hemH-Δ347* mutant lost most of its Chl during 20 hours of the stress.

4.3.2 Substitution of the conserved Glu(356) and Asn(359) of the FeCh LHC motif slows down the adaptation to cold/light stress

The *hemH-Δ347* mutant is lacking the last 40 C-terminal amino-acids (LHC-helix; Figure 30a). I had another FeCh mutant available, the *hemH-ΔChl* (ΔChl - mutated Chl-binding residues), which has two conserved charged amino acids of the LHC motif Glu(356) and Asn(359) replaced by non-polar amino acids Ala and Gly, respectively (see strain construction). The homologous side-chains of Glu(356) and Asn(359) in LHCII antennas coordinate Chl and both these residues also stabilize the structure of LHCII by forming ion pairs between the two central helices (Figure 25d) (Standfuss et al., 2005; Wei et al., 2016)). I found that the disruption of these two amino acids impaired the MPP induced dimerization of the FeCh enzyme (Figure 30b); similarly to the deletion of the whole FeCh LHC-helix (Figure 14). Importantly, the *hemH-ΔChl* mutation also caused the same phenotype as the deletion of the whole helix (Figure 30a). Note that when *hemH-ΔChl* grew as a biofilm on an agar plate, much lower light intensity (30 uE) was sufficient to trigger a growth defect when combined with sub-optimal temperature (Figure 30a). Light intensity of about 100 μE is minimal to observe a growth defect (Figure 32), in

liquid cultures, probably due to shading. These results show that at least one of the two conserved charged intra-membrane amino acids in the LHC helix (Glu and Asn) is essential under cold/light stress.

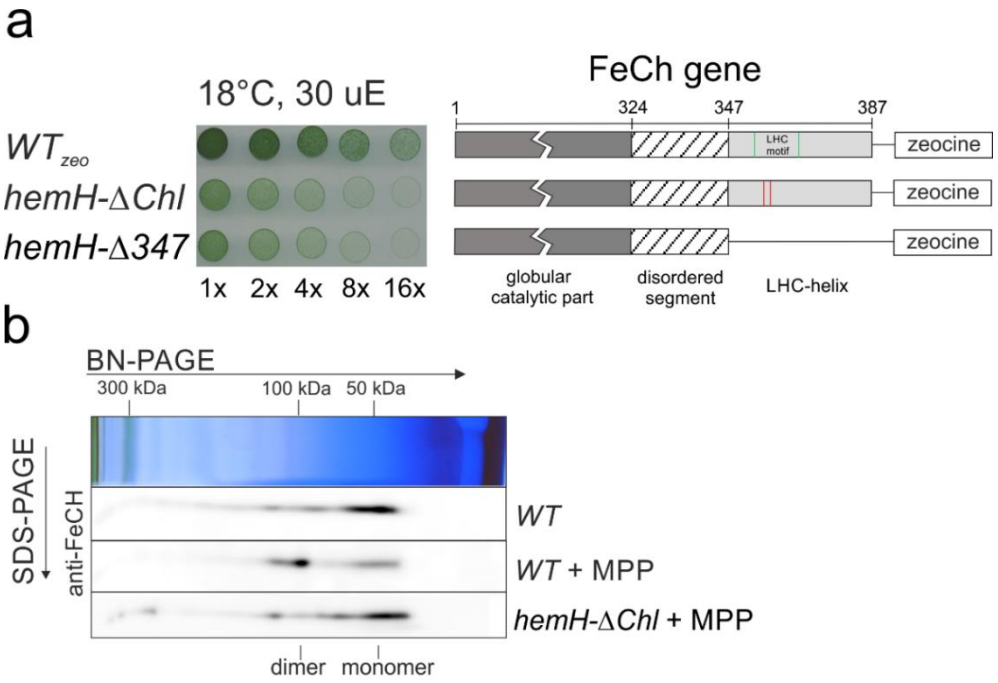

Figure 30. ***hemH-ΔChl*** **(mutant with disrupted Chl binding amino-acids) displays the same growth retardation as** ***hemH-Δ347*** **(missing the whole LHC-helix). a**) *WT*$_{zeo}$, *hemH-ΔChl* and *hemH-Δ347* strains were grown from identical optical density on BG11 agar plates at indicated dilutions under cold/light stress. **b**) Membrane fractions from indicated strains were solubilized and separated on 2D BN-PAGE, blotted and probed by the anti-FeCh antibody. Only slices of the western blot membrane are displayed. The expected positions of FeCh monomer and dimer are indicated. Note that FeCh-ΔChl does not form a dimer after MPP treatment. In the FeCh-ΔChl protein the Glu(356) and Asn(359) in Chl-binding motif are replaced by Ala and Gly, respectively.

It is well known that *Synechocystis* cells can relatively quickly spontaneously mutate if exposed to a selection pressure (Tichy et al., 2016). To verify that the *hemH-ΔChl* mutation is solely responsible for the observed phenotype I constructed *hemH-ΔChl/Chl*$^{+}$ strain, where I reintroduced the LHC-helix to its original sequence and, as the zeocine resistance was replaced by kanamycin, I constructed also WT$_{km}$ strain as a control for the *hemH-ΔChl/Chl*$^{+}$ strain (see strain construction). Reintroduction of Glu and Asp residues back into the FeCh LHC motif restored the growth under stress conditions (Figure 31).

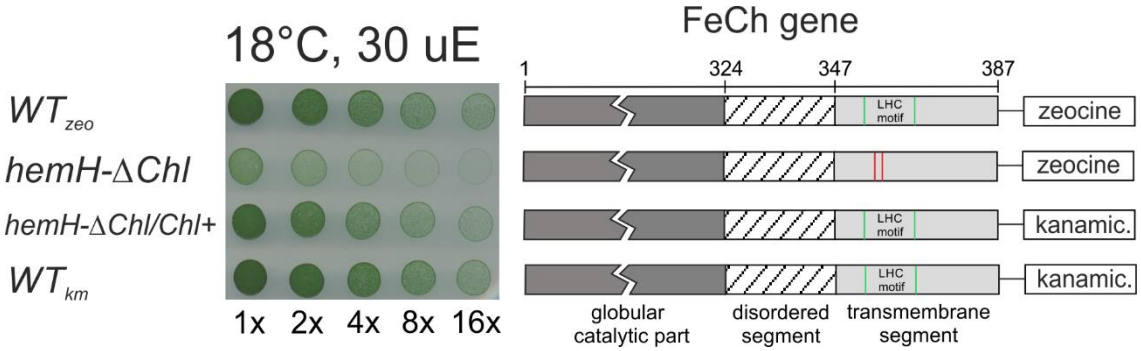

Figure 31. **Complementation control of the *hemH*-Δ*Chl* strain**. Displayed strains were grown from the identical optical density on BG-11 agar plates at indicated dilutions. *HemH*-Δ*Chl* protein has the Chl binding amino-acids Glu(356) and Asn(359) replaced by Ala and Gly respectively. *HemH*-Δ*Chl/Chl*$^{+}$ strain has the Glu(356) and Asn(359) reintroduced back into the LHC motif.

To prevent pleiotropic effects of drastic photooxidation of the mutant under 18 °C and 600 μE (Figure 29) I decreased light intensity from 600 μE to 150 μE. This resulted in a much milder phenotype, which could be followed for several days. Figure 32a shows that under standard conditions (28°C, 30 μE) WT_{zeo} and *hemH*-Δ*Chl* had nearly identical absorption spectra. After 48 hours at 18 °C and 150 μE, both strains end up with a very different color (Figure 32b). Comparison of WT_{zeo} and *hemH*-Δ*Chl* cell spectra after 48 h of cold/light stress shows that the mutant ended up with lower optical density (Figure 32c). Normalization of these spectra to 750 nm shows, that under these less stressful conditions, the mutant has nearly the same amount of Chl per OD as WT_{zeo} after 48 hours, but a much lower amount of carotenoids (Figure 32d). The amount of carotenoids in the *hemH*-Δ*Chl* mutant did increase under cold/light stress but not to such level as observed in WT_{zeo} (not shown). *Synechocystis* contains five major carotenoid species: β-carotene, echinenone, zeaxanthin, synechoxanthin, and myxoxanthophyll. HPLC analysis revealed, that the accumulation of all five carotenoid types was lower in the mutant (not shown). The increased amount of carotenoids protects the cell from oxidative damage and also plays a role in increased membrane fluidity under low temperature (Saini et al., 2019). Limited membrane fluidity will likely affect globally the function of membrane proteins/complexes in the cell, making more focused interpretation of the phenotype very complicated. Therefore, from these data, I just concluded that *hemH*-Δ*Chl* is acclimating to the cold/light stress, but at a slower rate compared to WT_{zeo}.

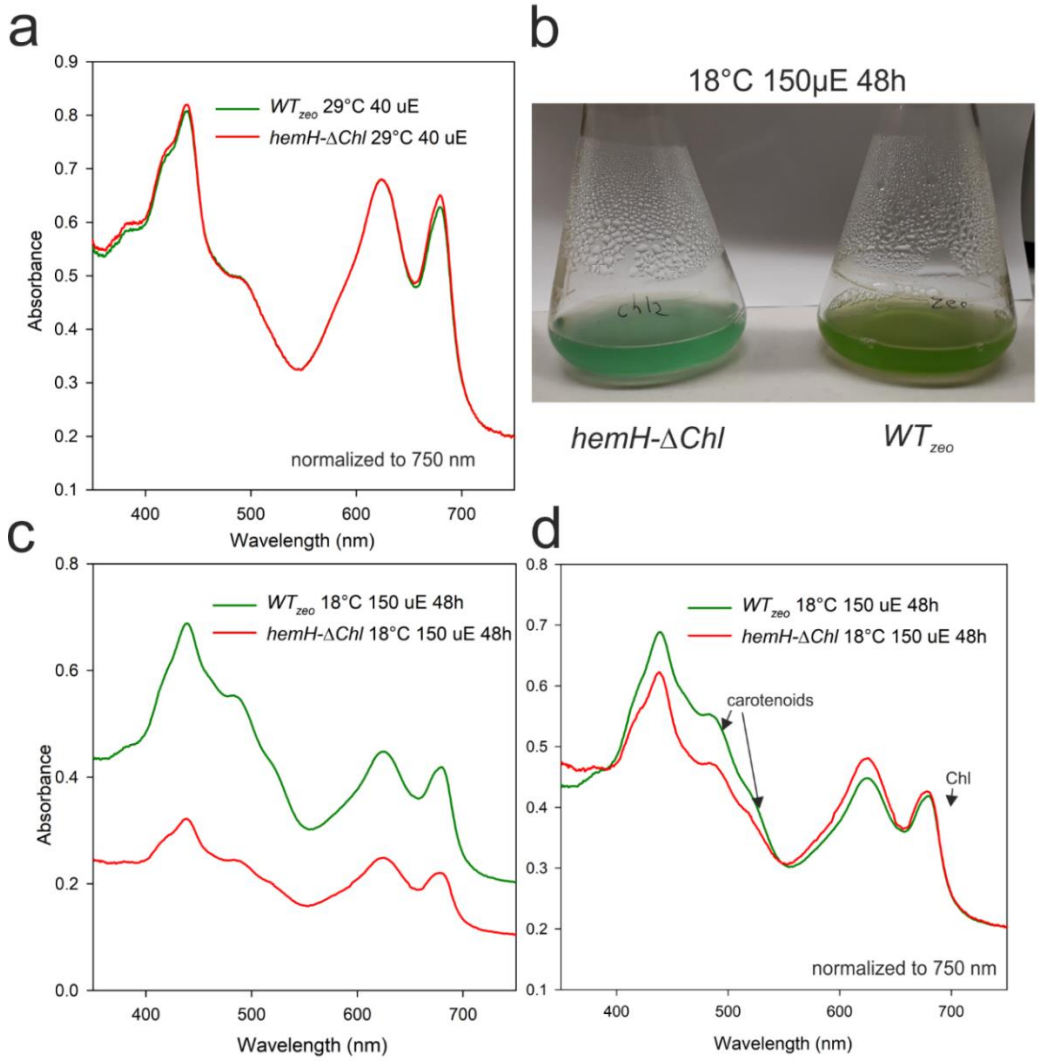

Figure 32. **Disruption of the FeCh LHC motif results in an impaired adaptation to cold/light stress. a**) Absorbance spectra of *WT*$_{zeo}$ and *hemH*-Δ*Chl* strains under standard laboratory conditions (**b**) at 18 °C and 150 µE for 48 hours. **c**) Absorbance spectra of displayed strains after 48 hours of cold/light stress. **d**) Spectra from (c) when normalized to 750 nm. Note the lower level of carotenoids in the mutant.

4.3.3 Disruption of the FeCh LHC motif affects heme accumulation under cold/light stress

In order to acquire a more detailed view of the phenotype of the *hemH*-Δ*Chl*, I used a shorter timescale (24 hours) to pinpoint the initial defect of the mutant. FeCh is an enzyme in the tetrapyrrole pathway (Figure 1), therefore I focused on measuring the pools of tetrapyrroles. During the first 24 hours of moderate cold/light stress (18 °C, 150 µE), the *WT*$_{zeo}$ culture increased its optical density by 300 % and its heme-*b* content by 60 %. In contrast, the *hemH*-Δ*Chl* culture increased its optical density by only 200% and its heme-*b* content by only 10% (Figure 33 a,b). These results suggest that the accumulation

of heme-binding protein(s) was severely impaired in the mutant, which signalizes a potential defect in heme synthesis. A low FeCh activity would be expected to increase the amount of PPIX as shown by its inhibition and by mutations impairing its activity (Papenbrock et al., 2001; Sobotka et al., 2008). However, the pool of PPIX in the *hemH-ΔChl* mutant did not show any increase (Figure 34a). In the first 24 hours of cold/light stress, the tetrapyrrole pathway was strongly downregulated in both WT_{zeo} and *hemH-ΔChl* (Figure 34a), thus other regulatory mechanisms may be dominant over the FeCh activity in the regulation of the tetrapyrrole pathway under these conditions. This would explain why the mutant did not accumulate PPIX. However, the lowered content of heme-*b* in the mutant (Figure 33a) can also be explained by excessive heme degradation. Therefore, at this point, it cannot be clearly stated whether the FeCh-ΔChl enzyme has low *in vivo* activity under the stress conditions.

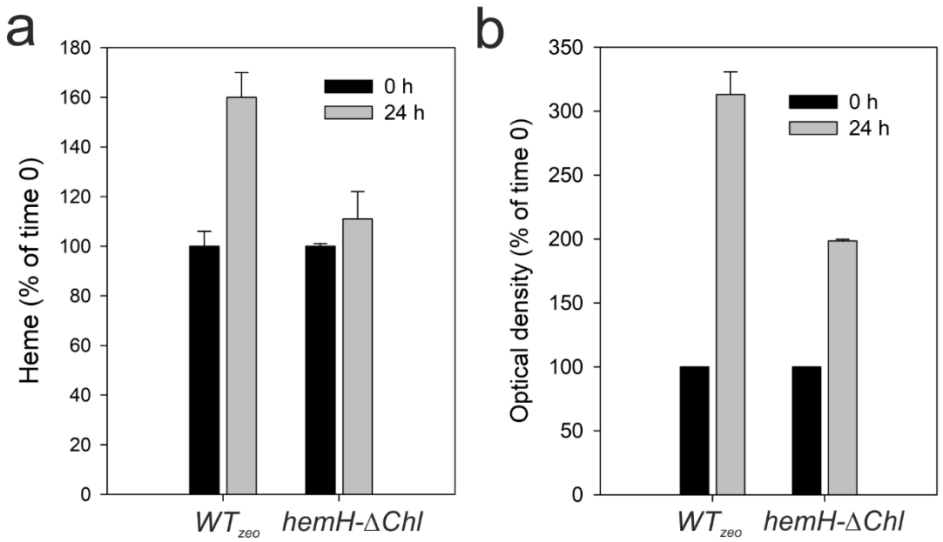

Figure 33. **Heme-*b* accumulation and growth are deficient in *hemH-ΔChl* (strain with the disrupted FeCh LHC motif) under cold/light stress**. **a**) WT_{zeo} and h*emH-ΔChl* cells were grown at 18 °C and 150 μE for 24 hours. Heme-*b* was extracted from 2 mL of each culture and quantified using HPLC coupled with a diode array detector. **b**) Identical cultures from a; the optical density was measured at 750 nm. Error bars indicate S.D., n= 2 biological replicates.

Because the optical density only doubled in the mutant, while it tripled in the control WT_{zeo} culture during the first 24 hours of cold/light stress (Figure 33b), interestingly, when heme-*b* content is displayed per OD, and not per total culture volume, the mutant cells do not appear to be heme deficient (Figure 34b), even though almost no heme-*b* accumulated during the 24 hours in the mutant (Figure 33a). A possible explanation is

that the availability of heme is the limiting factor under these stress conditions, therefore the cells cannot expand their size and divide above a certain heme/OD ratio.

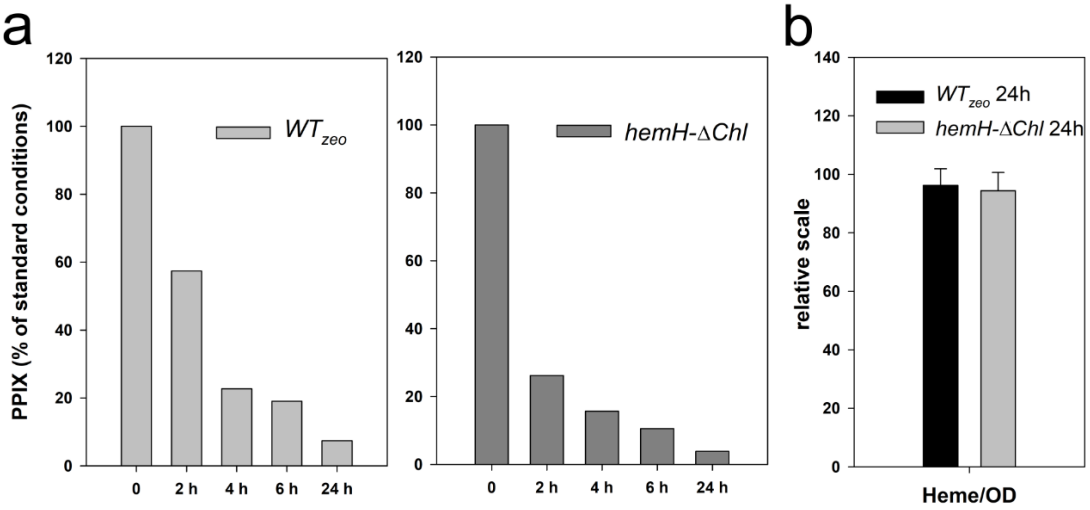

Figure 34. **The levels of PPIX and heme-*b* per optical density are similarly regulated in the *hemH*-Δ*Chl* (strain with interrupted FeCh LHC motif) under cold/light stress.** **a**) *WT*$_{zeo}$ and *hemH*-Δ*Chl* cultures were grown at 18 °C and 150 μE for 24 hours. PPIX was extracted from the cultures and quantified using HPLC coupled with a fluorescent detector at the indicated time intervals. **b**) The relative ratio of heme-*b* per optical density in displayed cultures. Non-covalently bound heme was extracted from WT and mutant cells after 24 h of cold/light stress and quantified using HPLC coupled with a diode array detector. Optical density (OD) was measured at 750 nm. Error bars indicate S.D., n= 2 biological replicates.

Figure 34a shows that the PPIX level is strongly downregulated after the first 24 hours of cold/light stress (about 20 times). During these 24 hours, the *WT*$_{zeo}$ culture increased its heme content by 60 %, however, the Chl content increased in *WT*$_{zeo}$ culture during these 24 hours only by 4 % (Figure 35a). This can be explained by a near-exclusive heme accumulation occurring in the WT, as an initial adaptation to the cold/light stress. This preferential channeling of PPIX towards heme synthesis results in an altered heme : Chl ratio. Interestingly, due to the aberrant accumulation of heme-*b* in the *hemH*-Δ*Chl* (Figure 33a), the mutants heme-*b* : Chl ratio did not adjust properly under the cold/light stress in the first 24 hours (Figure 35b). Although these data are somewhat preliminary, I suggest, that the remaining flux through the tetrapyrrole pathway under cold/light stress is preferentially channeled to heme, and that the *hemH*-Δ*Chl* mutant either cannot sufficiently make the heme or degrades the heme aberrantly fast. If the remaining tetrapyrrole flux was not preferentially directed towards heme synthesis in *WT*$_{zeo}$ under cold/light stress, the only way to explain the altered heme-*b* : Chl ratio after 24 hours

(Figure 35b) would be a situation where the *WT*$_{zeo}$ culture degrades about 40% of total Chl during these first 24 hours, which I find unlikely; however, it cannot be excluded, especially during severe stress conditions. This should be investigated further.

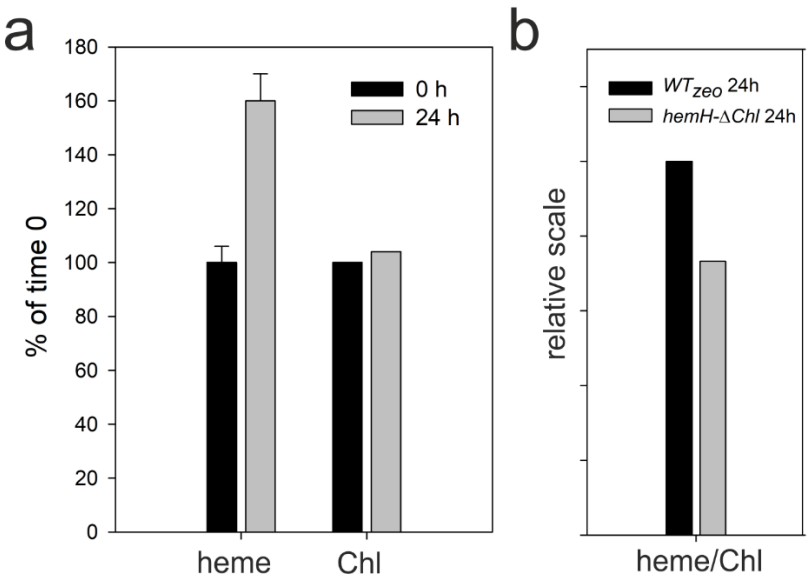

Figure 35. **Cold/light stress results in a preferential synthesis of heme. a**) Non-covalently bound heme and Chl were extracted from 2 mL of *WT*$_{zeo}$ culture and quantified using HPLC coupled with a diode-array detector. Note that only heme accumulated during the 24 hours of cold/light stress. **b**) The relative ratio of heme-*b* : Chl extracted from the same volume of *WT*$_{zeo}$ and *hemH*-Δ*Chl* cultures after 24 hours of cold/light stress.

The *hemH*-Δ*Chl* strain, which possesses mutation preventing FeCh dimerization, shows a growth defect during cold/high light stress. In order to check whether the WT FeCh dimerizes and binds pigments under these conditions, I isolated membrane fractions from *WT* after 4, 12, 24 and 48 hours of cold/light stress and analyzed the FeCh oligomerization by 2D BN-PAGE combined with Western blot. However, no significant increase in the dimeric form of FeCh during the time-course of the stress was detected (not shown). This result suggests that the stress-related function of the FeCh LHC-helix may not be connected to FeCh dimerization and pigment binding. However, it is also possible that the FeCh dimerizes and potentiality associates with pigments only transiently and thus the FeCh-pigment complex may never really accumulate *in vivo* unless the Chl and heme synthesis is artificially imbalanced by FeCh inhibitor.

Specialized proteins promoting the integration of translated proteins into membrane are expressed under low temperatures in bacteria (Sawasato et al., 2019), which suggests that cold stress poses a challenge for the proper folding of membrane proteins. The FeCh-ΔChl protein immunodetected in solubilized membranes after BN-

PAGE displays several spots that are not observed for the WT FeCh (Figure 30b, see the region around 300 kDa). These 'aberrant' interactions could block some other interactions required for the proper cold acclimation in the mutant. However, the *hemH-*Δ*347* strain, which lacks the whole LHC-helix displays no higher-mass spots on BN-gel (Figure 14), has the same phenotype as *hemH-*Δ*Chl* (Figure 30a). Therefore, I can conclude that these aberrant interactions are not the cause of the observed phenotype.

4.3.4 Transcriptomic analysis of WT_{zeo} and hemH-ΔChl cells cultivated under cold/light stress

To obtain more information about the acclimation of *Synechocystis* to cold/light stress and to clarify possible effects of the mutated FeCh, RNA from WT_{zeo}, and *hemH-*Δ*Chl* strains was isolated at 0, 2, 12 and 24 hours after stress initiation (18°C, 150uE) and sequenced; 2 biological replicates were sequenced for each strain and time. The RNAseq data were processed with CLC genomics workbench using annotation containing 3641 genes. All results are reported as transcripts per kilobase million (TPM). At least one transcript was assigned to 3635 genes, no transcript was detected for 6 genes. Figure 36 shows the principal component analysis (PCA) of all 16 samples. A few outliers were eliminated, as they were likely false positives due to extremely high variance between replicates and/or due to some persistent error in the data processing/sequencing (*slr1452* gene is given as an example of an outlier, Table 3D).

Under standard conditions (time 0 h) only *psbA2* gene coding for the D1 subunit of PSII was significantly differentially expressed; the amount of *psbA2* mRNA was almost doubled in the *hemH-*Δ*Chl* mutant (Table 3A). The transcript of *psbA3*, coding for another copy of the D1 subunit, was also increased in the mutant (Table 3A), however, the difference in *psbA3* was not evaluated as significant by the false discovery rate adjusted p-value (FDR p-value). *PsbAII* and *psbAIII* genes are upregulated with increased light intensity (Komenda et al., 2012) suggesting that perhaps the mutation in the FeCh LHC motif results in slightly accelerated PSII repair even under standard conditions. The *hemH-*Δ*Chl* mutant, however, did not exhibit a reduced growth rate under standard conditions (not shown); if there is a faster D1 turnover, it does not affect the cell viability.

Comparison of WT_{zeo} transcriptome at 0 h and after 2 h of stress showed 1909 genes (roughly half of the genome) differentially expressed (below a 0.05 FDR p-value). This is not surprising giving the combination of two stress conditions. Similarly, mutant samples, at 0 h and after 2 h of cold/light stress revealed 1879 genes with changed expression (below the 0.05 FDR value), suggesting a nearly identical acclimation as the

control cells. Indeed, a direct comparison of *WT*$_{zeo}$ and *hemH*-Δ*Chl* after 2 h stress showed that (again apart from 3 outliers) expression of only one operon differed. *Sll0381*, *sll0382*, *sll0383*, *sll0384* and *sll0385* had about 2.5 x lower transcript in the mutant than in the control. However, for all 5 genes, the variance in transcription between replicates was about 2 times, but even the lower *WT*$_{zeo}$ TPM value was about 2 times higher than the mutant TPM value (Table 3C). This difference in expression thus may not be a false-positive result. According to Cyanobase these 5 genes code for ATP-binding protein of ABC transporter (*sll0385*), a cobalt transport protein (*sll0384*), cobalt transporter (*sll0383*), a protein containing carboxypeptidase regulatory-like domain (*sll0382*) and a protein containing domain of unknown function (*sll0381*).

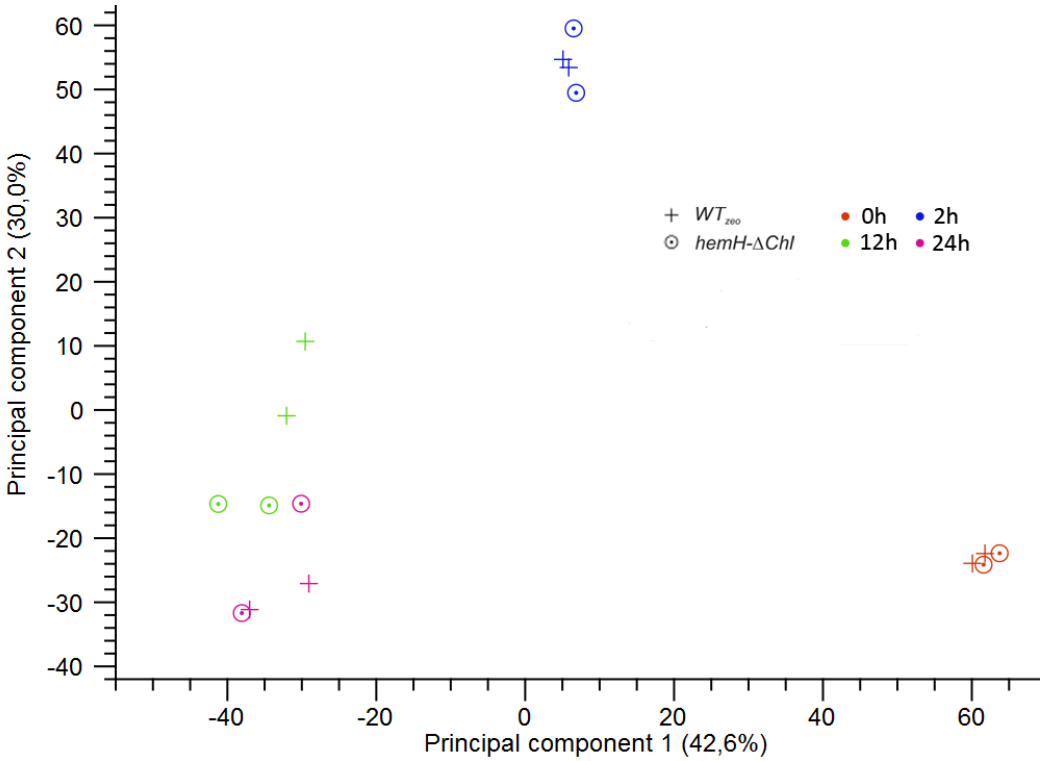

Figure 36.: Changes in *WT*$_{zeo}$ and *hemH*-Δ*Chl* transcriptome during acclimation to cold/light stress (18 °C, 150 µE). Total RNA was isolated from *WT*$_{zeo}$ and *hemH*-Δ*Chl* strains at indicated time-points and sequenced. The principal component analysis was done using TPM of the sequenced RNA fragments which were annotated to 3635 genes.

After 12 hours of cold/light stress, the difference in expression of 16 genes between WT and mutant scored below 0.05 FDR (336 genes were below the regular p-value). This was the largest difference of all time points, which is also visible on PCA graph (Figure 36). Interestingly, out of the 16 genes, 13 genes are coding for tRNA. From the other 3 genes, *ssr2016*, coding for a homolog (63% identity) of plant proton gradient regulation 5 protein PGR5 (Munekage et al., 2002; Takagi and Miyake, 2018), had 3x

lower expression in the mutant (Table 3b). *Sll0330*, a sepiapterine reductase and *slr1747* a putative cell death suppressor protein, had both also higher expression in the WT_{zeo} three and two times respectively (Table 3b). The 13 tRNA genes had all two or three times higher expression in the mutant. The level of $tRNA^{Glu}$, an initial precursor for all tetrapyrroles (Figure 1), was increased in the mutant. However, only a small fraction of

Table 3. Transcripts Per Kilobase Million (TPM) of selected genes in RNAseq dataset of *WT_{zeo}* and *hemH-ΔChl* analyzed after cold/light stress. 0h = standard conditions (28 °C, 30 µE), 2h and 12h denote the length of cold/light stress (18 °C, 150 µE). TPM of each sample is displayed for both biological replicates. **a**) *hemH-ΔChl* had increased transcription of D1 subunit under standard conditions. **b**) WT_{zeo} had a higher transcription of several genes after 12h of cold/light stress. **c**) WT_{zeo} had a higher transcription of one operon after 2 hours of cold/light stress. **d**) Example of an outlier excluded from the analysis. Red = aberrant transcription of a single replicate.

a

	TPM	
	slr1311 (psbA2)	***sll1867 (psbA3)***
WT_{zeo} 0h-1	15018	2068
WT_{zeo} 0h-2	16808	2730
hemH-ΔChl 0h-1	29423	4204
hemH-ΔChl 0h-2	26230	4607

b

	TPM		
	ssr2016 (pgr5)	***sll0330***	***slr1747***
WT_{zeo} 12h-1	317	168	65
WT_{zeo} 12h-2	431	214	61
hemH-ΔChl 12h-1	137	79	32
hemH-ΔChl 12h-2	101	50	27

c

	TPM				
	sll0381	***sll0382***	***sll0383***	***sll0384***	***sll0385***
WT_{zeo} 2h-1	516	265	207	131	135
WT_{zeo} 2h-2	280	136	122	72	68
hemH-ΔChl 2h-1	148	78	60	37	42
hemH-ΔChl 2h-2	119	70	55	37	35

d

	TPM	
	slr1452	
WT_{zeo} 0h-1	354	
WT_{zeo} 0h-2	13	
hemH-ΔChl 0h-1	10	
hemH-ΔChl 0h-2	16	
WT_{zeo} 2h-1		4.3
WT_{zeo} 2h-2		6.4
hemH-ΔChl 2h-1		46
hemH-ΔChl 2h-2		13

the charged $tRNA^{Glu}$ is used for the Chl/heme biosynthesis and, moreover, from the RNAseq data, it is not possible to say of how much of the $tRNA^{Glu}$ carries glutamate. Additionally, the tetrapyrrole pathway did not seem to be out of balance under these conditions (Figure 34a). In comparison, at 24 h, differential transcription of no genes scored below 0.05 FDR. From the PCA graph, it is evident that one WT_{zeo} and one mutant replicate had extremely similar overall transcription at this time point.

When I compared WT_{zeo} samples harvested after 12 h and 24 h of cold/light stress, 782 genes were differentially expressed. In contrast, only 7 genes were differentially expressed between mutant samples harvested at the same time-points. I'm aware that these numbers may look very different if two more replicates were analyzed for each time point. However, given the fact the mutant transcriptome after 12 h of stress is more similar to WT_{zeo} transcriptome after 24 h, I conclude that the mutant transcriptome responded faster to the cold conditions.

In summary, unless some large differences in gene expression occur around 6 hours after the stress induction, and thus were missed in this sequencing experiment, I do not think that any of the small differences observed in these RNAseq data could explain the phenotype of *hemH*-Δ*Chl*. Perhaps, a weaker expression of *ssr2016* (PGR5 homolog) and *slr1747* after 12 hours may play some role in the observed phenotype. Therefore, I propose that differences in carotenoid and heme levels and retarded growth of the *hemH*-Δ*Chl* mutant under cold/light stress are likely caused by a translational or post-translational defect(s).

4.3.5 The function of the FeCh LHC motif is connected to the catalytic domain

Synechocystis contains 4 Hlips. They bind PSII subunits and Chl synthase and function in photoprotection (Komenda and Sobotka, 2016). Hlips contain very similar LHC-like helix to the LHC-helix of FeCh and the cyanobacterial FeCh likely obtained the LHC-helix by fusing with an ancient Hlip (Jansson, 1999; Pazdernik et al., 2019). In theory, it is possible that the function of the FeCh LHC-helix does not influence the function of the catalytic domain, especially since the sequence of the linker between FeCh LHC-helix and the catalytic domain is not conserved between oxygenic phototrophs (not shown). In such a case the reason for the fusion of FeCh and an Hlip would be the presence of both proteins at the same subcellular location. To investigate whether this can be the case, I combined the genetic background expressing already the His-C-tn protein (the separate FeCh LHC-domain) from *psbAII* promoter with the *hemH*-Δ*Chl* mutation (see strain construction). Figure 17 shows that the His-C-tn protein dimerizes, binds pigments and most importantly quenches Chl fluorescence the same way as the full-length FeCh does. In theory, if the FeCh LHC-helix would not be functionally connected with the catalytic domain, the His-C-tn protein should complement the phenotypes of *hemH*-Δ*Chl* and *hemH*-Δ*347* (Figure 38a) as it retains the properties of the FeCh LHC-helix. However, it is not the case; the growth of the *His-C-tn*/*hemH*-Δ*Chl*

strain is apparently slower during cold/light stress compared to the *His-C-tn* (Figure 37), identically to *hemH-ΔChl* compared to WT_{zeo} (Figure 31). Based on this result, I conclude that the FeCh LHC-helix plays its physiological role only if physically connected to the FeCh catalytic domain.

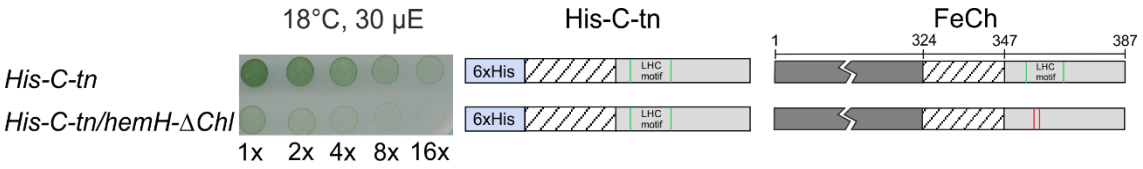

Figure 37. **A separate expression of the FeCh LHC-helix (His-C-tn protein) does not complement the phenotype of the *hemH-ΔChl* mutant.** Displayed strains were grown from the identical optical density on BG11 agar plates at indicated dilutions.

5. General discussion

5.1 The function of the FeCh LHC-helix

As reported in this thesis, the elimination of the Chl-binding site in the FeCh LHC-helix as well as the deletion of the helix cause aberrant response of *Synechocystis* cells to suboptimal temperature if combined with moderately-high light intensity. In cold/light stress the *hemH-ΔChl* and *hemH-Δ347* strains show retarded growth (Figure 30a) and lower heme (Figure 33a) and carotenoid accumulation when normalized to Chl (Figure 32d, Figure 35). Dimerization of *Synechocystis* FeCh via its LHC domain has been reported previously (Sobotka et al., 2011) and I show here that this process is induced by a low activity of this enzyme (Figures 13, 14). Since I found that the dimeric FeCh can bind Chl and carotenoids on its LHC domain (Figures 9, 17) it was intuitive to expect that under cold/light stress, where the FeCh LHC mutants display a growth phenotype, the FeCh in WT is a pigmented dimer. However, I did not observe any increased level of dimeric FeCh under such conditions (not shown). I propose two explanations. The first possibility is that the FeCh dimerizes and binds pigments for only a brief moment, perhaps to trigger some response signal. In this case, the pigment-bound dimeric FeCh would be a kind of short-lived "transition-state" and a pool of dimeric FeCh would not be observable by immunodetection.

Alternatively, the FeCh LHC-helix plays a role as a monomer even under stress conditions. My data suggest that the LHC-helix localizes FeCh to a specific membrane domain. This is supported by the observation that the thylakoid membranes are heterogeneous in cyanobacteria (MacGregor-Chatwin et al., 2017). The FeCh-Δ347 and

FeCh-ΔChl proteins could be mislocalized due to the lack of the LHC-helix and the intramembrane charged amino acids. Incorrect localization and/or the lack of putative binding partners might affect the FeCh activity as supported by the low heme accumulation under cold/light stress (Figure 33). The presence of hydrophilic charged intramembrane amino-acids Glu(-) and Arg(+) in the LHC-helix should force the monomeric FeCh to find a binding partner to neutralize these charges. My data suggest that the complex between the monomeric FeCh and Slr0483 (CurT) is mediated by the LHC-helix (Figure 22). Alignment of FeCh LHC domain and Slr0483 TM segment with respect to the position in the membrane might indicate that the Glu of FeCh is neutralized by interaction with the Arg of CurT (Figure 25e). In this case, the dimerization of FeCh via the LHC-helix and pigment binding would effectively block the interaction between FeCh and CurT as in the pigment-associated FeCh dimer the amino-acid side-chains of the LHC-helix are covered by Chls and carotenoids (Liu et al., 2004). FeCh dimerization and pigment binding thus could serve as a "switch-off" mechanism, preventing the LHC helix from performing another (monomer-related) function(s). If this second scenario is true, it might be possible to observe an increase in the level of dimeric FeCh under conditions in which the tetrapyrrole pathway needs to be upregulated and the PPIX preferentially channeled into Chl branch; just opposite to the situation described for the cold/light stress (see above).

I show, that under cold/light stress the tetrapyrrole pathway is strongly downregulated in the first 24 hours (Figure 34a) and that the residual tetrapyrrole synthesis is diverted preferentially into heme (Figures 33, 35a). Mutation in the FeCh LHC motif results in an insufficient accumulation of heme under these conditions (Figure 33a), thus the levels of Chl and heme become imbalanced in the mutant after 24 hours of stress (Figure 35b). Theoretically, when the WT culture is transferred from the stress conditions back to standard conditions, it will need to re-equilibrate the heme/Chl ratio back to the normal levels, by the preferential synthesis of Chl. Such a situation with a preferential synthesis of Chl is a likely candidate for the formation of a larger pool of dimeric FeCh. Interestingly, cells with increased Chl biosynthesis (after FeCh inhibition) possess dimeric and pigmented FeCh (Figure 6b). Although this stimulation of Chl biosynthesis is not due to environmental conditions, this observation could indeed mean that the FeCh dimerizes as a result of the increased amount of free Chl during preferential synthesis of Chl. If so, the formation of dimeric FeCh could prevent production of excess of heme which would be wasteful and could feedback inhibit the tetrapyrrole pathway when the cell needs to synthesize a large amount of Chl.

Nevertheless, the correct downregulation of PPIX in the *hemH*-ΔChl mutant under cold/light stress (Figure 34a) suggests that the FeCh LHC-helix (neither monomeric or dimeric) is not important for the regulation of tetrapyrrole synthesis via a heme feedback loop (Czarnecki and Grimm, 2012; Brzezowski et al., 2015; Richter et al., 2019). On the other hand, the monomeric FeCh (LHC-helix) seems to allow preferential partitioning of PPIX into heme when it is required by environmental conditions (Figures 33, 35). It cannot be however excluded that the impaired heme accumulation in the mutant (Figure 33a) is caused by accelerated heme degradation (oxidation by heme oxygenase) rather than by an insufficient heme synthesis. The mechanism of such a regulation would then need a completely new model; more experiments are needed to distinguish which model is closer to the situation in the cell.

5.2 Dimerization of FeCh and its binding to CurT protein

SEPs and Hlips can form homodimers via their LHC-domains resembling most likely the structure of the central pair of helices in LHCII proteins (Sobotka et al., 2011; Takahashi et al., 2014; Mork-Jansson et al., 2015) including pigment binding (Mork-Jansson et al., 2015; Shukla et al., 2018). As shown here the FeCh enzyme is also capable to dimerize and bind pigments via the LHC-domain; however, I found that the formation of FeCh dimer depends on the FeCh enzymatic activity (Figures 9, 14). Under standard laboratory conditions, the FeCh enzyme is either a monomer or in a complex that gets solubilized by β-DDM (Figure 14). A large portion of FeCh in the cells is most likely bound to Slr0483 (CurT) via the LHC-helix (Figures 22, 24). Homologs of the *slr0483* gene are present in genomes of all so far sequenced cyanobacteria except the most basal clades of the cyanobacterial tree (*Gloeobacter, Synechococcus,* and *Pseudanabaena*; Jan Mareš, personal communication). Interestingly, these strains also do not possess a FeCh with the LHC domain (Pazdernik et al., 2019). CurT protein and the FeCh LHC domain are highly conserved also in plants and green algae (Figure 25c). This suggests that the interaction between FeCh and Slr0483 could be conserved in the whole green lineage of oxygenic phototrophs. If the monomeric FeCh is interacting with Slr0483 via its LHC domain, this interaction must be reversible (weak) to allow FeCh to dissociate and dimerize. This is in line with my observation, that this interaction is preserved only upon solubilization with very mild detergent digitonin.

Hlips were always purified only as pigment-bound dimers or larger oligomers (Staleva et al., 2015; Shukla et al., 2018). A question is, why the FeCh does not bind pigments under standard conditions (like Hlips do) *in vivo* but preferentially binds to

CurT. The affinity of FeCh LHC-helices for homo-dimerization may be quite weak, thus the LHC dimer may require association with pigments for a stable configuration. Under standard conditions, the *Synechocystis* Hlip (HliD) is pigmented (Chidgey et al., 2014). Other Hlips (HliA/B/C) are expressed only under stress conditions but all of them appear also pigmented when present in the cell (Shukla 2018, Koskela M., unpublished data), which contrasts to FeCh (Figure 9a). Thus a lower affinity or limited access to Chl of the FeCh LHC-domain compared to Hlips may explain why FeCh is preferentially monomeric under standard conditions. A second reason for the prevalence of monomeric FeCh *in vivo* (Figure 14) may be the abundance of its interaction partner. The concentration of CurT (a structural protein) in the membranes is very likely much higher compared to FeCh (an enzyme), this would also explain why it's much more probable that the pigment-less FeCh is bound to Slr0483 rather than to another FeCh.

What mechanism, however, controls FeCh dimerization remains an open question. I see two possible explanations. An equilibrium may exist between dimeric and monomeric (CurT bound) FeCh, strongly in favor of the monomeric form, for reasons mentioned above. Binding of Chl on the dimeric FeCh, when Chl is overabundant, could shift this equilibrium towards the dimeric form by reinforcing the stability of the dimer (Figure 38A). Alternatively, monomeric FeCh could already be able to partially bind Chl, if the concentration of free Chl is above normal, thus the increased amount of free Chl molecules in the thylakoid membranes (Figure 7a) could disrupt the FeCh-CurT interaction by shielding the intramembrane charged amino acids of the LHC-domain, and thus release FeCh from the complex. Partially pigmented monomeric FeCh would then dimerize (Figure 38 b). Since one amino acid (FeCh - Glu356) is responsible for both dimerization and binding of Chl (Liu et al., 2004), it is difficult to design an experiment that could reliably show whether monomeric FeCh can bind some Chl. Nevertheless, in both hypothetical scenarios, the FeCh reacts to the increased amount of free Chl by increasing the level of the pigmented dimer. Binding of Chl and carotenoids on the FeCh LHC-helix will significantly alter the surface of the LHC helix by covering its amino-acid side chains, thus this might result in the relocation of FeCh to a different membrane domain.

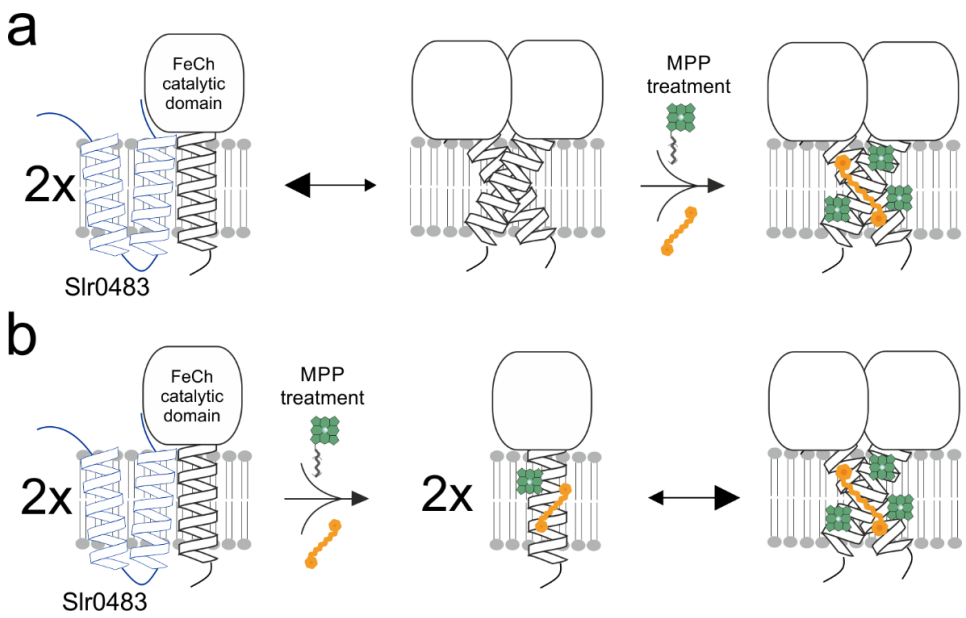

Figure 38. Proposed mechanisms of the MMP-induced dimerization of *Synechocystis* FeCh. A) An equilibrium between monomeric and dimeric FeCh, strongly in favor of the monomer may exist. Dimeric FeCh, in contrary to the monomeric enzyme, is able to bind Chl and carotenoids. Free Chl in membranes, which level is increased by MPP treatment, binds dimeric FeCh and removes it from the equilibrium, thus results in accumulation of the pigmented dimer. **B**) A high concentration of free Chl could directly disrupt the interaction between FeCh and CurT (Slr0483) by binding on the monomeric FeCh.

Lil3 protein was reported to have a higher *in vitro* affinity to dimerization compared to Chl binding (Mork-Jansson et al., 2015). The binding constant of Chl-Lil3 interaction (231 nM) was reported to be about 10 times larger than Lil3-Lil3 binding constant (25 nM). Although the i*n vitro* thermophoretic system can be far from the situation *in vivo*, this result suggests that the FeCh dimerization could proceed Chl binding, which favors the first (A) variant in Figure 38. The so-far single study, which investigated *in vivo* role of the LHC domain in the Lil3 protein proposed that it has a dual function to anchor Lil3 into the membrane and to dimerize Lil3 (Takahashi et al., 2014). In contrast, the LHC-domain of FeCh is required for the FeCh dimerization but actually not for the association of FeCh with the membrane (Sobotka et al., 2011). Whether the dimerization and pigment binding on Lil3 and other LIL proteins is similarly conditional as in the FeCh and reflects the state of the tetrapyrrole pathway is unknown. However, I see it as probable, since the function of Lil3 seems to be connected to the regulation of the tetrapyrrole pathway (Hey et al., 2017; Zhou et al., 2017).

5.3 Pigment binding on the FeCh LHC domain

To my knowledge, this work is the first observation of Chl and carotenoid binding on the FeCh LHC-helix. Previously, the pigment binding ability *in vivo* has been already reported for a few other members of the Lil protein superfamily (Adamska et al., 1999; Reisinger et al., 2008; Shukla et al., 2018). However, I clearly demonstrated that the *Synechocystis* FeCh can be present in the cell in both pigmented and non-pigmented forms depending on the state of the tetrapyrrole synthesis (Figure 9, 14). Such a specifically-induced pigment binding has not been reported for any other Lil protein. Two different *Synechocystis* Hlips (HliC and HliD) bind β-carotene and Chl in a 2 : 4 or 2 : 6 ratio, respectively (Staleva et al., 2015; Shukla et al., 2018). In contrast, the FeCh LHC-domain binds β-carotene, zeaxanthin and a small amount of echinenon (Figures 10b, 17c). The calculated molar ratio of Chl : β-car : zeaxanthin (6 : 0.9 : 1) (Figure 17c) corresponds to the ratio reported for HliD (Staleva et al., 2015). However, in FeCh, one carotenoid-binding site seems to be less specific and more polar than that in HliC/D proteins and accommodates preferentially xanthophylls or keto-carotenoids, indicating the presence of on carotenoid-binding pocket selective for polar xanthophylls. Both full-length FeCh and separately expressed FeCh C-terminus (His-C-tn) bind Chl and the same carotenoids in an energy dissipative configuration (Figure 16, Table 1, Figure 17a). These results strongly suggest that the FeCh catalytic domain does not have any structural function in the pigment binding. The observed Chl quenching in FeCh resembled the efficient quenching described in Hlips (Staleva et al., 2015).

The virtual absence of detectable dimeric FeCh under standard conditions (Figures 9, 14) suggests that Chl does not play any role in the incorporation of the FeCh LHC-helix into the thylakoid membrane. Although, increased amount of free Chl increased the half-life of the His-C-tn (Figure 19, 20), which suggests that Chl-binding does have a stabilizing role on the LHC-helix as proposed for LHC proteins by (Eggink and Hoober, 2000).

5.4 Do pigments on the LHC-helix influence the FeCh catalytic activity?

It remains an open question whether the pigmented FeCh dimer shows different enzymatic parameters than the monomeric enzyme. The usage of FeCh inhibitor to induce the pigment binding makes a direct activity measurement impossible. *In vitro* reconstitution of *Synechocystis* FeCh with pigments is not a feasible way to obtain a non-inhibited FeCh-pigment complex (Storm et al., 2013). Also, I did not yet find any physiological conditions where the pigmented FeCh dimer would significantly

accumulate. The FeCh LHC domain, if produced as a separated protein, dimerizes and binds Chl and carotenoids in a dissipative configuration, essentially as the dimeric FeCh (Figure 17). This artificial protein even dimerizes with FeCH via its LHC-domain (Sobotka et al., 2011); however, it does not complement the FeCh-ΔChl mutation during cold/light stress. It indicates that the functional LHC domain (with intact Chl-binding motif) needs to be physically linked to the catalytic part FeCh for the acclimation to stress. Since the removal of the FeCh LHC-helix results in an active enzyme both *in vivo* and *in vitro* (Sobotka et al., 2011; Storm et al., 2013), a possible co-enzymatic role of Chl in the FeCh catalytic reaction can be excluded, at least under standard conditions. In theory, I see two ways how pigment-binding on the LHC domain could affect the activity of the catalytic domain.

Allosteric regulation, where a ligand binding is coupled to a functional change at a remote site, is a typical regulation of enzymes (Changeux and Edelstein, 2005; Tsai et al., 2009). Thus, the binding of pigments on the LHC domain could affect the properties of the catalytic domain. However, there are two arguments why this should not be the case for the FeCh. Firstly, the pigments bound on the separately expressed FeCh LHC domain seem to be in correct amounts and conformations (Figure 17a) when compared to the full-length protein (Figure 16a). This result suggests that the FeCh catalytic domain does not have any structural (allosteric) effect on the pigment binding on the LHC domain, which makes a possible reverse allosteric effect of the bound pigments towards the catalytic domain unlikely. The second argument is that the first half of the linker between the catalytic and LHC domain does not have a conserved sequence even between cyanobacteria. In addition, in green algae and plants, the linker is near twice as long compared to *Synechocystis* (~40 versus ~20 amino acids, Figure 4). Such a long linker with no clear secondary structure is very unlikely to transmit a signal between the LHC domain and the catalytic FeCh domain. However, the limited heme-*b* accumulation in the *hemH*-Δ*Chl* mutant during stress conditions suggests an impaired function of the catalytic domain (Figure 33), when the LHC-helix is disrupted.

In my opinion, the more favorable explanation is that upon dimerization and pigment binding FeCh changes localization and/or binding partner. Dimeric and pigment-associated LHC-helix will have very different surface compared to a monomeric helix, thus it would not be a surprise if the FeCh changed localization in the cell during such an event. In theory, the association of FeCh with various proteins could modulate access of FeCh to PPIX and/or iron, thus effectively influencing the rate of heme synthesis. FeCh was shown to form a complex with the preceding enzyme PPOX in the cyanobacterium *Thermosynechococcus elongates* (Masoumi et al., 2008).

5.5 FeCh LHC-helix and PSII

In the first published study dealing with the FeCh LHC domain (Funk and Vermaas, 1999), authors reported a decreased energy transfer between phycobilisomes and PSII, but only when the FeCh LHC domain deletion was combined with the deletion of PSI. However, the full segregation of PSI deletion strains is probably only possible when other (secondary) mutations are formed as shown by results of the whole-genome sequencing (Martin Tichý, personal communication). Therefore, the observed decrease in PSII efficiency may not be attributed solely to the FeCh LHC domain. Although, I observed an increase in *psbA* transcript in the *hemH*-Δ*Chl* mutant during standard conditions (Table 3a), which suggests a direct or indirect effect of the FeCh LHC-helix on the PSII biogenesis. Plant OHPs and two *Synechocystis* Hlips (HliC and HliD, most likely homologs of plant OHP1/2) have been shown to facilitate the synthesis of RCII core complex of PSII (Komenda and Sobotka, 2016; Myouga et al., 2018). However, because the separately expressed FeCh LHC-domain (His-C-tn protein) does not complement the cold/light stress phenotype of *hemH*-ΔChl (Figure 37), I conclude that the role of FeCh-LHC helix in PSII assembly is not analogous to HliC/D or OHPs. However, the interaction of FeCh with Slr0483 (CurT) (Figures 22, 24e) further supports a role of FeCh LHC-helix in the PSII biosynthesis since the CurT protein is expected to participate in the formation of special membrane domains where the PSII assembly/repair preferentially occurs, both in plants and cyanobacteria (Armbruster et al., 2013; Heinz et al., 2016). Localization of FeCh into this domain may be another role of the FeCh LHC-helix.

It should be noted that I did observe a decrease in PSII activity (oxygen evolution) in the *hemH*-Δ*Chl* mutant after a 6-hour exposition to cold/light stress (not shown). At the moment I am unable to say whether the lower PSII activity in the mutant is caused by the observed heme deficiency (Figure 33a) or vice versa, this will be the subject of a future study. It should be noted that heme is non-covalently bound to the cytochrome *b*-559 (Cyt559) subunit of PSII and covalently in the lumenal PsbV (Cyt550) subunit. The exact physiological function of Cyt559 is unknown, however it has definitely a structural role in PSII as in the absence of Cyt559 the process of PSII assembly is completely blocked (Chu and Chiu, 2016). In theory, the heme deficiency in the *hemH*-ΔChl under cold/light stress (Figure 33a) may result in an aberrant supply of heme to the Cyt559, which would result in aberrant PSII assembly and thus explain lower PSII activity. It is possible that proper PSII assembly requires a specific mechanism for the delivery of heme to the Cyt559 or Cyt550 subunits, and the inability of the FeCh LHC mutant to localize

to the CurT-dependant domain (Figure 22), may result in a misallocation of heme, thus lowering the amount of PSII.

Improper assembly of PSII, due to lack of heme, could result in Chl "leaking" from unassembled PSII Chl-proteins. This leaked Chl could bind to the FeCh LHC-helix, which is localized in the vicinity of PSII assembly due to interaction with Slr0483 (Figure 22), and dimerize it. Dimerization of FeCh could be a signal that heme and Chl are out of balance. Although I do observe a strong misbalance between heme and Chl in the *hemH*-Δ*Chl* mutant (Figure 35b), I do not observe an increase in the dimeric FeCh under these conditions using immunodetection (not shown). However, the total conservation of the FeCh LHC motif from cyanobacteria to higher plants (Figure 3) suggests a function that must be important for the cell/chloroplast and common to all of these organisms. PSII biogenesis is an energetically demanding process conserved in the whole green lineage (Komenda et al., 2012; Lu, 2016). The role of FeCh LHC-helix in PSII assembly would thus be important enough to be conserved for billions of years.

5.6 Conservation of the tetrapyrrole pathway in cyanobacteria and plants

The synthesis of heme and Chl in cyanobacteria includes the same enzymatic steps as in plants (Czarnecki and Grimm, 2012). The question is whether the knowledge about the regulation of the tetrapyrrole pathway obtained using an algal or cyanobacterial model organism can be applied to plants and vice versa. There seem to be noticeable differences in the regulation of tetrapyrrole synthesis between plants and cyanobacteria. For example, the penultimate step in Chl synthesis is catalyzed by protochlorophyllide oxidoreductase (POR, Figure 1). Light-independent and light-dependent PORs are present in genomes of cyanobacteria, algae and gymnosperms. However, the genomes of angiosperms contain only the light-dependent POR enzyme, which uses light as an energy source for the reaction, and thus angiosperms cannot synthesize Chl in dark. To prevent the accumulation of protochlorophyllide (substrate of POR), the tetrapyrrole pathway is strongly downregulated minutes after the transition to darkness as reported in barley (Richter et al., 2010). In plants, FLU protein is required for this rapid downregulation of the pathway (Meskauskiene et al., 2001). The FLU protein interacts with GluTR (Fang et al., 2016), the initial enzyme of the tetrapyrrole pathway, and somehow inhibits the GluTR activity when protochlorophyllide starts to accumulate (Meskauskiene et al., 2001). As I show in Figure 39, the tetrapyrrole pathway in *Synechocystis* is downregulated similarly to plants upon transition to darkness, even though it possesses the light-independent POR. Although cyanobacteria do not contain a homolog of the FLU

protein, this measurement suggests that they are able to perform a similar type of fast regulation that occurs in higher plants, perhaps by using a different protein.

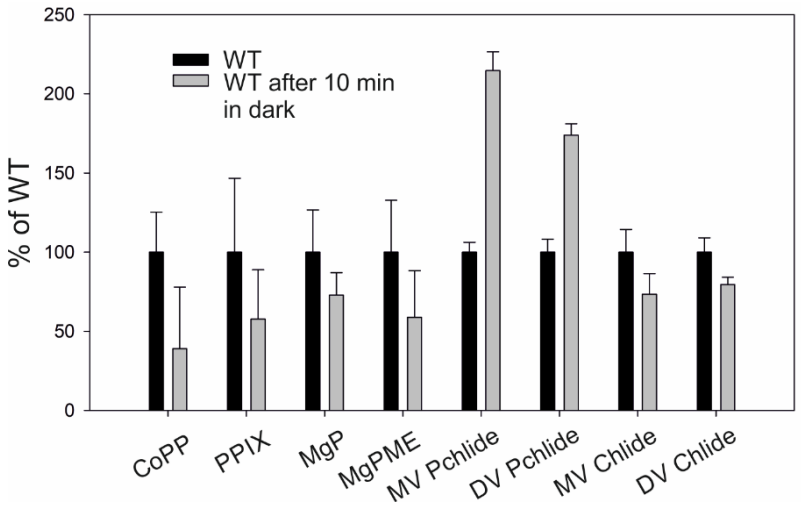

Figure 39. **The tetrapyrrole synthesis in *Synechocystis* is downregulated within minutes after transfer to darkness**. Metabolites of the tetrapyrrole pathway were extracted and quantified using HPLC coupled with fluorescence detectors from WT and WT transferred to darkness for 10 minutes. CoPP - coproporphyrin III, PPIX - protoporphyrin IX, MgP - Mg-protoporphyrin IX, MgPME - Mg-protoporphyrin IX monomethyl ester, MV/DV Pchlide - monovinyl/divinyl protochlorophyllide, MV/DV Chlide - monovinyl/divinyl chlorophyllide. Error bars give S.D., n = 3 biological replicates.

An example of the transferability of knowledge between cyanobacteria and plants is the redox-regulation of the ChlI subunit of Mg-chelatase, first reported in *Synechocystis* (Jensen et al., 2000). Later, it was shown in *A. thaliana* that the ChlI subunit interacts with thioredoxin *f* (Luo et al., 2012) and by reduction of the ChlI cysteine residues the thioredoxin increases the activity of ChlI (Luo et al., 2012). A comparison of the ChlI sequence between *Synechocystis* and *A. thaliana* shows that three cysteines of ChlI are conserved along with the amino acids around them (Figure 40). Also, the thioredoxin *f* is conserved in *Synechocystis*. It is therefore likely that some post-translational regulations of the tetrapyrrole pathway work very similarly in cyanobacteria and in chloroplasts.

```
ChlI (synecho.) 104: KVTMVDLPLGATEDRVCGTIDIEKALSEGVKAFEPGLLAKANRGILYVDEVNLLDDHLVDVLLDSA
ChlI (arabido.) 170: KINMVDLPLGATEDRVCGTIDIEKALTEGVKAFEPGLLAKANRGILYVDEVNLLDDHLVDVLLDSA

ChlI (synecho.) 275: RVKVSEVCAELDVDGLRGDIVTNRAAKALAAFEGRTEVTVDDISRVIVLCLRHRLRKDPLESIDSG
ChlI (arabido.) 341: KVKISKVCAELDVDGLRGDMVINRAARALAALQGRDQVTAEDVGIVIPNCLRHRLRKDPLESMDSG
```

Figure 40. **Sequence alignment of ChlI subunit of Mg-chelatase from *Synechocystis*** (U35144.1) **and *A. thaliana*** (AT5G45930.1). Conserved regions around the cysteine residues are highlighted in grey.

Whether the FeCh LHC-helix has the same function in plants and algae as in *Synechocystis* remains an open question. In plants and green algae, the linker between FeCh catalytic and LHC domains contains a ~20 aa insert that is absent in cyanobacteria (not shown). However, the FeCh catalytic domain remained linked with its LHC-domain for >billion years (Pazdernik et al., 2019) suggesting an essential role of this ancient fusion in oxygenic phototrophs; the sequence of the linker may be thus less crucial but this needs to be tested experimentally.

6. Conclusion

My experiments show that *Synechocystis* cells actively maintain a certain ratio between Chl and heme, which is shifted towards heme during stress conditions. In very challenging growth conditions such as cold stress combined with high-light, *Synechocystis* cells seem to synthesize preferentially heme for the first 24 hours. Importantly, in the mutant possessing an aberrant FeCh, which lacks the Chl-binding and dimerization motif, this stress-induced heme synthesis is not observed. It suggests that the FeCh LHC-motif facilitates channeling of PPIX towards heme. My data show that the FeCh LHC-helix localizes FeCh to a CurT dependant membrane domain. I also show that the FeCh LHC-helix dimerizes and binds Chl when the FeCh activity is lowered. This further supports the role of the LHC-helix in balancing the synthesis of Chl and heme. Based on my data I propose that the role of the FeCh LHC-domain is to monitor the availability of Chl during the assembly of photosystems and coordinate Chl availability with the synthesis of heme.

7. References

Adamska, I., Kruse, E., and Kloppstech, K. (2001). Stable insertion of the early light-induced proteins into etioplast membranes requires chlorophyll-alpha. Journal of Biological Chemistry **276,** 8582-8587.

Adamska, I., Roobol-Boza, M., Lindahl, M., and Andersson, B. (1999). Isolation of pigment-binding early light-inducible proteins from pea. European Journal of Biochemistry **260,** 453-460.

Adhikari, N.D., Froehlich, J.E., Strand, D.D., Buck, S.M., Kramer, D.M., and Larkin, R.M. (2011). GUN4-Porphyrin Complexes Bind the ChlH/GUN5 Subunit of Mg-Chelatase and Promote Chlorophyll Biosynthesis in Arabidopsis. Plant Cell **23,** 1449-1467.

Armbruster, U., Labs, M., Pribil, M., Viola, S., Xu, W.T., Scharfenberg, M., Hertle, A.P., Rojahn, U., Jensen, P.E., Rappaport, F., Joliot, P., Dormann, P., Wanner, G., and Leister, D. (2013). Arabidopsis CURVATURE THYLAKOID1 Proteins Modify Thylakoid Architecture by Inducing Membrane Curvature. Plant Cell **25,** 2661-2678.

Ballottari, M., Mozzo, M., Girardon, J., Hienerwadel, R., and Bassi, R. (2013). Chlorophyll Triplet Quenching and Photoprotection in the Higher Plant Monomeric Antenna Protein Lhcb5. Journal of Physical Chemistry B **117,** 11337-11348.

Brzezowski, P., Richter, A.S., and Grimm, B. (2015). Regulation and function of tetrapyrrole biosynthesis in plants and algae. Biochimica Et Biophysica Acta-Bioenergetics **1847,** 968-985.

Burkhart, J.M., Schumbrutzki, C., Wortelkamp, S., Sickmann, A., and Zahedi, R.P. (2012). Systematic and quantitative comparison of digest efficiency and specificity reveals the impact of trypsin quality on MS-based proteomics. Journal of Proteomics **75,** 1454-1462.

Changeux, J.P., and Edelstein, S.J. (2005). Allosteric mechanisms of signal transduction. Science **308,** 1424-1428.

Chen, G.Y.E., Canniffe, D.P., Barnett, S.F.H., Hollingshead, S., Brindley, A.A., Vasilev, C., Bryant, D.A., and Hunter, C.N. (2018). Complete enzyme set for chlorophyll biosynthesis in Escherichia coli. Science Advances **4**.

Chidgey, J.W., Linhartova, M., Komenda, J., Jackson, P.J., Dickman, M.J., Canniffe, D.P., Konik, P., Pilny, J., Hunter, C.N., and Sobotka, R. (2014). A Cyanobacterial Chlorophyll Synthase-HliD Complex Associates with the Ycf39 Protein and the YidC/Alb3 Insertase. Plant Cell **26,** 1267-1279.

Chow, K.S., Singh, D.P., Walker, A.R., and Smith, A.G. (1998). Two different genes encode ferrochelatase in Arabidopsis: mapping, expression and subcellular targeting of the precursor proteins. Plant Journal **15,** 531-541.

Chu, H.A., and Chiu, Y.F. (2016). The Roles of Cytochrome b(559) in Assembly and Photoprotection of Photosystem II Revealed by Site-Directed Mutagenesis Studies. Frontiers in Plant Science **6**.

Cormann, K.U., Moller, M., and Nowaczyk, M.M. (2016). Critical Assessment of Protein Cross-Linking and Molecular Docking: An Updated Model for the Interaction Between Photosystem II and Psb27. Frontiers in Plant Science **7**.

Czarnecki, O., and Grimm, B. (2012). Post-translational control of tetrapyrrole biosynthesis in plants, algae, and cyanobacteria. Journal of Experimental Botany **63,** 1675-1687.

Czarnecki, O., Hedtke, B., Melzer, M., Rothbart, M., Richter, A., Schroter, Y., Pfannschmidt, T., and Grimm, B. (2011). An Arabidopsis GluTR Binding Protein Mediates Spatial Separation of 5-Aminolevulinic Acid Synthesis in Chloroplasts. Plant Cell **23,** 4476-4491.

Da, Q.G., Wang, P., Wang, M.L., Sun, T., Jin, H.L., Liu, B., Wang, J.F., Grimm, B., and Wang, H.B. (2017). Thioredoxin and NADPH-Dependent Thioredoxin Reductase C Regulation of Tetrapyrrole Biosynthesis. Plant Physiology **175,** 652-666.

Dobakova, M., Sobotka, R., Tichy, M., and Komenda, J. (2009). Psb28 Protein Is Involved in the Biogenesis of the Photosystem II Inner Antenna CP47 (PsbB) in the Cyanobacterium Synechocystis sp PCC 6803. Plant Physiology **149,** 1076-1086.

Dolganov, N.A.M., Bhaya, D., and Grossman, A.R. (1995). CYANOBACTERIAL PROTEIN WITH SIMILARITY TO THE CHLOROPHYLL A/B BINDING-PROTEINS OF HIGHER-PLANTS - EVOLUTION AND REGULATION. Proceedings of the National Academy of Sciences of the United States of America **92,** 636-640.

Eggink, L.L., and Hoober, J.K. (2000). Chlorophyll binding to peptide maquettes containing a retention motif. Journal of Biological Chemistry **275,** 9087-9090.

Engelken, J., Brinkmann, H., and Adamska, I. (2010). Taxonomic distribution and origins of the extended LHC (light-harvesting complex) antenna protein superfamily. BMC Evolutionary Biology **10**.

Engelken, J., Funk, C., and Adamska, I. (2012). The extended light-harvesting complex (LHC) protein superfamily: classification and evolutionary dynamics. In Functional Genomics and Evolution of Photosynthetic Systems, R.L. Burnap and W.F.J. Vermaas, eds, pp. 265-284.

Fang, P., Liu, M.Q., Xue, Y., Yao, J., Zhang, Y., Shen, H.L., and Yang, P.Y. (2015). Controlling nonspecific trypsin cleavages in LC-MS/MS-based shotgun proteomics using optimized experimental conditions. Analyst **140,** 7613-7621.

Fang, Y., Zhao, S., Zhang, F.L., Zhao, A.G., Zhang, W.X., Zhang, M., and Liu, L. (2016). The Arabidopsis glutamyl-tRNA reductase (GluTR) forms a ternary complex with FLU and GluTR-binding protein. Scientific Reports **6**.

Funk, C., and Vermaas, W. (1999). A cyanobacterial gene family coding for single-helix proteins resembling part of the light-harvesting proteins from higher plants. Biochemistry **38,** 9397-9404.

Gotze, M., Pettelkau, J., Schaks, S., Bosse, K., Ihling, C.H., Krauth, F., Fritzsche, R., Kuhn, U., and Sinz, A. (2012). StavroX-A Software for Analyzing Crosslinked Products in Protein Interaction Studies. Journal of the American Society for Mass Spectrometry **23,** 76-87.

Griesbeck, O., Baird, G.S., Campbell, R.E., Zacharias, D.A., and Tsien, R.Y. (2001). Reducing the environmental sensitivity of yellow fluorescent protein - Mechanism and applications. Journal of Biological Chemistry **276,** 29188-29194.

Heddad, M., Engelken, J., and Adamska, I. (2012). Light stress proteins in viruses, cyanobacteria and photosynthetic eukaryota. In Photosynthesis: Plastid Biology, Energy Conversion and Carbon Assimilation, J.J. EatonRye, B.C. Tripathy, and T.D. Sharkey, eds, pp. 299-317.

Heinz, S., Rast, A., Shao, L., Gutu, A., Gugel, I.L., Heyno, E., Labs, M., Rengstl, B., Viola, S., Nowaczyk, M.M., Leister, D., and Nickelsen, J. (2016). Thylakoid Membrane Architecture in Synechocystis Depends on CurT, a Homolog of the Granal CURVATURE THYLAKOID1 Proteins. Plant Cell **28,** 2238-2260.

Hey, D., and Grimm, B. (2018). ONE-HELIX PROTEIN2 (OHP2) Is Required for the Stability of OHP1 and Assembly Factor HCF244 and Is Functionally Linked to PSII Biogenesis. Plant Physiology **177,** 1453-1472.

Hey, D., Rothbart, M., Herbst, J., Wang, P., Muller, J., Wittmann, D., Gruhl, K., and Grimm, B. (2017). LIL3, a Light-Harvesting Complex Protein, Links Terpenoid and Tetrapyrrole Biosynthesis in Arabidopsis thaliana. Plant Physiology **174,** 1037-1050.

Hontani, Y., Kloz, M., Polivka, T., Shukla, M.K., Sobotka, R., and Kennis, J.T.M. (2018). Molecular Origin of Photoprotection in Cyanobacteria Probed by Watermarked Femtosecond Stimulated Raman Spectroscopy. Journal of Physical Chemistry Letters **9,** 1788-1792.

Janouskovec, J., Sobotka, R., Lai, D.H., Flegontov, P., Konik, P., Komenda, J., Ali, S., Prasil, O., Pain, A., Obornik, M., Lukes, J., and Keeling, P.J. (2013). Split Photosystem Protein, Linear-Mapping Topology, and Growth of Structural Complexity

in the Plastid Genome of Chromera velia. Molecular Biology and Evolution **30,** 2447-2462.

Jansson, S. (1999). A guide to the Lhc genes and their relatives in Arabidopsis. Trends in Plant Science **4,** 236-240.

Jarvi, S., Suorsa, M., and Aro, E.M. (2015). Photosystem II repair in plant chloroplasts - Regulation, assisting proteins and shared components with photosystem II biogenesis. Biochimica Et Biophysica Acta-Bioenergetics **1847,** 900-909.

Jensen, P.E., Reid, J.D., and Hunter, C.N. (2000). Modification of cysteine residues in the ChlI and ChlH subunits of magnesium chelatase results in enzyme inactivation. Biochemical Journal **352,** 435-441.

Kaneko, T., and Tabata, S. (1997). Complete genome structure of the unicellular cyanobacterium Synechocystis sp. PCC6803. Plant and Cell Physiology **38,** 1171-1176.

Kaul, S., Koo, H.L., Jenkins, J., Rizzo, M. … and Ar Gen, I. (2000). Analysis of the genome sequence of the flowering plant Arabidopsis thaliana. Nature **408,** 796-815.

Ke, S.H., and Madison, E.L. (1997). Rapid and efficient site-directed mutagenesis by single-tube 'megaprimer' PCR method. Nucleic Acids Research **25,** 3371-3372.

Komenda, J., and Sobotka, R. (2016). Cyanobacterial high-light-inducible proteins - Protectors of chlorophyll-protein synthesis and assembly. Biochimica Et Biophysica Acta-Bioenergetics **1857,** 288-295.

Komenda, J., Lupinkova, L., and Kopecky, J. (2002). Absence of the psbH gene product destabilizes photosystem II complex and bicarbonate binding on its acceptor side in Synechocystis PCC 6803. European Journal of Biochemistry **269,** 610-619.

Komenda, J., Sobotka, R., and Nixon, P.J. (2012). Assembling and maintaining the Photosystem II complex in chloroplasts and cyanobacteria. Current Opinion in Plant Biology **15,** 245-251.

Kopecna, J., de Vaca, I.C., Adams, N.B.P., Davison, P.A., Brindley, A.A., Hunter, C.N., Guallar, V., and Sobotka, R. (2015). Porphyrin Binding to Gun4 Protein, Facilitated by a Flexible Loop, Controls Metabolite Flow through the Chlorophyll Biosynthetic Pathway. Journal of Biological Chemistry **290,** 28477-28488.

Koreny, L., Sobotka, R., Kovarova, J., Gnipova, A., Flegontov, P., Horvath, A., Obornik, M., Ayala, F.J., and Lukes, J. (2012). Aerobic kinetoplastid flagellate Phytomonas does not require heme for viability. Proceedings of the National Academy of Sciences of the United States of America **109,** 3808-3813.

Kuchmina, E., Wallner, T., Kryazhov, S., Zinchenko, V.V., and Wilde, A. (2012). An expression system for regulated protein production in Synechocystis sp PCC 6803 and its application for construction of a conditional knockout of the ferrochelatase enzyme. Journal of Biotechnology **162,** 75-80.

Larkin, R.M., Alonso, J.M., Ecker, J.R., and Chory, J. (2003). GUN4, a regulator of chlorophyll synthesis and intracellular signaling. Science **299,** 902-906.

Lee, J., Lee, H.J., Shin, M.K., and Ryu, W.S. (2004). Versatile PCR-mediated insertion or deletion mutagenesis. Biotechniques **36,** 398-+.

Liu, Z.F., Yan, H.C., Wang, K.B., Kuang, T.Y., Zhang, J.P., Gui, L.L., An, X.M., and Chang, W.R. (2004). Crystal structure of spinach major light-harvesting complex at 2.72 angstrom resolution. Nature **428,** 287-292.

Lu, Y. (2016). Identification and Roles of Photosystem II Assembly, Stability, and Repair Factors in Arabidopsis. Frontiers in Plant Science **7**.

Luo, T., Fan, T.T., Liu, Y.N., Rothbart, M., Yu, J., Zhou, S.X., Grimm, B., and Luo, M.Z. (2012). Thioredoxin Redox Regulates ATPase Activity of Magnesium Chelatase CHLI Subunit and Modulates Redox-Mediated Signaling in Tetrapyrrole Biosynthesis and Homeostasis of Reactive Oxygen Species in Pea Plants. Plant Physiology **159,** 118-130.

MacGregor-Chatwin, C., Sener, M., Barnett, S.F.H., Hitchcock, A., Barnhart-Dailey, M.C., Maghlaoui, K., Barber, J., Timlin, J.A., Schulten, K., and Hunter, C.N. (2017).

Lateral Segregation of Photosystem I in Cyanobacterial Thylakoids. Plant Cell **29,** 1119-1136.

Masoumi, A., Heinemann, I.U., Rohde, M., Koch, M., Jahn, M., and Jahn, D. (2008). Complex formation between protoporphyrinogen IX oxidase and ferrochelatase during haem biosynthesis in Thermosynechococcus elongatus. Microbiology-Sgm **154,** 3707-3714.

Meskauskiene, R., Nater, M., Goslings, D., Kessler, F., den Camp, R.O., and Apel, K. (2001). FLU: A negative regulator of chlorophyll biosynthesis in Arabidopsis thaliana. Proceedings of the National Academy of Sciences of the United States of America **98,** 12826-12831.

Mork-Jansson, A.E., Gargano, D., Kmiec, K., Fumes, C., Shevela, D., and Eichacker, L.A. (2015). Lil3 dimerization and chlorophyll binding in Arabidopsis thaliana. Febs Letters **589,** 3064-3070.

Munekage, Y., Hojo, M., Meurer, J., Endo, T., Tasaka, M., and Shikanai, T. (2002). PGR5 is involved in cyclic electron flow around photosystem I and is essential for photoprotection in Arabidopsis. Cell **110,** 361-371.

Myouga, F., Takahashi, K., Tanaka, R., Nagata, N., Kiss, A.Z., Funk, C., Nomura, Y., Nakagami, H., Jansson, S., and Shinozaki, K. (2018). Stable Accumulation of Photosystem II Requires ONE-HELIX PROTEIN1 (OHP1) of the Light Harvesting-Like Family. Plant Physiology **176,** 2277-2291.

Normile, D., and Cohen, J. (2019). Government report blasts creator of CRISPR twins. Science **363,** 328-328.

Olsen, J.V., Ong, S.E., and Mann, M. (2004). Trypsin cleaves exclusively C-terminal to arginine and lysine residues. Molecular & Cellular Proteomics **3,** 608-614.

Pagliano, C., Barera, S., Chimirri, F., Saracco, G., and Barber, J. (2012). Comparison of the alpha and beta isomeric forms of the detergent n-dodecyl-D-maltoside for solubilizing photosynthetic complexes from pea thylakoid membranes. Biochimica Et Biophysica Acta-Bioenergetics **1817,** 1506-1515.

Papenbrock, J., Mock, H.P., Tanaka, R., Kruse, E., and Grimm, B. (2000). Role of magnesium chelatase activity in the early steps of the tetrapyrrole biosynthetic pathway. Plant Physiology **122,** 1161-1169.

Papenbrock, J., Mishra, S., Mock, H.P., Kruse, E., Schmidt, E.K., Petersmann, A., Braun, H.P., and Grimm, B. (2001). Impaired expression of the plastidic ferrochelatase by antisense RNA synthesis leads to a necrotic phenotype of transformed tobacco plants. Plant Journal **28,** 41-50.

Pazdernik, M., Mares, J., Pilny, J., and Sobotka, R. (2019). The antenna-like domain of the cyanobacterial ferrochelatase can bind chlorophyll and carotenoids in an energy-dissipative configuration. Journal of Biological Chemistry **294,** 11131-11143.

Pilný, J., Kopečná, J., Noda, J., and Sobotka, R. (2015). Detection and quantification of heme and chlorophyll precursors using a High Performance Liquid Chromatography (HPLC) system equipped with two fluorescence detectors. Bio-protocol **5,** e1390.

Price, M.N., Wetmore, K.M., Waters, R.J., Callaghan, M., Ray, J., Liu, H.L., Kuehl, J.V., Melnyk, R.A., Lamson, J.S., Suh, Y., Carlson, H.K., Esquivel, Z., Sadeeshkumar, H., Chakraborty, R., Zane, G.M., Rubin, B.E., Wall, J.D., Visel, A., Bristow, J., Blow, M.J., Arkin, A.P., and Deutschbauer, A.M. (2018). Mutant phenotypes for thousands of bacterial genes of unknown function. Nature **557,** 503-+.

Reisinger, V., Ploscher, M., and Eichacker, L.A. (2008). Lil3 assembles as chlorophyll-binding protein complex during deetiolation. Febs Letters **582,** 1547-1551.

Richter, A., Peter, E., Pors, Y., Lorenzen, S., Grimm, B., and Czarnecki, O. (2010). Rapid Dark Repression of 5-Aminolevulinic Acid Synthesis in Green Barley Leaves. Plant and Cell Physiology **51,** 670-681.

Richter, A.S., and Grimm, B. (2013). Thiol-based redox control of enzymes involved in the tetrapyrrole biosynthesis pathway in plants. Frontiers in Plant Science **4**.

Richter, A.S., Banse, C., and Grimm, B. (2019). The GluTR-binding protein is the heme-binding factor for feedback control of glutamyl-tRNA reductase. Elife **8**.

Richter, A.S., Peter, E., Rothbart, M., Schlicke, H., Toivola, J., Rintamaki, E., and Grimm, B. (2013). Posttranslational Influence of NADPH-Dependent Thioredoxin Reductase C on Enzymes in Tetrapyrrole Synthesis. Plant Physiology **162,** 63-73.

Rinalducci, S., Pedersen, J.Z., and Zolla, L. (2004). Formation of radicals from singlet oxygen produced during photoinhibition of isolated light-harvesting proteins of photosystem II. Biochimica Et Biophysica Acta-Bioenergetics **1608,** 63-73.

Rizzo, M.A., Springer, G.H., Granada, B., and Piston, D.W. (2004). An improved cyan fluorescent protein variant useful for FRET. Nature Biotechnology **22,** 445-449.

Ruban, A.V. (2016). Nonphotochemical Chlorophyll Fluorescence Quenching: Mechanism and Effectiveness in Protecting Plants from Photodamage. Plant Physiology **170,** 1903-1916.

Saini, R.K., Sivanesan, I., and Keum, Y.S. (2019). Emerging Roles of Carotenoids in the Survival and Adaptations of Microbes. Indian Journal of Microbiology **59,** 125-127.

Sawasato, K., Suzuki, S., and Nishiyama, K. (2019). Increased expression of the bacterial glycolipid MPIase is required for efficient protein translocation across membranes in cold conditions. Journal of Biological Chemistry **294,** 8403-8411.

Sawicki, A., Zhou, S.X., Kwiatkowski, K., Luo, M.Z., and Willows, R.D. (2017). 1-N-histidine phosphorylation of ChlD by the AAA(+) ChlI2 stimulates magnesium chelatase activity in chlorophyll synthesis. Biochemical Journal **474,** 2095-2105.

Schagger, H., and Vonjagow, G. (1991). BLUE NATIVE ELECTROPHORESIS FOR ISOLATION OF MEMBRANE-PROTEIN COMPLEXES IN ENZYMATICALLY ACTIVE FORM. Analytical Biochemistry **199,** 223-231.

Shipovskov, S., Karlberg, T., Fodje, M., Hansson, M.D., Ferreira, G.C., Hansson, M., Reimann, C.T., and Al-Karadaghi, S. (2005). Metallation of the transition-state inhibitor N-methyl mesoporphyrin by ferrochelatase: Implications for the catalytic reaction mechanism. Journal of Molecular Biology **352,** 1081-1090.

Shukla, M.K., Llansola-Portoles, M.J., Tichy, M., Pascal, A.A., Robert, B., and Sobotka, R. (2018). Binding of pigments to the cyanobacterial high-light-inducible protein HliC. Photosynthesis Research **137,** 29-39.

Sobotka, R., Komenda, J., Bumba, L., and Tichy, M. (2005). Photosystem II assembly in CP47 mutant of Synechocystis sp PCC 6803 is dependent on the level of chlorophyll precursors regulated by ferrochelatase. Journal of Biological Chemistry **280,** 31595-31602.

Sobotka, R., Tichy, M., Wilde, A., and Hunter, C.N. (2011). Functional Assignments for the Carboxyl-Terminal Domains of the Ferrochelatase from Synechocystis PCC 6803: The CAB Domain Plays a Regulatory Role, and Region II Is Essential for Catalysis. Plant Physiology **155,** 1735-1747.

Sobotka, R., McLean, S., Zuberova, M., Hunter, C.N., and Tichy, M. (2008). The C-terminal extension of ferrochelatase is critical for enzyme activity and for functioning of the tetrapyrrole pathway in synechocystis strain PCC 6803. Journal of Bacteriology **190,** 2086-2095.

Staleva, H., Komenda, J., Shukla, M.K., Slouf, V., Kana, R., Polivka, T., and Sobotka, R. (2015). Mechanism of photoprotection in the cyanobacterial ancestor of plant antenna proteins. Nature Chemical Biology **11,** 287-U296.

Standfuss, R., van Scheltinga, A.C.T., Lamborghini, M., and Kuhlbrandt, W. (2005). Mechanisms of photoprotection and nonphotochemical quenching in pea light-harvesting complex at 2.5A resolution. Embo Journal **24,** 919-928.

Storm, P., Tibiletti, T., Hall, M., and Funk, C. (2013). Refolding and Enzyme Kinetic Studies on the Ferrochelatase of the Cyanobacterium Synechocystis sp. PCC 6803. Plos One **8**.

Storm, P., Hernandez-Prieto, M.A., Eggink, L.L., Hoober, J.K., and Funk, C. (2008). The small CAB-like proteins of Synechocystis sp PCC 6803 bind chlorophyll. Photosynthesis Research **98,** 479-488.

Straskova, A., Knoppova, J., and Komenda, J. (2018). Isolation of the cyanobacterial YFP-tagged photosystem I using GFP-Trap (R). Photosynthetica **56,** 300-305.

Tabrizi, S.T., Sawicki, A., Zhou, S.X., Luo, M.Z., and Willows, R.D. (2016). GUN4-Protoporphyrin IX Is a Singlet Oxygen Generator with Consequences for Plastid Retrograde Signaling. Journal of Biological Chemistry **291,** 8978-8984.

Takagi, D., and Miyake, C. (2018). PROTON GRADIENT REGULATION 5 supports linear electron flow to oxidize photosystem I. Physiologia Plantarum **164,** 337-348.

Takahashi, K., Takabayashi, A., Tanaka, A., and Tanaka, R. (2014). Functional Analysis of Light-harvesting-like Protein 3 (LIL3) and Its Light-harvesting Chlorophyll-binding Motif in Arabidopsis. Journal of Biological Chemistry **289,** 987-999.

Tanaka, R., Rothbart, M., Oka, S., Takabayashi, A., Takahashi, K., Shibata, M., Myouga, F., Motohashi, R., Shinozaki, K., Grimm, B., and Tanaka, A. (2010). LIL3, a light-harvesting-like protein, plays an essential role in chlorophyll and tocopherol biosynthesis. Proceedings of the National Academy of Sciences of the United States of America **107,** 16721-16725.

Tichy, M., and Vermaas, W. (2000). Combinatorial mutagenesis and pseudorevertant analysis to characterize regions in loop E of the CP47 protein in Synechocystis sp PCC 6803. European Journal of Biochemistry **267,** 6296-6301.

Tichy, M., Beckova, M., Kopecna, J., Noda, J., Sobotka, R., and Komenda, J. (2016). Strain of Synechocystis PCC 6803 with Aberrant Assembly of Photosystem NN Contains Tandem Duplication of a Large Chromosomal Region. Frontiers in Plant Science **7**.

Tsai, C.J., Del Sol, A., and Nussinov, R. (2009). Protein allostery, signal transmission and dynamics: a classification scheme of allosteric mechanisms. Molecular Biosystems **5,** 207-216.

Vavilin, D., and Vermaas, W. (2007). Continuous chlorophyll degradation accompanied by chlorophyllide and phytol reutilization for chlorophyll synthesis in Synechocystis sp PCC 6803. Biochimica Et Biophysica Acta-Bioenergetics **1767,** 920-929.

Verdecia, M.A., Larkin, R.M., Ferrer, J.L., Riek, R., Chory, J., and Noel, J.P. (2005). Structure of the Mg-chelatase cofactor GUN4 reveals a novel hand-shaped fold for porphyrin binding. Plos Biology **3,** 777-789.

Viklund, H., and Elofsson, A. (2008). OCTOPUS: improving topology prediction by two-track ANN-based preference scores and an extended topological grammar. Bioinformatics **24,** 1662-1668.

Wang, L.Y., Elliott, M., and Elliott, T. (1999). Conditional stability of the HemA protein (glutamyl-tRNA reductase) regulates heme biosynthesis in Salmonella typhimurium. Journal of Bacteriology **181,** 1211-1219.

Wei, X.P., Su, X.D., Cao, P., Liu, X.Y., Chang, W.R., Li, M., Zhang, X.Z., and Liu, Z.F. (2016). Structure of spinach photosystem II-LHCII supercomplex at 3.2 angstrom resolution. Nature **534,** 69-+.

Zhao, A.G., Fang, Y., Chen, X.M., Zhao, S., Dong, W., Lin, Y.J., Gong, W.M., and Liu, L. (2014). Crystal structure of Arabidopsis glutamyl-tRNA reductase in complex with its stimulator protein. Proceedings of the National Academy of Sciences of the United States of America **111,** 6630-6635.

Zhou, F., Wang, C.Y., Gutensohn, M., Jiang, L., Zhang, P., Zhang, D.B., Dudareva, N., and Lu, S. (2017). A recruiting protein of geranylgeranyl diphosphate synthase controls metabolic flux toward chlorophyll biosynthesis in rice. Proceedings of the National Academy of Sciences of the United States of America **114,** 6866-6871.

Zoschke, R., Chotewutmontri, P., and Barkan, A. (2017). Translation and Co-translational Membrane Engagement of Plastid-encoded Chlorophyll-binding Proteins Are Not Influenced by Chlorophyll Availability in Maize. Frontiers in Plant Science **8**.

8. Appendix

8.1 Primers used in this study

Ara1	CTAGAGGCGGCCGCAGTTATCTCCGATGCCATTTCC
Ara2	GAGATCAGATCTTTATAAGGAAGGCAAGATGCC
Ara3	TTGTCATCCTCGACTGTGC
Ara4	AGCTAATTACGATGCCGG
Hemh1	GCCATCTATTGTTACACTTG
Hemh2	GATCTTGACACTGCGTTAGG
Cit1	CTAGAGGGTACCGGTCGTGTTGGGGTCTTACTG
Cit2	CAGGAGCTGCAGCTAAAGCAAGCCGACAAAATG
Cit3	GCCATCTATTGTTACACTTG
Cit4	CCAAAGCTATGTGGATGAAGC
Zeo1	GACGATCTATTGGTGGTGCC
Zeo2	CATCAATTGGAGGAAGCCTG
Chl3	CTAGAGCATATGGGTCGTGTTGGGGTCTTA
Chl4	CAGGAGCTGCAGCTAAAGCAAGCCGACAAAATG
Chl5	GACGATCTATTGGTGGTGCC
Chl6	AACGGGCAAAATTAGGGC

8.2 Biological (BR) and technical (TR) replicates of crosslink candidate between FeCh (K337-E345) and CurT (Y125-K131)

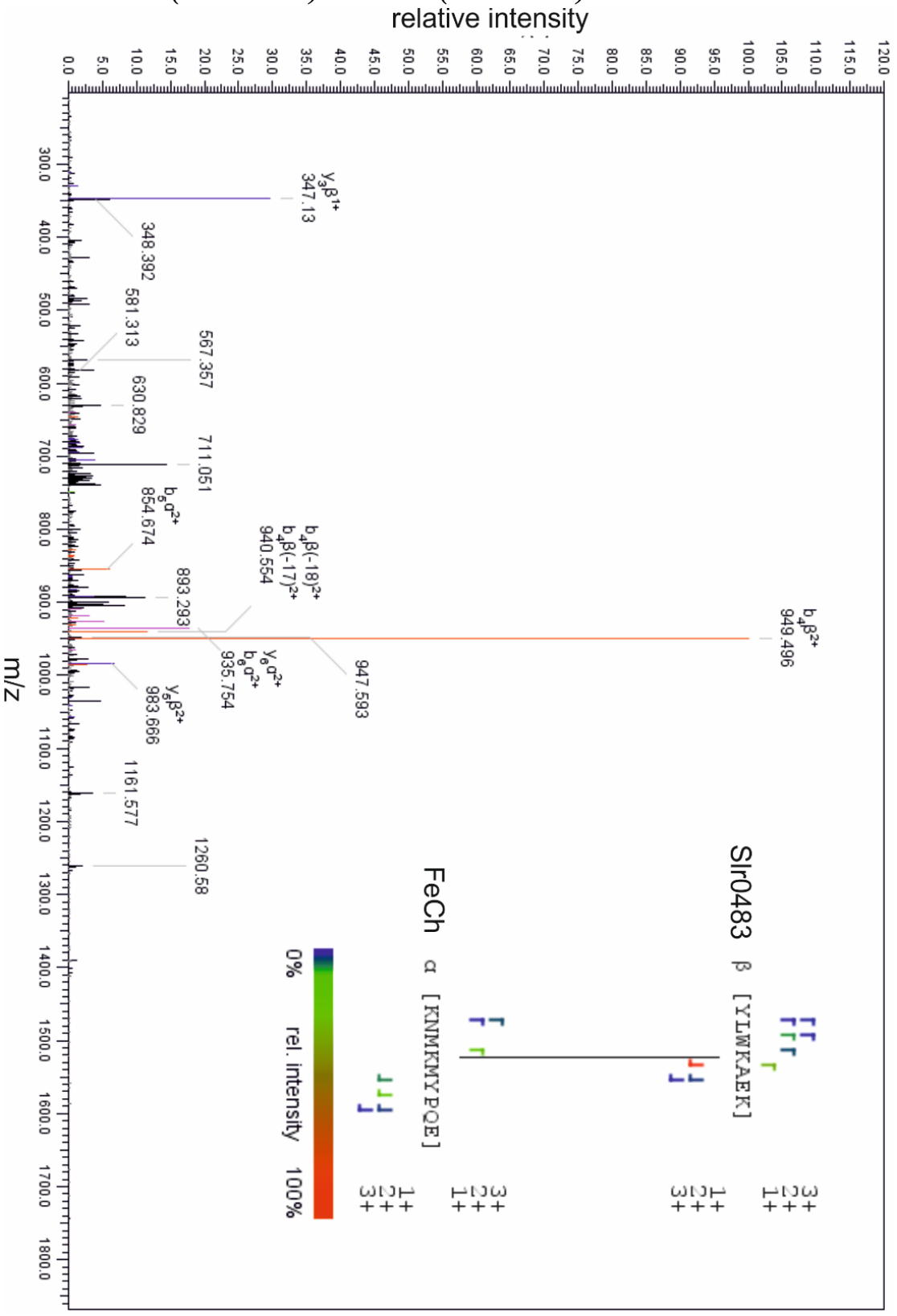

BR-1 TR-2 BS^3, FeCh 337-345 - Slr0483 125-131

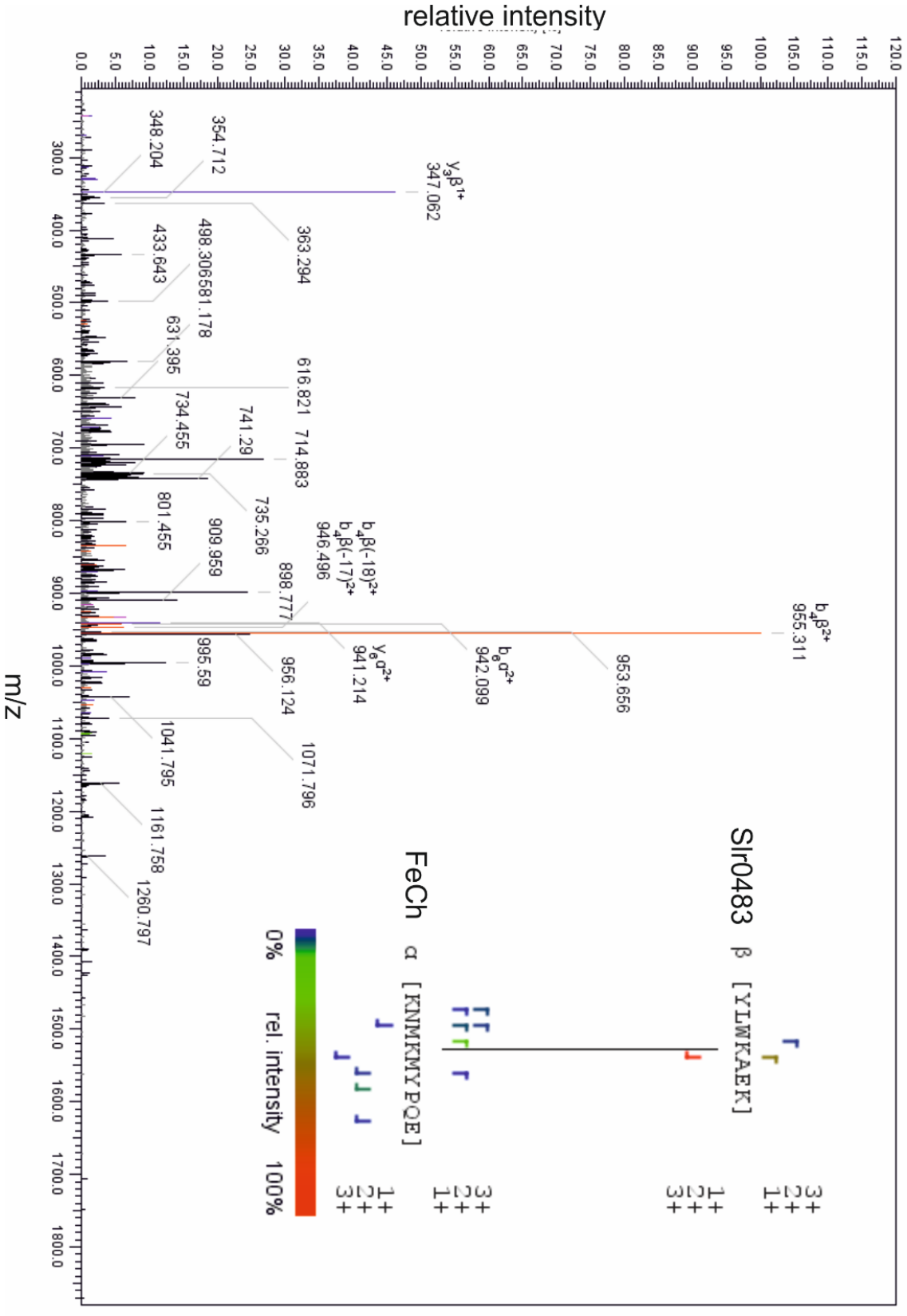

BR-1 TR-2 BS^3(deuter) , FeCh 337-345 - Slr0483 125-131

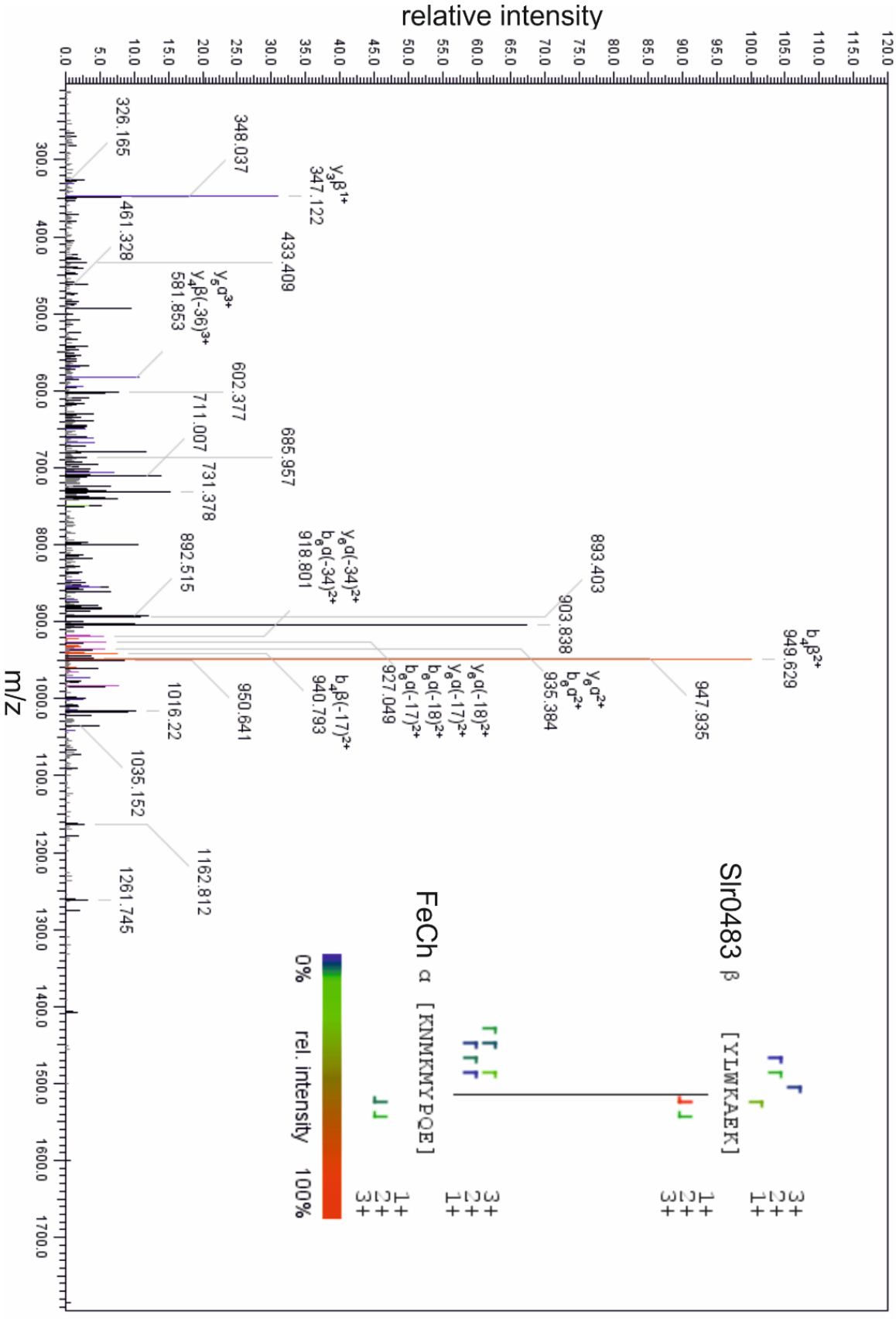

BR-2 TR-1 BS^3, FeCh 337-345 - Slr0483 125-131

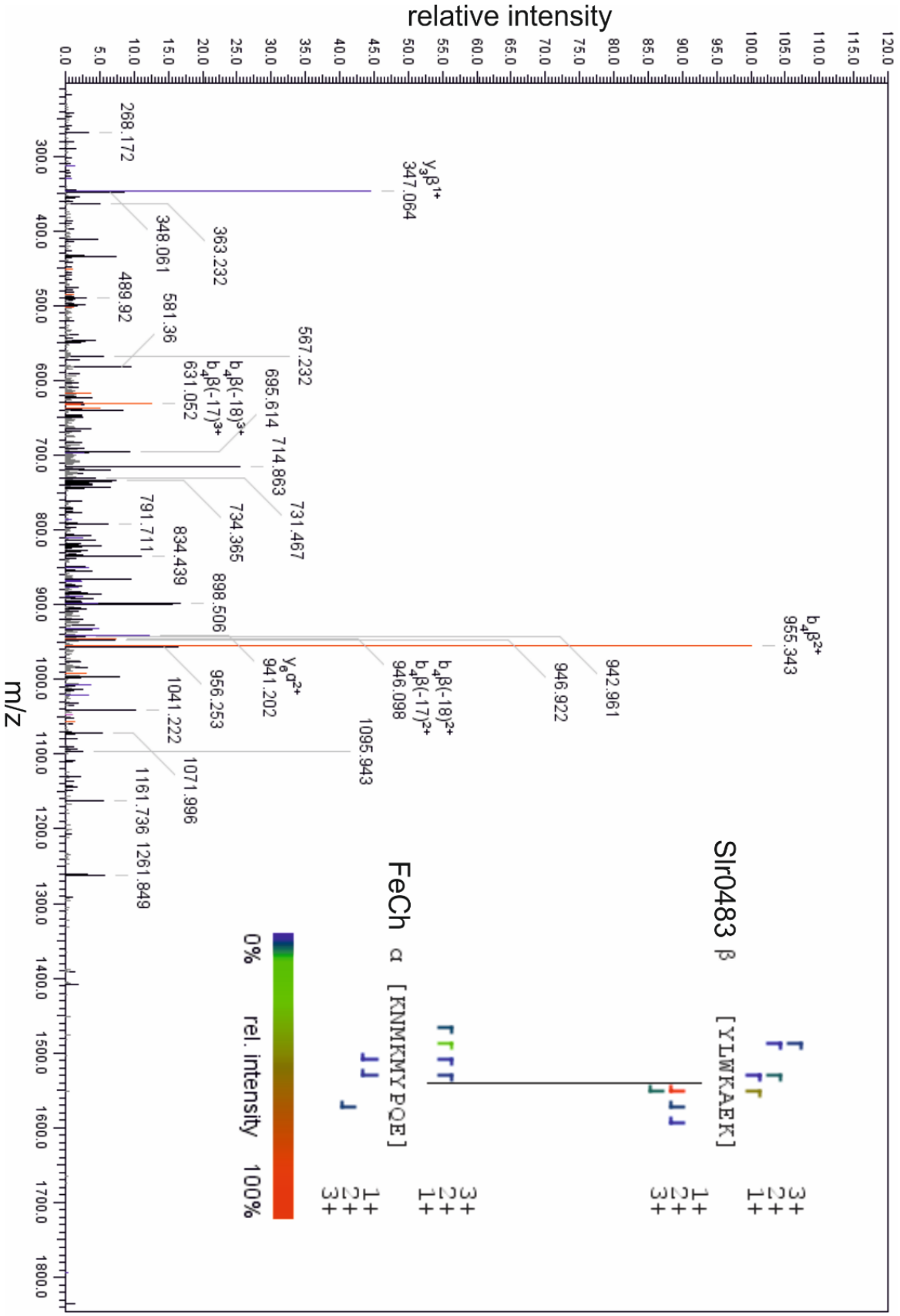

BR-2 TR-1 BS^3(deuter) , FeCh 337-345 - Slr0483 125-131

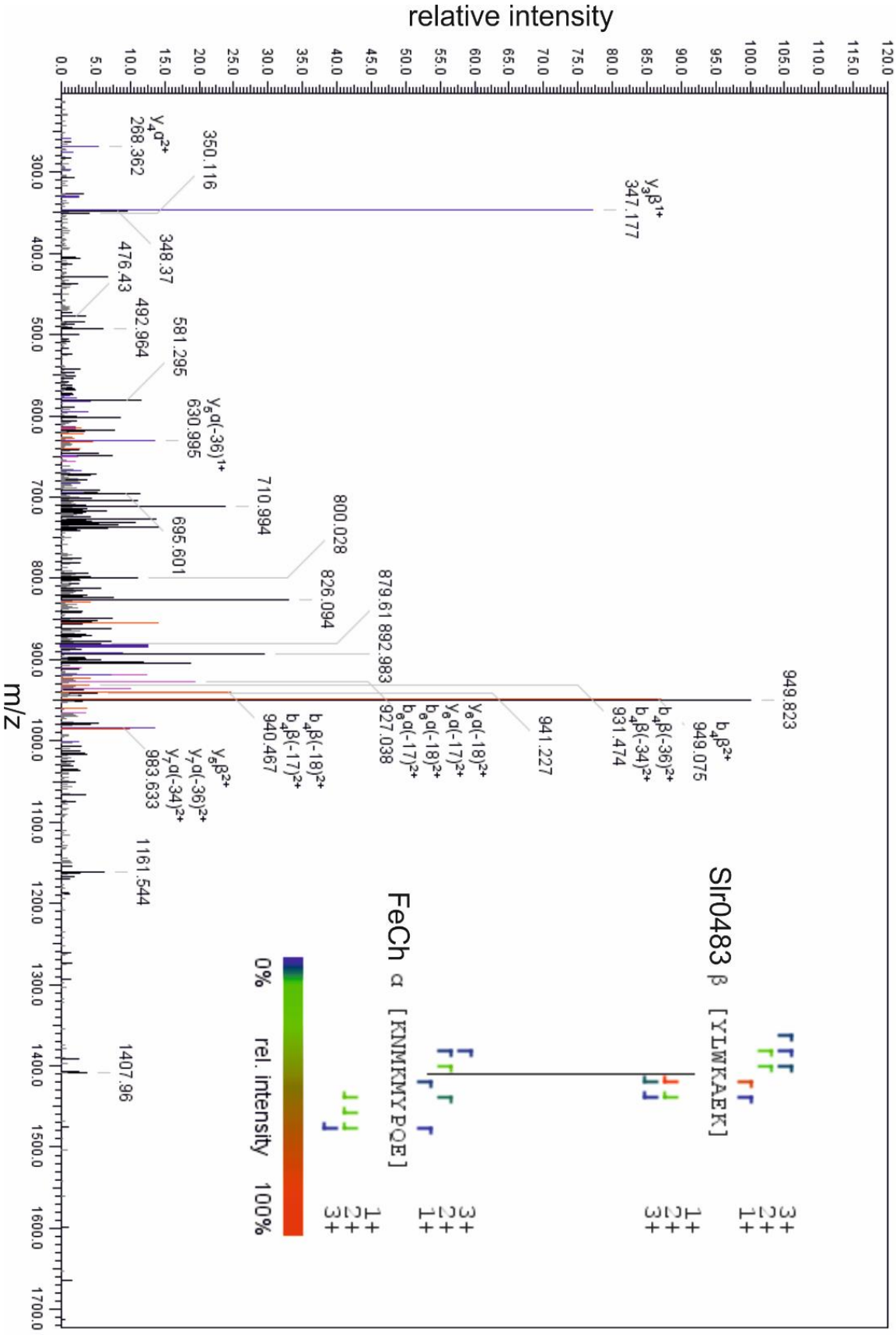

BR-2 TR-2 BS[3], FeCh 337-345 - Slr0483 125-131

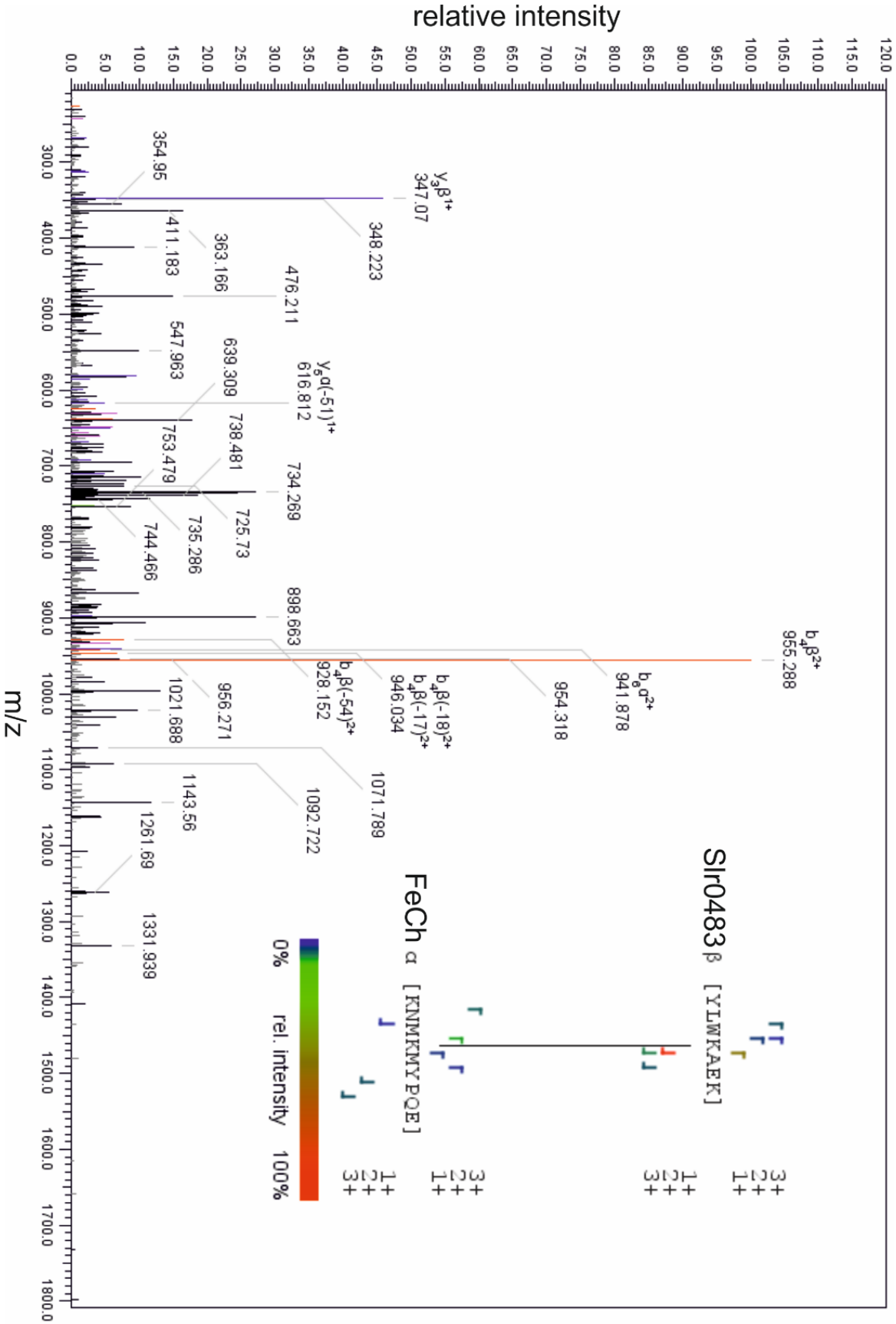

BR-2 TR-2 BS^3(deuter) , FeCh 337-345 - Slr0483 125-131

8.3 Sequences of inserted genes

3xFlag-Arabidopsis FeCh2 (*f.ara-hemH*), yellow = 3xFlag

ATGGATTACAAAGATGATGATGATAAAGATTACAAAGATGATGATGATAAAGATTACAAAGATGATGATG
ATAAAGCGGCCGCAGTTATCTCCGATGCCATTTCCTCCTCCTCCGTTATCACCGATGATGCCAAAATTGG
TGTCTTGTTATTAAACCTTGGCGGTCCTGAGACCTTAGATGATGTACAACCCTTTTTGTTTAACCTCTTC
GCCGACCCGGACATTATTCGGTTGCCGCCGGTATTCCAGTTTCTTCAGAAGCCATTAGCCCAGTTTATTT
CAGTAGCCCGCGCCCCCAAAAGCAAGGAAGGCTATGCCTCCATTGGTGGGGGTTCTCCTCTTCGGCACAT
TACCGATGCCCAGGCCGAAGAATTACGGAAATGCCTTTGGGAAAAAAATGTACCAGCCAAGGTATATGTT
GGTATGCGGTATTGGCATCCATTCACCGAGGAAGCCATTGAACAGATTAAACGGGATGGAATTACAAAAC
TAGTTGTTCTACCACTTTATCCTCAATTTTCTATTTCCACCAGTGGTTCCAGCCTACGGCTCTTGGAGCG
GATTTTTCGGGAGGACGAGTATCTTGTTAACATGCAACATACTGTTATTCCATCCTGGTATCAGCGGGAG
GGCTATATTAAGGCCATGGCCAATCTAATCCAAAGCGAGTTGGGCAAATTTGGTTCTCCTAATCAGACCT
GCTTCAAACCAAAATATATGTTACAGGTTGTAATTTTTTTCAGTGCCCATGGCGTGCCTCTTGCCTATGT
CGAAGAAGCCGGTGATCCTTACAAGGCCGAGATGGAAGAATGTGTTGATCTAATCATGGAGGAATTAGAC
AAGCGGAAGATTACCAATGCCTACACCCTTGCCTATCAGAGCCGGGTTGGCCCAGTTGAATGGCTGAAAC
CATACACCGAAGAAGCCATTACCGAACTTGGTAAAAAAGGTGTTGAAAATCTTCTGGCCGTACCCATTAG
TTTTGTGAGCGAGCACATTGAAACCCTGGAGGAGATTGATGTTGAGTATAAAGAGTTGGCCTTGAAGTCT
GGTATCAAAAACTGGGGGCGGGTACCTGCCCTAGGAACCGAACCTATGTTTATTTCTGACTTGGCCGATG
CCGTTGTGGAAAGTCTTCCATACGTTGGTGCCATGGCCGTCTCAAACCTTGAAGCCCGGCAGTCCTTAGT
TCCGCTCGGGAGTGTAGAAGAATTATTAGCCACGTATGATTCCCAGCGGCGGGAGTTACCAGCCCCGGTG
ACCATGTGGGAATGGGGCTGGACAAAAAGTGCCGAAACCTGGAACGGCCGGGCCGCCATGTTAGCCGTGC
TAGCCCTCTTGGTGCTCGAAGTCACCACCGGCAAAGGGTTTCTGCATCAGTGGGGCATCTTGCCTTCCTT
ATAA

Citrine-FeCh (*citrine-hemH*), yellow = citrine, cyan = FeCh

ATGGTGAGCAAGGGCGAGGAGCTGTTCACCGGGGTGGTGCCCATCCTGGTCGAGCTGGACGGCGACGTAA
ACGGCCACAAGTTCAGCGTGTCCGGCGAGGGCGAGGGCGATGCCACCTACGGCAAGCTGACCCTGAAGTT
CATCTGCACCACCGGCAAGCTGCCCGTGCCCTGGCCCACCCTCGTGACCACCTTCGGCTACGGCCTGATG
TGCTTCGCCCGCTACCCCGACCACATGAAGCAGCACGACTTCTTCAAGTCCGCCATGCCCGAAGGCTACG
TCCAGGAGCGCACCATCTTCTTCAAGGACGACGGCAACTACAAGACCCGCGCCGAGGTGAAGTTCGAGGG
CGACACCCTGGTGAACCGCATCGAGCTGAAGGGCATCGACTTCAAGGAGGACGGCAACATCCTGGGGCAC
AAGCTGGAGTACAACTACAACAGCCACAACGTCTATATCATGGCCGACAAGCAGAAGAACGGCATCAAGG
TGAACTTCAAGATCCGCCACAACATCGAGGACGGCAGCGTGCAGCTCGCCGACCACTACCAGCAGAACAC
CCCCATCGGCGACGGCCCCGTGCTGCTGCCCGACAACCACTACCTGAGCTACCAGTCCGCCCTGAGCAAA
GACCCCAACGAGAAGCGCGATCACATGGTCCTGCTGGAGTTCGTGACCGCCGCCGGGATCACTCTCGGCA
TGGACGAGCTGTACAAGGGCGGTACCGGTCGTGTTGGGGTCTTACTGCTAAATCTTGGCGGACCGGAGAA
GTTAGAGGATGTACGCCCCTTCCTTTTTAACCTGTTTGCGGATCCGGAAATCATTCGTCTCCCTTTTCCT
TGGTTGCAAAAACCCCTGGCATGGCTGATTTCTACCCTACGGGCGAAAAAATCCCAGGCCAACTACGCCG
AAATCGGTGGTGGTTCCCCCCTGTTGCAGATTACCGAAGCCCAAGCCTCCGCCCTCACGACCCGTCTGGA
ACGCCTTGGCCAGGATGCAAAAGTGTACATTGGCATGCGCTACTGGCACCCCTTTACGGAGGAAGCCGTC
GAAAAAATTAAAGGCGATCGCCTGCAACGGCTGGTGATTTTGCCTCTATATCCCCATTTTTCCATTAGCA
CTAGCGGCTCCAGTTTCCGGGTGTTGGAGGAAATGTGGCATAACGACCCCAGTTTGCGGCAATTGGACTA
TAGCCTGATCCCCTCTTGGTACGACCATCCGGGCTATCTCCAGGCCATGGCGGATTTGATTGCTCAAGAA
TTAAAGAAATTCCCCAATCCAGACCAAGCCCATATTTTCTTCAGTGCCCACGGTGTGCCCCAAAGCTATG
TGGATGAAGCGGGAGACCCCTACCAGGCAGAAATTGAAGCCTGTACCCGTTTGATAATGCGGACTCTCGA
TCGTCCGAACCAATACACGTTGGCCTACCAAAGTCGGGTGGGGCCAGTGGAATGGCTCAAGCCCTACACG
GAAGAAGCTCTGCAAAAACTGGGGGCGGAGGGCATTGACGATCTATTGGTGGTGCCCATTAGCTTTGTGT

CAGAACATATTGAAACCCTCCAGGAAATTGACATCGAGTATCGGGAAATTGCCGAAGAAGCCGGCATTGA
TAATTTTCAGCGGGTACCGGCCCTAAACACCCATCCAGTTTTCATCGACGCCTTGGCCCAGATGGTGATG
GATTCCCTCAACGATCCTCCCTGCACCTTTGAAACGGTGCCCCATCCCAAAAAGAACATGAAAATGTATC
CCCAGGAAAGATGGGAATGGGGTTTGACTACGGCGGCGGAAGTATGGAATGGTCGCCTCGCCATGTTGGG
TTTCATTGCCCTGTTGGTGGAGTTGATCAGCGGCCAGGGCCCGTTGCATTTTGTCGGCTTGCTTTAG

8.4 Published data

The antenna-like domain of the cyanobacterial ferrochelatase can bind chlorophyll and carotenoids in an energy-dissipative configuration

Pazderník, M., Mares, J., Pilny, J., and Sobotka, R. (2019)

Journal of Biological Chemistry 294, 11131-11143

JBC ARTICLE

The antenna-like domain of the cyanobacterial ferrochelatase can bind chlorophyll and carotenoids in an energy-dissipative configuration

Received for publication, March 13, 2019, and in revised form, May 29, 2019 Published, Papers in Press, June 5, 2019, DOI 10.1074/jbc.RA119.008434

Marek Pazderník[‡§], Jan Mareš[‡§¶], Jan Pilný[‡], and Roman Sobotka[‡§1]

From the [‡]Institute of Microbiology, Czech Academy of Sciences, Centre Algatech, Třeboň, 379 81, Czech Republic, the [§]Faculty of Science, University of South Bohemia, České Budějovice 370 05, Czech Republic, and [¶]Institute of Hydrobiology, Biology Centre of the Czech Academy of Sciences, České Budějovice 370 05, Czech Republic

Edited by Chris Whitfield

Ferrochelatase (FeCh) is an essential enzyme catalyzing the synthesis of heme. Interestingly, in cyanobacteria, algae, and plants, FeCh possesses a conserved transmembrane chlorophyll *a*/*b* binding (CAB) domain that resembles the first and the third helix of light-harvesting complexes, including a chlorophyll-binding motif. Whether the FeCh CAB domain also binds chlorophyll is unknown. Here, using biochemical and radiolabeled precursor experiments, we found that partially inhibited activity of FeCh in the cyanobacterium *Synechocystis* PCC 6803 leads to overproduction of chlorophyll molecules that accumulate in the thylakoid membrane and, together with carotenoids, bind to FeCh. We observed that pigments bound to purified FeCh are organized in an energy-dissipative conformation and further show that FeCh can exist *in vivo* as a monomer or a dimer depending on its own activity. However, pigmented FeCh was purified exclusively as a dimer. Separately expressed and purified FeCH CAB domain contained a pigment composition similar to that of full-length FeCh and retained its quenching properties. Phylogenetic analysis suggested that the CAB domain was acquired by a fusion between FeCh and a single-helix, high light-inducible protein early in the evolution of cyanobacteria. Following this fusion, the FeCh CAB domain with a functional chlorophyll-binding motif was retained in all currently known cyanobacterial genomes except for a single lineage of endosymbiotic cyanobacteria. Our findings indicate that FeCh from *Synechocystis* exists mostly as a pigment-free monomer in cells but can dimerize, in which case its CAB domain creates a functional pigment-binding segment organized in an energy-dissipating configuration.

Heme is an essential cofactor for virtually all forms of life, and it is produced by a conserved tetrapyrrole pathway. The last step of heme biosynthesis is catalyzed by ferrochelatase (FeCh; protoheme ferro-lyase, EC 4.99.1.1),[2] which inserts iron into protoporphyrin IX (PPIX), a metal-free tetrapyrrole ring. Apart from serving as a cofactor for a myriad of redox and sensor proteins and as a precursor for the synthesis of bilins, heme is also a crucial regulatory molecule (1). Among many other recognized regulatory functions, heme availability controls total metabolite flow through the tetrapyrrole pathway. This heme feedback loop, although not fully understood, seems to operate universally from unicellular bacteria to animals (mitochondria) and plants (plastids) (2–4).

In photosynthetic organisms, regulation of the tetrapyrrole pathway is more complicated, because PPIX is also a substrate for magnesium chelatase, which diverts PPIX toward the chlorophyll (Chl) branch (Fig. S1*A*) (4). Considering the general phototoxicity of tetrapyrroles, there must be regulatory mechanisms to prevent an overproduction of one of the tetrapyrrole products at the expense of the others or a harmful accumulation of intermediates. Thus, in Chl producing organisms, the activity of FeCh not only just controls a regulatory pool of heme but also competes with magnesium chelatase for PPIX, the last common substrate of both the heme and Chl branches. Indeed, the activity of FeCh has been shown to be crucial for the regulation of the tetrapyrrole pathway in both plants and cyanobacteria; an impairment of FeCh causes a massive accumulation of PPIX (5, 6). In contrast, low activity of magnesium chelatase resulted in a total down-regulation of the pathway but not in the accumulation of PPIX (7–9).

Interestingly, a unique feature of the FeCh enzymes of Chl-producing organisms is a conserved C-terminal transmembrane helix that resembles the first and third helix of light-harvesting complex (LHC) proteins including a Chl-binding motif (the so-called LHC or CAB domain; Fig. 1 and Fig. S1*B*). The FeCh in oxygenic phototrophs is thus the only known enzyme belonging to the LHC protein superfamily, a large and diverse group of proteins characterized by the presence of at

This work was supported by Czech Science Foundation Grant 17-08755S and Czech Ministry of Education Project LO1416. This work was also supported by University of South Bohemia Grant 04-026/2017 (to M. P.). The authors declare that they have no conflicts of interest with the contents of this article.

This article contains Table S1 and Figs. S1–S7.

[1] To whom correspondence should be addressed: Institute of Microbiology, Czech Academy of Sciences, Centre Algatech, Novohradská 237, Opatovický mlýn, 37981 Třeboň, Czech Republic. Tel.: 420384340491; E-mail: sobotka@alga.cz.

[2] The abbreviations used are: used are: FeCh, ferrochelatase; Chl, chlorophyll; MPP, *N*-methyl mesoporphyrin; CAB, chlorophyll *a*/*b*– binding; DDM, *n*-dodecyl β-D-maltoside; LHC, light-harvesting complex; Hlip, high light–inducible protein; ELIP, early light–inducible protein; PPIX, protoporphyrin IX; MV/DV Pchlide, monovinyl/divinyl protochlorophyllide; OHP, one-helix protein; SEC, size-exclusion chromatography; PSI, photosystem I; β-car, β-carotene; BN/SDS-PAGE, blue-native/SDS polyacrylamide gel electrophoresis; HS, high-salt; BI, Bayesian inference; RCF, relative centrifugal force.

© 2019 Pazderník et al. Published under exclusive license by The American Society for Biochemistry and Molecular Biology, Inc.

Downloaded from http://www.jbc.org/ at Institute of Physiology AS CR on July 24, 2019

least one LHC/CAB-domain. Apart from light-harvesting antennas, the superfamily includes LHC-like proteins that are apparently not involved in light harvesting but rather have regulatory or photoprotective functions (10–15). Cyanobacterial LHC-like proteins are limited to the single-helix high light-inducible proteins (Hlips) and FeCh, but in algae and plants, the spectrum of these proteins is much broader. Apart from FeCh and the homologs of Hlips called one-helix proteins (OHPs), eukaryotes possess various two- and three-helix LHC-like proteins such as Lil3 proteins, early light-inducible proteins (ELIPs), and Psb33 (16–21). ELIPs, Lil3s, and Hlips were already reported to bind Chl and carotenoids *in vivo* (22–25). Based on the known structure of various LHC proteins (26, 27), it is expected that two helices, each containing an LHC/CAB motif, must dimerize to create a functional Chl-binding site (25).

The function of the FeCh CAB domain has been previously addressed by genetic and biochemical approaches (28–30); however, its role remains unclear. The CAB domain is connected to the catalytic part of FeCh via a variable linker (Fig. 1), and in the cyanobacterium *Synechocystis* PCC 6803 (hereafter *Synechocystis*), the FeCh enzyme lacking both the LHC domain and the linker still appeared to be fairly active but was unstable, and its accumulation in the cell was impaired (6). A truncation preserving the linker but eliminating the CAB domain yields an active and stable enzyme (29, 30). Such a truncated enzyme is, however, strictly monomeric, whereas the full-length enzyme can dimerize, at least *in vitro* (29, 30). In addition, a *Synechocystis* strain expressing FeCh without the CAB domain was sensitive to high light conditions (29).

In this work, we demonstrate that *Synechocystis* FeCh is present in the cell mostly as a pigment-less monomer but can conditionally dimerize, and in such cases, its CAB domain creates a functional pigment-binding segment. Interestingly, the Chl and carotenoids bound to the CAB domain are organized in an energy-dissipative configuration, as previously reported for Hlips (24). This is consistent with our phylogenetic analysis, suggesting that the FeCh CAB domain originates from a fusion between an ancient Hlip and FeCh enzyme early in cyanobacterial evolution.

Results

Partially inhibited FeCh binds Chl and carotenoids

To address the longstanding question of whether the FeCh enzyme in oxygenic phototrophs can bind Chl, we affinity-purified a 3×FLAG-tagged version of FeCh (f.FeCh; Fig. 1) ectopically expressed in a *Synechocystis* strain with the original *hemH* gene deleted (29). The obtained eluate was further separated by size-exclusion chromatography (SEC), and the Chl absorbance was measured by a diode-array detector. However, the only detectable Chl in the eluate comigrated with traces of photosystem I complexes (PSI) and with detergent micelles (DDM), but not with the purified f.FeCh (Fig. 2*A*). The FeCh, migrating close to DDM micelles, was the only protein detectable on the stained gel after the separation of all fractions collected from the SEC column (Fig. S2). It should be noted that PSI complexes are extremely Chl-rich (90 Chl molecules per monomeric PSI),

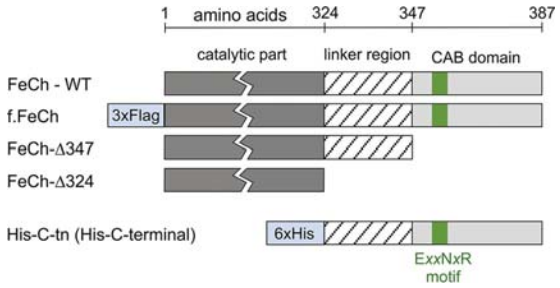

Figure 1. A schematic presentation of the FLAG-tagged and truncated *Synechocystis* FeCh proteins used in this study and the His-tagged C-terminal part of FeCh (His-C-tn protein) that possesses the FeCh linker and the CAB domain. The highly conserved Chl-binding motif (E*XX*N*X*R), which is characteristic for the whole LHC protein family, is also indicated.

and thus their Chl absorbance is typically detectable even if the level of PSI protein subunits is below the detection limit of our protein stain (compare Fig. 1*A* and Fig. S2). We hypothesized that the FeCh could only bind (sense) Chl molecules if there was an abnormally large pool of unbound "free" Chl in the thylakoid membranes. Low FeCh activity in *Synechocystis* was previously shown to up-regulate the levels of Chl precursors (6, 31); however, whether such up-regulation leads to an accumulation of free Chl molecules in the membrane was not known.

To clarify this point we treated the *Synechocystis* cells with a specific FeCh inhibitor, *N*-methyl mesoporphyrin IX (MPP) (32). After 4 h of the MPP treatment, the cells were fed with ^{14}C-labeled glutamate to follow the rate of *de novo* Chl formation. The concentration of MPP (275 nM) was not significantly toxic to *Synechocystis* under our standard conditions, because the proliferation rate of the cells treated with this concentration of MPP for 24 h was only 6% slower than that of untreated cells (Fig. S3). However, the partial FeCh inhibition significantly accelerated Chl biosynthesis compared with untreated cells (Fig. 3, *A* and *B*). Further, to assess the amount of free (or loosely bound) Chl in the cell, the membrane fraction was isolated after 4 h of MPP-treatment and separated by clear-native electrophoresis. In the case of MPP-treated cells, the Chl fluorescence detected in the zone of free pigments (DDM micelles) was more than doubled than in untreated control (Fig. 4, *A* and *B*). We eluted and quantified pigments from this part of the gel, and the content of Chl correlated well with the fluorescence measurement (Fig. 4*B*). According to these results, ~0.7% of the total Chl loaded on the clear-native gel comigrated with DDM micelles, and this amount is roughly doubled after treatment with MPP (Fig. 4*B*). Given these results, we concluded that decreased FeCh activity results in excess production of Chl in the cell.

Notably, when we purified f.FeCh from the cells treated with MPP, it eluted from the SEC column as a higher-mass protein complex than when it was purified from cells without the inhibitor. Moreover, a peak of Chl absorbance (675 nm) clearly comigrated with the f.FeCh (Fig. 2*B*), and the absorbance spectrum of the f.FeCh peak (450–500 nm region; Fig. 2*C*) also signaled the presence of carotenoids. We extracted pigments from the collected f.FeCh peak and separated the extract by HPLC, which revealed a complex mixture of carotenoids in addition to Chl molecules. β-Carotene (β-car) was the most abundant

Downloaded from http://www.jbc.org/ at Institute of Physiology AS CR on July 24, 2019

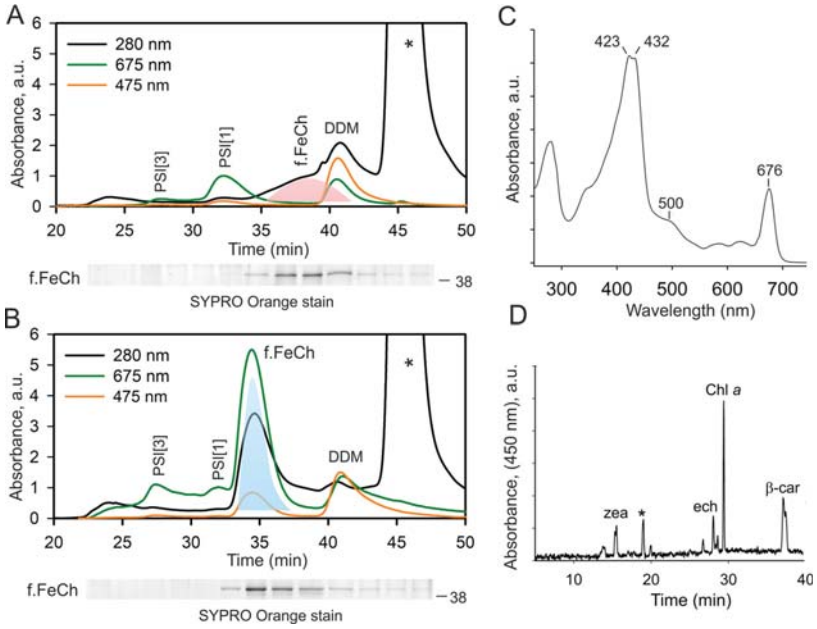

Figure 2. Synechocystis FeCh binds Chl and carotenoids when its enzymatic activity is low. *A*, SEC separation of f.FeCh purified from *Synechocystis* cells. Chl, carotenoids, and UV absorptions were recorded by a diode-array detector; minute fractions were collected and separated by SDS-electrophoresis, and f.FeCh protein was stained by SYPRO Orange (below SEC chromatogram, see Fig. S2 for full-sized gel pictures). The peak of f.FeCh is highlighted by *pink shading*. The *asterisk* marks the absorption of the 3×FLAG peptide used to elute the f.FeCh protein from the anti-FLAG gel; DDM marks detergent micelles containing Chl molecules. *PSI[3]* and *PSI[1]* indicate Chl bound to traces of trimeric and monomeric photosystem I, respectively. *B*, SEC separation of f.FeCh purified from *Synechocystis* cells treated for 4 h with a specific FeCh inhibitor (MPP). The f.FeCh peak, highlighted by *cyan shading*, was collected for pigment analysis. *C*, absorbance spectrum of the pigmented form of f.FeCh; the unusually high absorbance in the region of 415–435 nm is due to the MPP bound to f.FeCh (see Fig. S4 for an HPLC analysis). *D*, pigments were extracted by methanol from the collected f.FeCh peak (*B*) and separated on a C18 column. *Zea*, *ech*, and *β-car* denote zeaxanthin, echinenone and, *β*-carotene, respectively. An *asterisk* indicates an unknown carotenoid species.

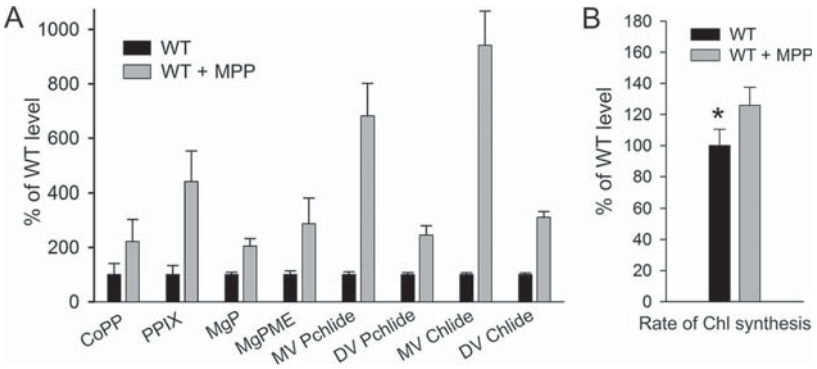

Figure 3. Low activity of FeCh accelerates the *de novo* synthesis of Chl molecules. *A*, tetrapyrrolic Chl precursors were extracted from WT and from WT cells treated for 4 h with MPP and separated using HPLC. Individual precursor species were detected and quantified using two fluorescence detectors essentially as described in Ref. 68. *Error bars* show the S.D., $n = 3$ independent experiments. *CoPP*, coproporphyrin III; *MgP*, magnesium protoporphyrin IX; *MgPME*, magnesium protoporphyrin IX monomethyl ester; *MV/DV Pchlide*, monovinyl/divinyl protochlorophyllide; *MV/DV Chlide*, monovinyl/divinyl chlorophyllide. *B*, WT control cells and cells treated with MPP for 3.5 h were supplemented with radiolabeled ^{14}C[Glu]. After 60 min-pulse, pigments were extracted by methanol and separated on an HPLC equipped with a diode-array detector and a flow scintillation detector. The rate of Chl synthesis was quantified as the ratio of Chl absorbance and radioactivity peaks. *Error bars* show the S.D., $n = 4$ independent experiments. *, $p = 0.029$; Student's *t* test.

carotenoid but zeaxanthin, echinenone, and an unknown carotenoid species were present as well (Fig. 2*D*). We also found MPP bound to f.FeCh, which explains the high absorbance of f.FeCh in the blue spectral region (Fig. 2*C* and Fig. S4). By recording Chl fluorescence during SEC, we discovered that the fluorescence of Chl molecules bound to f.FeCh is quenched: the fluorescence yield of Chl was only ~14% when compared with the fluorescence of Chl molecules in detergent micelles (Fig. 5). From these observations, we conclude that the *Synechocystis* FeCh possesses a functional Chl and carotenoid-binding motif, which coordinates pigments in an energy-dissipative configuration.

The pigment-binding form of FeCh is a homodimer

Based on the elution time from the SEC column, the apparent mass of f.FeCh was greater after incubation with MPP (Fig. 2, *A* and *B*). However, on the stained gel, we detected no other proteins except f.FeCh (Fig. S2), which implies the formation of a

Downloaded from http://www.jbc.org/ at Institute of Physiology AS CR on July 24, 2019

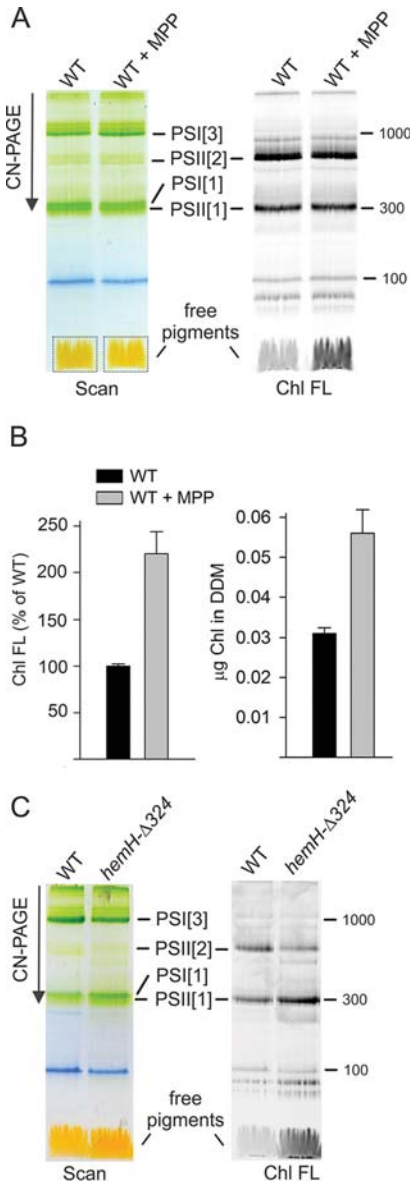

Figure 4. Oversynthesized Chl accumulates in thylakoid membranes. *A*, membrane complexes prepared from WT and from WT treated for 4 h with MPP were separated by clear native electrophoresis on 4–12% acrylamide gel and scanned (*left panel*); 4 μg of Chl was loaded per each sample. Chl fluorescence (*right panel*, *Chl FL*) in the gel was detected after excitation with blue light. *PSI[1]* and *PSI[3]*, monomeric and trimeric photosystem I, respectively. *PSII[1]* and *PSII[2]*, monomeric and dimeric photosystem II, respectively. Pigments migrating in gel with DDM micelles are indicated by *dotted boxes*. *B*, Chl fluorescence in the gel region marked by *dotted boxes* in *A* was quantified. This part of gel was further cut, the pigments were eluted by repeated incubation in an elution buffer containing DDM (see "Experimental procedures"), and the Chl content was quantified by HPLC. *Error bars* show S.D., $n = 3$ independent experiments. *C*, membrane complexes prepared from WT and *hemH-Δ324* mutant were separated by clear native electrophoresis, and Chl fluorescence was detected as described for *A*.

f.FeCh oligomer. According to the known structure of LHCII (33) and a structural model of Hlips (24, 25), two LHC/CAB domains should dimerize to create a canonical 4-Chls and 2-carotenoid binding motif. The observed shift in f.FeCh mobility suggests that the capability of the *Synechocystis* FeCh to bind Chl is related to its dimerization. To exclude the possibility that the f.FeCh oligomerization is an artifact of protein purification or its tagging, we separated *Synechocystis* membrane complexes by SEC and immunodetected FeCh in the collected minute fractions. A similar shift in the mass of FeCh was detected in membranes from WT cells: MPP treatment resulted in a higher-mass FeCh complex (Fig. 6*A*). According to the column calibration (Fig. S5), this shift corresponds to 50 kDa, which is very close to the shift expected for the presence of a FeCh dimer. Therefore, the discrepancy (~2 min) in the elution times of FeCh and f.FeCh from the SEC column is most likely because of the presence of the highly charged 3×FLAG tag.

To verify the inducible FeCh dimerization by an independent approach, we separated WT membrane proteins by 2D blue-native/SDS electrophoresis (BN/SDS-PAGE), blotted, and immunodetected FeCh. Although the FeCh pattern was a bit smeared, after treatment with MPP, it was evident that a new spot corresponding to a size of a FeCh dimer appeared (Fig. 6*B*). We repeated the same experiment using membranes isolated from the *Synechocystis hemH*-Δ347 strain containing FeCh without the CAB domain (Fig. 1) (29). As expected, the FeCh-Δ347 enzyme was exclusively monomeric, and its mobility was not affected by MPP (Fig. 6*B*). These data demonstrate that the *Synechocystis* FeCh can exist *in vivo* as a monomer or as a homodimer, and the formation of FeCh dimer is stimulated by MPP.

To prove that the FeCh CAB domain is the pigment-binding site, the FeCh C terminus, including the linker, was expressed in *Synechocystis* as a His_6-tagged protein (His-C-tn, 9 kDa; Fig. 1). We have previously shown that the His-C-tn protein interacts *in vivo* with the FeCh CAB domain and can be copurified with the full-length FeCh but not with a truncated, CAB-less derivative (29). To isolate the His-C-tn domain not "contaminated" by His-C-tn-FeCh heterodimers, we expressed this protein in the *Synechocystis hemH-Δ324* strain containing FeCh lacking both the linker and the LHC domain (Fig. 1) (6). The FeCh-Δ324 truncation, apart from its inability to bind His-C-tn (29), lowers the cellular activity of FeCh because of impaired stability of the enzyme, thus mimicking the free Chl accumulation effect of MPP (Fig. 4*C*). We purified His-C-tn using a nickel affinity column, and after removing contaminating proteins and pigments by anion-exchange chromatography, we obtained pure His-C-tn protein (Fig. 7*A*). Fig. 7*B* shows the absorption spectrum of the isolated His-C-tn protein; as revealed by HPLC analysis of the extracted pigments, the protein binds Chl, β-car, and zeaxanthin at a molar ratio 6: 0.9: 1. A small amount of echinenone and the unknown carotenoid copurified with full-length FeCh was also detectable (Fig. 7*C*). Furthermore, the fluorescence of Chls bound to His-C-tn was also quenched (Fig. 7*A*) as in the case of purified FeCh. Therefore, we can conclude that the FeCh CAB domain is solely responsible for the binding of pigments; the catalytic domain is not required for its folding into a Chl-binding protein structure.

Occurrence and phylogeny of FeCh in cyanobacterial genomes

The FeCh enzyme found in distinct groups of oxygenic phototrophs, such as plants, green algae, diatoms, haptophytes, and

Downloaded from http://www.jbc.org/ at Institute of Physiology AS CR on July 24, 2019

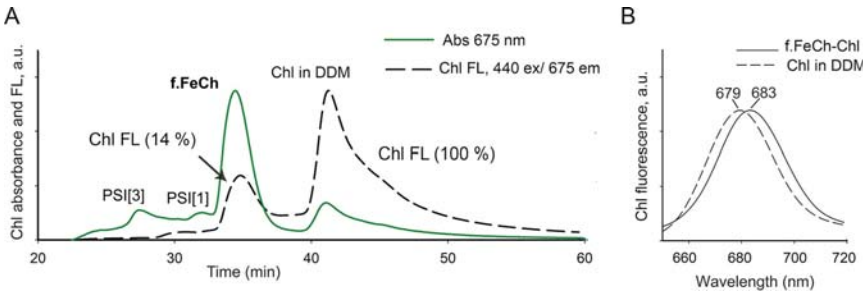

Figure 5. Quenching of Chl fluorescence in the FeCh–pigment complex. *A*, SEC separation of f.FeCh purified from *Synechocystis* cells treated for 4 h with MPP. Chl absorption and fluorescence were recorded by diode array and fluorescent detectors, respectively. *PSI[3]* and *PSI[1]* indicate Chl bound to traces of trimeric and monomeric PSI, respectively. *Numbers* in *parentheses* indicate Chl fluorescence yield. The efficiency of quenching was calculated from the ratio of fluorescence/absorbance at their respective maxima for Chls bound to FeCh and for Chl molecules in detergent micelles. The same extinction coefficient was assumed for both Chl populations. *B*, fluorescence maxima of the f.FeCh–pigment complex and free Chl molecules in DDM micelles recorded during SEC chromatography by a fluorescence detector after excitation at 440 nm.

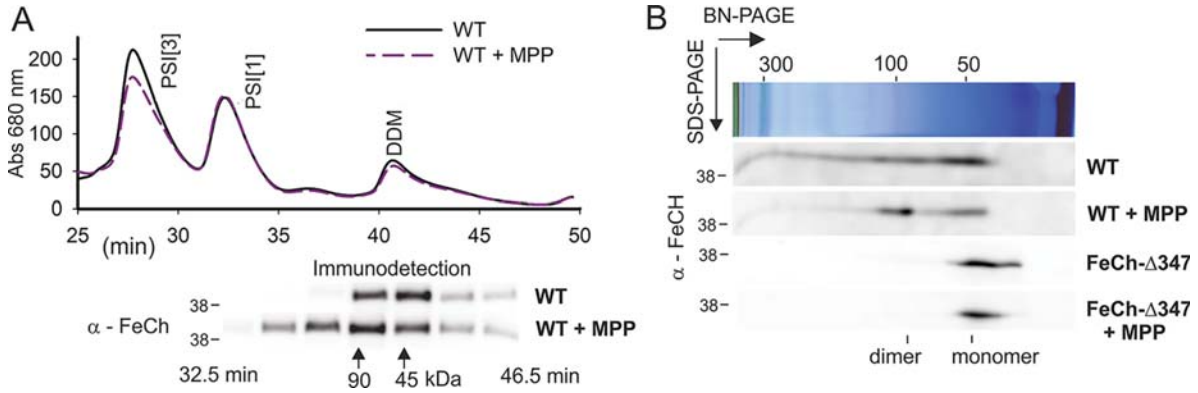

Figure 6. MPP-treatment induces dimerization of *Synechocystis* FeCh via its CAB domain. *A*, membrane complexes prepared from WT cells and WT cells treated for 4 h with MPP were separated by SEC, and minute fractions were collected. Individual fractions were separated by SDS-electrophoresis, blotted, and probed with an anti-FeCh antibody. Calibration of the SEC column is indicated by *arrows* (see Fig. S5 for details). *PSI[3]* and *PSI[1]* show the position of trimeric and monomeric PSI complexes. *B*, solubilized membrane fractions were separated by 2D BN-PAGE and blotted, and the FeCh was immunodetected. Only slices of the blot with the signal of FeCh are shown (see Fig. S6 for full-sized gels). The position of monomeric and dimeric FeCh is indicated.

glaucophytes, is of cyanobacterial origin and possesses a conserved CAB domain (Fig. S1) (34). However, the origin of the FeCh CAB domain, as well as its distribution in currently sequenced cyanobacterial species, remains unclear. We searched for *hemH* genes in all of the currently available cyanobacterial genomes (a total of 462 genomes) and found that the vast majority (453 genomes) code for FeCh with the CAB domain. The only exceptions are the most basal clades of the cyanobacterial evolutionary tree (primordial *Gloeobacter*, *Synechococcus*, and *Pseudanabaena* strains) and two members of a derived clade of unicellular endosymbionts of diatoms (Fig. 8 and Table 1). A complete list of the analyzed genomes is provided in Table S1. In all analyzed CAB domains (453 genomes), the E*XX*N*X*R Chl-binding motif is conserved.

Three *Pseudoanabena* strains, forming a sister group to the basal, CAB domain-less clade, (Fig. 8) possess two similar *hemH* genes (identity ~60%); one *hemH* copy contains the CAB domain, but this domain is absent in the second gene. This situation is unique, because no other cyanobacterial genomes contain a combination of *hemH* genes with and without the CAB domain (Table 1). Intriguingly, 90 cyanobacterial genomes code for a "FeCh-like" protein with very limited similarity to the cyanobacterial FeCh (20–30%; Table 1). This gene also seems to be cyanobacteria-specific, because we found no homologs in the NCBI database (by BLAST search) after excluding cyanobacteria from the search. Whereas the FeCh-like protein substantially differs from archeal, bacterial, or eukaryotic FeChs on a sequence level (not shown), its tertiary structure predicted by I-TASSER (35) aligned very tightly with the structure of canonical human FeCh (root-mean-square deviation between 256 pruned atom pairs = 0.37 Å; Fig. S7*A*). Moreover, His-263, Asp-340, and Glu-343 residues (if counted according to the human FeCh), which are essential for the extraction of protons from PPIX nitrogens (36), are conserved in all 90 sequences of the FeCh-like proteins. The same is true for the absolutely conserved Phe-337 residue placed onto the PPIX-binding pocked (Fig. S7*B*) (37). Strains containing the putative second FeCh are listed in Table S1.

Single-helix Hlips have already been proposed as ancestors of the whole LHC superfamily (16). Indeed, genes coding for Hlips are present in all of the analyzed genomes, including the strains lacking thylakoids and/or the FeCh CAB domain (Table 1). We therefore conclude that the FeCh CAB domain most likely originates from an ancient fusion between an Hlip protein and the FeCh enzyme in the ancestor of all modern cyanobacteria except for the three deepest-branching lineages (Fig. 8).

Downloaded from http://www.jbc.org/ at Institute of Physiology AS CR on July 24, 2019

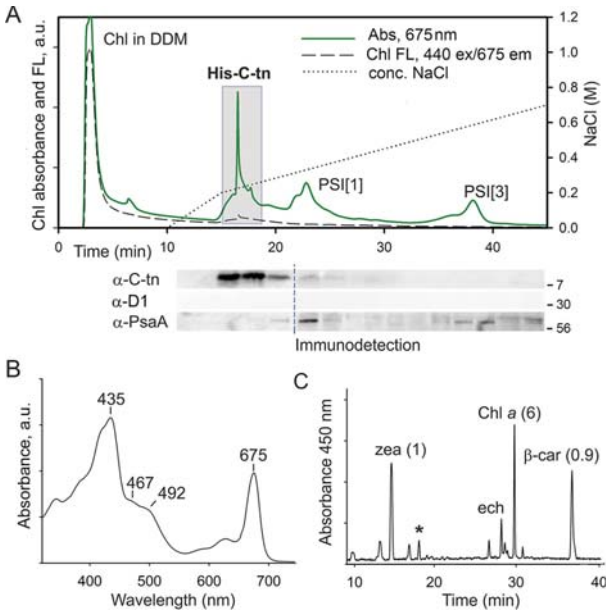

Figure 7. The C-terminal segment of FeCh lacking the catalytic domain (an artificial His-C-tn protein) binds Chl, β-car, and zeaxanthin *in vivo*. *A*, the His-C-tn protein was expressed in the *Synechocystis hemH-Δ324* genetic background and purified on a nickel column. The obtained eluate was further separated by anion-exchange chromatography, and the Chl absorbance (675 nm) and Chl fluorescence were recorded (*Chl FL*; 440-nm excitation/675-nm emission). Note the strikingly different emission intensity of Chls in DDM micelles and Chls bound to His-C-tn. Minute fractions were collected and separated by SDS-electrophoresis, and the presence of His-C-tn protein was detected by antibodies raised against the FeCh C terminus. The core photosystem I and II subunits PsaA and D1 were also immunodetected as a control of purity; *dashed line* indicates blot splicing. Fractions highlighted by the *gray box* were pooled and used for the analysis of pigments associated with His-C-tn. *B*, the absorption spectrum of the His-C-tn protein purified by a combination of nickel-affinity and anion-exchange chromatography as described above. *C*, the extracted pigments from the purified His-C-tn protein were separated on a C18 column; the molar stoichiometry of the major constituents is indicated. *zea*, zeaxanthin; *ech*, echinenone. The unknown carotenoid (see Fig. 2*D*) is marked by an *asterisk*.

Discussion

The FeCh enzyme equipped with the pigment-binding CAB domain is apparently an old invention of cyanobacteria (Fig. 8). Comparing our phylogenetic tree to the recent calibrated molecular clock analyses, the evolution of this fused protein can be dated back to the early Proterozoic, roughly coinciding with the Great Oxygenation Event (38). Our data support a scenario in which the CAB domain originates from a fusion between an ancient cyanobacterial FeCh and an Hlip. Although we cannot completely exclude the possibility that the FeCh CAB domain is the progenitor of the whole LHC superfamily including Hlips, it is indeed very unlikely that the CAB segment of FeCh, in such a case already present in the last common cyanobacterial ancestor, would be selectively lost in basal cyanobacterial lineages (Fig. 8). Furthermore, in the literature there is an example of another fusion between an Hlip and a conserved cyanobacterial protein, a homolog of the *Synechocystis* Ssl2148 protein (39), supporting the plausibility of FeCh–Hlip fusion.

The function of Hlips and their plant homologs (OHPs) has been connected to the biogenesis of Chl-binding proteins, particularly the subunits of PSII (21, 40). All four Hlips present in *Synechocystis* (HliA–D) interact with either the D1 subunit (HliC/D) or the CP47 subunit of PSII (HliA/B/C) soon after these Chl proteins are synthesized (21). Hlips then remain associated with D1/CP47 to support certain stages of PSII assembly or, possibly, PSII repair (21). In addition, the HliC/D proteins associate with the Chl-synthase enzyme (41). The exact roles that Hlips play are not clear yet, but they most likely fulfill several different tasks: (i) photoprotection of PSII biogenesis (dissipation of absorbed energy), (ii) delivery of Chl molecules, and (iii) regulation of Chl metabolism (HliC/D) (10). We suggest that once the FeCh enzyme linked physically with an Hlip, the FeCh became targeted to the machinery responsible for the biogenesis and assembly of Chl-binding proteins. There is general agreement about the existence of specific membrane compartments in which the photosystems are assembled, in both cyanobacteria (42) and plastids (43). As a crucial regulatory enzyme, FeCh probably got close to a site where Chl molecules are produced (44) and distributed into Chl-binding apoproteins (45).

The ability of Hlips to bind Chl and carotenoids in an energy dissipative configuration (24) has been preserved in the FeCh CAB domain. The absorbance spectrum of the His-C-tn-pigment complex is similar to two Hlips that have been previously characterized (HliC and HliD) (24, 46). However, unlike HliC and HliD proteins that exclusively contain β-car, the CAB domain also binds zeaxanthin and echinenone (Fig. 7*C*). The calculated molar ratio of Chl:β-car:zeaxanthin (6:0.9:1) in the CAB domain is very similar to the ratio of Chl:β-car identified in HliC and HliD (6 or 4 Chl per 2 β-car, respectively) (24, 25). Two different β-car–binding sites have been unambiguously identified in Hlips (24, 47). However, in CAB domain, one carotenoid-binding site could be less specific and more polar than that in Hlips, preferentially accommodating xanthophylls or keto-carotenoids. A similar shift to polar xanthophylls (lutein, violaxanthin) also happened during the evolution of the eukaryotic major and minor antenna proteins (26, 48).

The original cyanobacterial FeCh was probably monomeric, because it is strictly monomeric if the CAB domain is eliminated (Fig. 6*B*) (29), and the recombinant full-length *Synechocystis* FeCh can be prepared in an active monomeric form (30). Although there is a small fraction of dimeric FeCh in *Synechocystis* grown under our standard laboratory conditions (29), the vast majority of FeCh appears to be monomeric *in vivo* (Fig. 6*B*). Because the pigment-binding motif in Hlips is, however, formed by two parallel helices (24), the monomeric CAB domain cannot serve a photoprotective or Chl carrier role. To be capable of pigment binding the FeCh needs to dimerize via CAB domain (29); most likely by mimicking the LHC-like pair of helices (26) clipped together by salt bridges between Glu and Arg residues on the opposite helices (see also Fig. S1*B*).

A mechanistic explanation or a function of the observed conditional FeCh dimerization is beyond the scope of this report and must be addressed by future studies; however, based on the present data, we speculate that the formation of FeCh dimers is triggered in response to disturbed tetrapyrrole metabolism. The rather mild dose of MPP used in our study allows treated cells to produce enough heme for close to normal proliferation (Fig. S3); yet the regulatory function of heme was apparently

Downloaded from http://www.jbc.org/ at Institute of Physiology AS CR on July 24, 2019

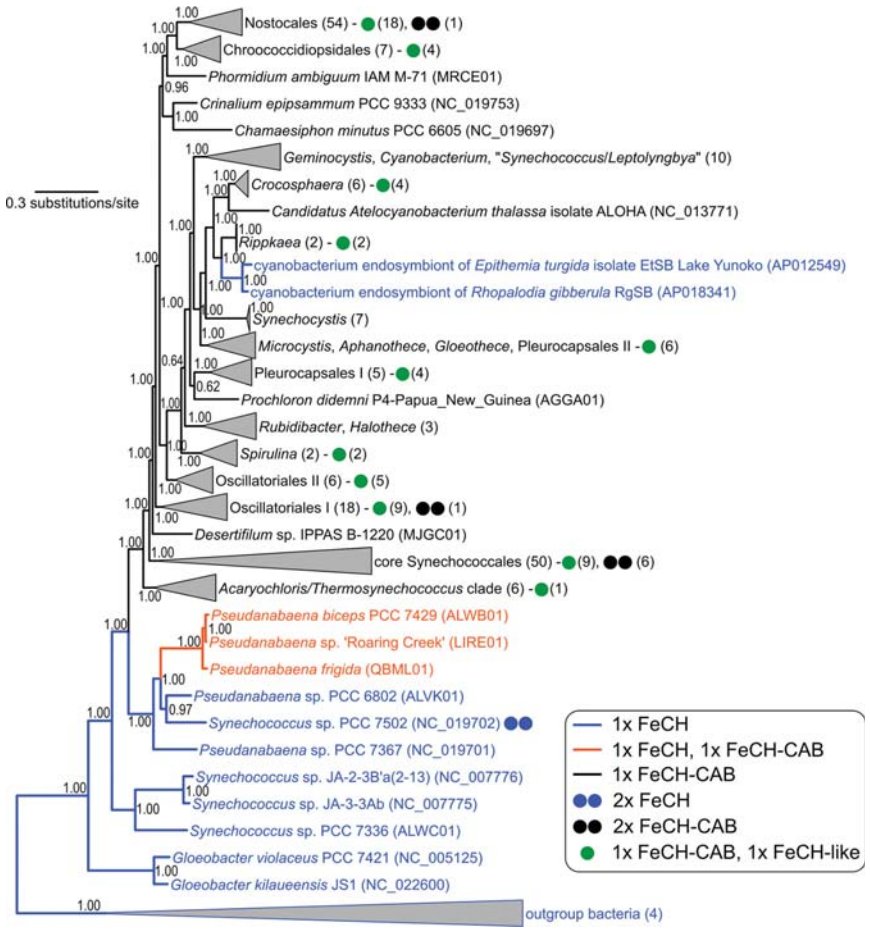

Figure 8. Distribution of *hemH* genes coding for FeCh with and without the CAB domain in an evolutionary tree of cyanobacteria. FeCH lacking the CAB domain is plesiomorphic in cyanobacteria. The fusion of FeCH and CAB may have occurred twice (the *orange clade* and the *black clade*) or may have been lost once (sister clade to the *orange one*) after duplication of *hemH*. The tree inferred from 22 conserved proteins in 220 genomes was calculated using Bayesian inference posterior probabilities are shown near the nodes. *Numbers* in *brackets* indicate the number of genomes in a collapsed clade or possessing a particular organization of FeCH-coding genes as explained in the legend.

disturbed, resulting in a strongly up-regulated tetrapyrrole pathway. Under such conditions, a large pool of FeCh dimerizes. It should be noted that the His-C-tn protein (an artificial CAB domain) readily attaches to full-length FeCh via its CAB domain *in vivo* (29), suggesting that there is a control mechanism such that two FeChs form a stable dimer only under certain conditions. A possible explanation is that the monomeric FeCh is incorporated into a protein complex. A colocalization of cyanobacterial FeCh with protoporphyrinogen oxidase, the preceding enzyme in the pathway, has been reported (49), and it is worth noting that the mitochondrial FeCh is a component of large protein assembly dealing with heme metabolism (50). The proposed spatial separation of FeCh monomers in the cell is consistent with the fact that purified pigment-less *Synechocystis* FeCh spontaneously dimerizes (29). However, there is the possibility of *in vitro* artifacts caused by the high concentrations of the protein and/or handling and freezing the sample. In this work, the purified sample was immediately loaded into a SEC column. An alternative scenario is that the *in vivo* stability of the pigment-less FeCh dimer is weak, but after association with Chl and carotenoids, the dissociation constant of the pigmented dimer becomes much lower, resulting in the accumulation of FeCh dimer. This is indeed an attractive hypothesis, providing a mechanism for how the FeCh enzyme senses a risky accumulation of Chl molecules in the membrane, particularly if this occurs in the specialized compartment for Chl-protein biogenesis. The *Synechocystis* mutant lacking FeCh CAB domain was reported to be sensitive to high light and to accumulate chlorophyllide, the substrate of Chl synthase (29). We did not observe a large pool of FeCh dimer under high light conditions (not shown); however, it is possible that under physiological conditions, the level of FeCh dimer does not exceed a certain threshold and/or it is short-lived.

The amount of FeCh in *Synechocystis* appears to be much higher than that needed for synthesizing a sufficient amount of heme: strains with ~10% of normal FeCh activity do not exhibit any signs of phycobilisome deficiency, at least under low-stress conditions (6, 31). This situation resembles the reserve flux capacity that enables an immediate (<1 min) rerouting of glucose-6-phosphate into the oxidative pentose phosphate path-

Downloaded from http://www.jbc.org/ at Institute of Physiology AS CR on July 24, 2019

Table 1
Numbers of cyanobacterial genomes coding for the Hlips, the FeCh with or without the CAB domain, and the FeCh-like proteins
A detailed list of all strains and identified *hemH* genes are provided in Table S1.

Deduced content of genes coding for Hlips and FeChs	Number of genomes (462 in total)
Hlips	462
1× FeCh[a]	9
Gloeobacter violaceus PCC 7421	
Gloeobacter kilaueensis JS1	
Synechococcus sp. JA-3-3Ab	
Synechococcus sp. JA-2-3B′a(2-13)	
Pseudanabaena sp. PCC 6802	
Synechococcus sp. PCC 7336	
Pseudanabaena sp. PCC 7367	
Cyanobacterium endosymbiont of *Epithemia turgida*	
Cyanobacterium endosymbiont of *Rhopalodia gibberula*	
2× FeCh[a]	1
Synechococcus sp. PCC 7502	
1× FeCh, 1× FeCh-CAB[b]	3
Pseudanabaena biceps PCC 7429	
Pseudanabaena sp. "Roaring Creek"	
Pseudanabaena frigida ULC066bin1	
1× FeCh-CAB	359
2× FeCh-CAB[c]	10
1× FeCh, 1× FeCh-like	0
1× FeCh-CAB, 1× FeCh-like	90

[a] High similarity to cyanobacterial FeCh but lacking CAB domain.
[b] A cyanobacterial-type of FeCh containing CAB domain.
[c] Genes sharing high identity.

way in *Escherichia coli* (51). *Synechocystis* could have a similar capacity to promptly reroute PPIX into the heme pathway, away from magnesium chelatase. Whether FeCh dimerization together with pigment binding on the CAB domain influences its activity is unknown at this point. Unfortunately, we cannot assess the activity of pigmented FeCh because of the presence of MPP in the active site. However, in an *in vitro* assay, FeCh lacking the CAB domain shows increased catalytic turnover number (30), suggesting that there is an effect of this segment on the enzymatic parameters *in vivo*. In the same report, the addition of a methanol extract from *Synechocystis* membranes containing pigments lowered the FeCh activity irrespectively of the CAB domain (30). This observation might indicate that free Chl molecules have a direct effect on the enzyme catalytic site. However, the conditions in *in vitro* assay are very artificial, and also the methanol extract is a complex mixture of compounds; in the work of Storm *et al.* (30), a measurement with chemically pure Chl *a* is not provided. Potential modulation of FeCh activity by Chl, either via CAB domain or by interfering with catalytic site, thus remains an open question. Alternatively, instead of changing the catalytic properties, dimerization and binding of pigments on the CAB domain may alter the availability of PPIX for chelation by changing the FeCh interactome (as discussed above). In this scenario, FeCh would be regulated by substrate availability rather than by enzymatic activity.

Although FeCh activity is undoubtedly very important for the regulation of Chl biosynthesis (31, 52), the molecular mechanism of this regulation is not known. The classical model of labile free heme directly controlling the formation of ALA (53) appears to be oversimplified. In plants, it has been proposed that two spatially separated pools of PPIX are located in plastids, each used for the synthesis of heme, but only one pool of PPIX also serving as a substrate for magnesium chelatase (52, 54). In addition, there seems to be a dedicated regulatory heme pool produced by plastid FeCh1 isozyme (lacking the CAB domain) that is involved in plastid to nucleus signaling (55). Plant cells are much more complex than cyanobacterial cells; yet the CAB domain (FeCh2 isozyme) is conserved in plants, and there is no reason to expect that it has a fundamentally different function than in cyanobacteria. Predictably, FeCh2 is the key regulator of plant tetrapyrrole metabolism; FeCh1 activity does not affect the synthesis of tetrapyrroles in plastids (56). Because many cyanobacterial stains contain a putative second FeCh (Table 1), we speculate that the FeCh-controlled ALA synthesis and flow of PPIX into the Chl branch are limited to a specific compartment. This is in line with our proposed targeting of FeCh with the CAB domain into a site of Chl-protein biogenesis, where enzymes of the Chl pathway should be also localized (44, 57).

Different oligomeric states of the FeCh enzyme are most likely involved in the sophisticated regulatory machinery controlling Chl metabolism, which in cyanobacteria also includes Hlips (10) and other proteins (58, 59). Intriguingly, *Synechocystis* lycopene cyclase (CruA), an enzyme in carotenoid biosynthesis, was recently reported to bind Chl and carotenoids (60). This enzyme does not possess a CAB domain or helical transmembrane segments; the mechanism through which the lycopene cyclase binds Chl and carotenoids in a ratio and spectral characteristics resembling a typical Chl-complexes such as photosystem I thus remains enigmatic. In plants and algae, the conserved CAB/LHC motif is present within a broader spectrum of proteins that are otherwise diverse but also generally connected to Chl biosynthesis. For instance, the Msf1 protein recently identified in the alga *Chlamydomonas reinhardtii* is required for the accumulation of photosystem I and interacts with the cyclase enzyme in Chl biosynthesis (61). In *Arabidopsis thaliana*, Lil3.1/2 proteins are crucial for the synthesis of the Chl phytol chain (12, 13, 62–65), whereas OHPs assist during the synthesis of photosystem II as described above for the cyanobacterial Hlips (14, 15). Association with a biogenesis compartment and (regulatory) pigment-driven dimerization could be thus common themes for LHC-like proteins.

Experimental procedures

Synechocystis strains and growth conditions

The glucose-tolerant *Synechocystis* WT-P substrain is referred to here as WT (66). The *Synechocystis* strain expressing 3×FLAG-tagged FeCh and lacking the native *hemH* gene has been described previously (29), as well as the strains possessing truncated FeCh derivatives (*hemH-Δ324*, *hemH-Δ347*) (6, 29) or expressing the FeCh C-terminal domain as a His_6-tagged protein (His-C-tn) (29). To express the His-C-tn protein in the *hemH-Δ324* genetic background, the His-*C-tn* cells were transformed with chromosomal DNA isolated from the *hemH-Δ324* cells, and transformants were selected on a BG-11 plate with Zeocin (3 mg/liter). Complete segregation of the mutant was verified by PCR. All strains were grown in BG-11 medium; solid media were further supplemented with 10 mM TES/NaOH (pH 8.2), 1.5% agar, and 0.3% sodium thiosulfate. Liquid cultures were grown either grown in 50 ml of BG-11 in 250-ml conical flasks on a rotary shaker or in 800 ml of BG-11 in 1-liter cylin-

Downloaded from http://www.jbc.org/ at Institute of Physiology AS CR on July 24, 2019

ders bubbled with air at 29 °C with a surface irradiance of 40 μmol photons m^{-2} s^{-1} of white light. The cultures were harvested in the exponential phase at a cell density of ~10^8/ml (A_{750} in a range of 0.8–1.0) by centrifugation (5000 RCF, 5 min). Where applicable the FeCh inhibitor MPP (32) (Frontier Scientific) was added from a 10 mM stock in DMSO to a final concentration of 275 nM.

Affinity, size-exclusion, and anion-exchange chromatography

Pelleted cells were resuspended in isolation buffer A (20 mM MES, pH 6.5, 150 mM NaCl, complete protease inhibitor mixture; Roche) and mixed with glass beads of 100–200 μM diameter at a 1:1 ratio (1 volume of dense cell solution to 1 volume of glass beads). This suspension was vortexed six times for 10 s with 1 min on ice in between each cycle. After vortexing, the glass beads were washed four times with buffer A, and the obtained suspension of broken cells was pooled and centrifuged (40,000 RCF, 20 min). The pelleted membranes were resuspended in buffer A and frozen (−80 °C) for further use. Isolated membranes containing 500 μg Chl/ml were solubilized using 1% (w/v) DDM for 5 min on ice. His- and FLAG-tagged proteins were purified in buffer A at 10 °C according to the manufacturer's instructions using Protino nickel–nitrilotriacetic acid–agarose (Macherey–Nagel) and an anti-FLAG M2 affinity gel (Sigma–Aldrich), respectively. Prior to ion-exchange/size-exclusion chromatography, samples were concentrated approximately four times using 10-kDa cutoff microconcentrators (AmiconR Ultra 0.5 ml; Merck). The eluted and concentrated f.FeCh protein was immediately injected onto an Agilent-1200 HPLC system and separated on a Yarra SEC-3000 column (Phenomenex) using mobile phase (20 mM MES, pH 6.5, 100 mM NaCl, pH 6.5, containing 0.06% (w/v) DDM) at a flow rate of 0.25 ml min^{-1} at 15 °C. Eluted proteins and complexes were detected using a diode-array detector and a fluorescence detector set to 440/680 nm (excitation/emission wavelengths). The membrane fraction solubilized by 1% (w/v) DDM was separated with an identical procedure as that of the f.FeCh eluate.

For anion-exchange separation of the His-C-tn protein, the concentrated eluate from the nickel column was injected onto an Agilent-1200 HPLC system and separated on a MonoQ 4.6/100 PE column (GE Healthcare) using a gradient of NaCl in 20 mM HEPES, pH 8.1, 5 mM $MgCl_2$, 0.06% (w/v) DDM. The high-salt (HS) buffer was identical to the low-salt buffer but contained 1 M NaCl. The gradient was run as follows: 10 min, 0% HS; 15 min, 20% HS; 45 min, 55% HS; and 47 min, 100% HS at a flow rate of 0.8 ml min^{-1} at 15 °C. Eluted proteins and complexes were detected using a diode-array detector and a fluorescence detector set to 440/675 nm (excitation/emission wavelengths).

Native and denaturing protein electrophoresis

Harvested cells were dissolved in isolation buffer B (25 mM MES, pH 6.5, 4 mM $MgCl_2$, 4 mM $CaCl_2$, 25% (w/v) glycerol, complete protease inhibitor mixture; Roche), mixed with glass beads of 100–200 μM diameter at a 1:1 ratio (1 volume of dense cell solution to 1 volume of glass beads), and broken (three times for 20 s) using a Mini-Beadbeater-16 (Biospec). The cells were kept on ice for 2 min between each cycle. The membranes were isolated as described above.

For the separation of membrane complexes on BN-PAGE, the isolated membranes containing 400 μg Chl/ml were solubilized using 1% (w/v) DDM for 5 min on ice. Nonsolubilized material was removed by centrifugation (20,000 RFC, 10 min). Extracted membrane proteins corresponding to 4 μg of Chl were mixed with 1/10 volume of sample buffer (750 mM aminocaproic acid, 5% (w/v) CBB-G) and separated at 4 °C on an 8–16% gradient polyacrylamide gel containing 500 mM aminocaproic acid and 50 mM Bis-Tris/HCl, pH 7.6, at room temperature according to Ref. 67. The starting blue cathode buffer (50 mM Tricine, 50 mM Bis-Tris/HCl, pH 7.0, 0.2% (w/v) CBB-G) was exchanged after one-third of the run for the clear cathode buffer (50 mM Tricine, 50 mM Bis-Tris/HCl, pH 7.0). As anode buffer, 50 mM Bis-Tris/HCl, pH 7.0, was used. In clear-native electrophoresis the cathode buffer contained 0.05% (w/v) sodium deoxycholate and 0.02% (w/v) DDM, and a 4–12% gradient polyacrylamide gel was used. After separation, Chl fluorescence in the gel was detected using LAS-4000 (Fuji) after illumination with blue light.

To separate proteins using denaturing SDS-PAGE, a 16–20% linear gradient polyacrylamide gel containing 7 M urea, 650 mM Tris/HCl, pH 8.6, was prepared according to (68). For the second dimension, gel strips from the native gel were excised and incubated for 30 min in 25 mM Tris/HCl, pH 7.5, containing 1% (w/v) SDS and 2% (w/v) DTT, and placed on top of the denaturing gel; two strips were analyzed on a single denaturing gel. Cathode buffer (25 mM Tris, 192 mM glycine, 0.2% (w/v) SDS) and anode buffer (25 mM Tris/HCl, pH 8.3) were used. A ratio of 1:60 for acrylamide to bis-acrylamide was used for all gels.

Protein immunodetection

Proteins separated by SDS-PAGE were stained for 50 min with SYPRO Orange (Thermo Fisher) 5000× diluted in 10 mM Tris/HCl, pH 7.6, 150 mM NaCl, 10% (v/v) methanol and subsequently transferred (3 mA/cm^2, 3h) onto an Immobilon-P membrane (0.45 μm; Millipore). After electrotransfer, the membrane was blocked by 0.05% (w/v) Tween 20 in 10 mM Tris/HCl, pH 7.6, 150 mM NaCl for 30 min and subsequently incubated with a specific primary antibody and then with a secondary antibody–horseradish peroxidase conjugate (Sigma). The peroxidase activity was visualized by incubating the membrane for 20 s in Luminata Crescendo Western HRP substrate (Sigma) and detected using LAS-4000 (Fuji).

The primary antibodies used in this study were as follows: anti-FeCh antibody (1:20,000 dilution) raised in rabbit against the *Synechocystis* recombinant FeCh (29); a rabbit polyclonal antiserum raised against residues 325–353 of the D1 protein from *Pisum sativum* (67) at a dilution of 1:5000; a polyclonal purified anti-PsaA antibody (Agrisera; dilution 1:10,000) raised against residues 2–18 of the *Synechocystis* PsaA; and a polyclonal purified antibody raised against the synthetic peptide VPHPKKNMKMYPQER, which corresponds to the linker region of *Synechocystis* FeCh (29) (dilution 1:10,000).

Downloaded from http://www.jbc.org/ at Institute of Physiology AS CR on July 24, 2019

Binding of pigments on the ferrochelatase CAB domain

Chl radiolabeling and measurement of Chl precursors and pigments

To assess the rate of *de novo* Chl synthesis, cells corresponding to 50 mg of Chl in an exponential growth phase at density ~5 × 10^7/ml (OD_{750} = 0.5) were harvested by centrifugation (2700 RCF, 3 min), washed, and resuspended in fresh BG-11 medium containing 20 mM TES to a final volume of 540 μl. The cell suspension was shaken in 10-ml glass tubes for 30 min at 29 °C at 40 μmol photons m^{-2} s^{-1}. Then 60 μl of [^{14}C]Glu with specific activity 248 mCi/mmol (Moravek Biochemicals) was added. After 60 min, the cells were harvested (10,000 RCF, 2 min) and frozen in liquid nitrogen. MPP (275 nM) was added to the cells 3.5 h before the addition of [^{14}C]Glu and also kept at the 275 nM concentration during radiolabeling. Pelleted cells were washed and resuspended in 50 μl of water; Chl was extracted with 1 ml of methanol, and insoluble material was discarded by centrifugation (10,000 RCF, 4 min). The extract was injected into an Agilent-1260 HPLC system equipped with a Radiomatic 150 TR scintillation detector (PerkinElmer Life Sciences) and a diode-array detector. Pigment separation was carried out on a Zorbax Eclipse Plus C18 column (4.6-μm particle size, 3.9 × 100 mm; Agilent) with 35% methanol, 15% acetonitrile in 0.25 M pyridine as solvent A and 20% methanol, 20% acetone in acetonitrile as solvent B. Pigments were eluted with a linear gradient of solvent B (30–95% in 25 min) followed by 95% solvent B at a flow rate of 0.8 ml min^{-1} at 40 °C. The relative rate of Chl synthesis was estimated from the ratio of Chl radio emission to Chl absorbance between MPP-treated and untreated samples.

To quantify free Chl in the native gel, a piece of gel (~4 × 5 mm) corresponding to the region of DDM micelles was cut and further chopped up into pieces (1 × 1 mm). The obtained gel pieces were incubated for 2 h in 125 μl of buffer A containing 0.04% DDM, and then the buffer was collected after centrifugation (10,000 RCF, 2 min). The incubation of gel pieces in the buffer A was repeated, the buffer fractions were pooled, and the eluted pigments were separated by HPLC as described above. The absolute Chl concentration was calculated from peak area using a Chl-*a* standard.

Chl precursors were quantified as described in Ref. 69. To identify pigments bound to the isolated f.FeCh and His-C-tn proteins, fractions collected during SEC and anion-exchange chromatography were concentrated on 10-kDa cutoff microconcentrators (AmiconR Ultra 0.5 ml; Merck). This concentrated solution was extracted with 90% methanol, and the extract was analyzed using the Agilent-1260 HPLC system, essentially as described above for the radiolabeled samples. Pigment stoichiometry was calculated from calibration curves prepared using authentic standards.

Nonphotochemical quenching of Chl bound to f.FeCh

Quenching of Chl fluorescence was estimated from the ratio of fluorescence/absorbance of Chl molecules bound to f.FeCh compared with unquenched Chl in DDM micelles. Identical fluorescence constants and extinction coefficients were assumed for both Chl populations.

Phylogenetic and bioinformatic analysis

A representative set of 550 publicly available cyanobacterial genome assemblies was downloaded from NCBI and utilized to create a custom BLAST database (70). FeCh protein from *Synechocystis* (*slr0839* gene) was used as the query for a tBLASTn search with a cutoff value of 1.e^{-10} against this database, allowing multiple hits for each genome. All hits were automatically harvested and aligned using MAFFT v. 7 (71). Sequence analysis in Geneious Prime v. 2019 allowed us to remove short hits, reducing the number of genomes in the final data set to 462 and to assess the presence of a terminal CAB domain, specific conserved residues (Chl-binding motif), and pairwise amino acid sequence identity between individual deduced proteins in the matrix.

The multilocus phylogenetic tree was generated using a set of 22 conserved single-copy orthologous protein-coding genes selected from loci previously tested for congruent cyanobacterial phylogenies (72, 73). The selection was made based on the presence of a full unambiguous sequence of the genes in a representative subset of genomes, and comprised these loci: *dnaG*, *frr*, *infC*, *nusA*, *pgk*, *pyrG*, *rplB*, *rplC*, *rplD*, *rplE*, *rplF*, *rplM*, *rplP*, *rplT*, *rpoB*, *rpsC*, *rpsE*, *rpsI*, *rpsK*, *rpsM*, *rpsS*, and *smpB*. First, BLAST queries were derived from respective proteins mined from *Synechocystis* (BA000022). Each of the 22 queries was then used in tBLASTn (cutoff value 1.e^{-15}) searches against the custom database. Hits for each protein were aligned using MAFFT v. 7, and the alignments were manually reviewed to remove ambiguous sites and gap regions. A maximum likelihood tree was calculated using each of the 22 alignments with 1000 bootstrap pseudoreplications in RaxML v. 8 (74). The resulting phylogenies were inspected manually for topological incongruence. Because individual gene trees were generally consistent, all alignments were concatenated into a 5117–amino acid–long matrix containing 220 sequence lines. A Bayesian inference (BI) tree was obtained using MrBayes v. 3.2.6 (75). Two independent runs of eight Markov chains were performed for 1 million generations, sampling every 100th tree, until the likelihood values were stable, and the divergence criterion was lower than 0.01. The BI calculation employed a common LG + I + G evolutionary model because of the excessive computational demands of a calculation using partitioned models. Posterior probabilities were estimated from branch frequencies in the sampled trees, discarding the first 25% of the harvested data as burn-in. The maximum likelihood and BI calculations were run via the CIPRES supercomputing facility (76).

Author contributions—M. P. and R. S. conceptualization; M. P., J. M., J. P., and R. S. data curation; M.P., J. M., J. P., and R. S. formal analysis; M. P. and R. S. funding acquisition; M. P. and R. S. investigation; M. P. and R. S. visualization; M.P., J. M., J. P., and R. S. methodology; M. P. and R. S. writing-original draft; M. P. and R. S. project administration; M.P., J. M., J. P., and R. S. writing-review and editing; J. M. software; R. S. resources; R. S. supervision; R. S. validation.

Acknowledgments—We thank Eva Kiss and Josef Komenda for reading the manuscript.

ASBMB

Downloaded from http://www.jbc.org/ at Institute of Physiology AS CR on July 24, 2019

References

1. Yuan, X., Rietzschel, N., Kwon, H., Walter Nuno, A. B., Hanna, D. A., Phillips, J. D., Raven, E. L., Reddi, A. R., and Hamza, I. (2016) Regulation of intracellular heme trafficking revealed by subcellular reporters. *Proc. Natl. Acad. Sci. U.S.A.* **113,** E5144–E5152 CrossRef Medline
2. Ikushiro, H., Nagami, A., Takai, T., Sawai, T., Shimeno, Y., Hori, H., Miyahara, I., Kamiya, N., and Yano, T. (2018) Heme-dependent inactivation of 5-aminolevulinate synthase from *Caulobacter crescentus*. *Sci. Rep.* **8,** 14228 CrossRef Medline
3. de Armas-Ricard, M., Levicán, G., Katz, A., Moser, J., Jahn, D., and Orellana, O. (2011) Cellular levels of heme affect the activity of dimeric glutamyl-tRNA reductase. *Biochem. Biophys. Res. Commun.* **405,** 134–139 CrossRef Medline
4. Brzezowski, P., Richter, A. S., and Grimm, B. (2015) Regulation and function of tetrapyrrole biosynthesis in plants and algae. *Biochim. Biophys. Acta* **1847,** 968–985 CrossRef Medline
5. Papenbrock, J., Mishra, S., Mock, H. P., Kruse, E., Schmidt, E. K., Petersmann, A., Braun, H. P., and Grimm, B. (2001) Impaired expression of the plastidic ferrochelatase by antisense RNA synthesis leads to a necrotic phenotype of transformed tobacco plants. *Plant J.* **28,** 41–50 CrossRef Medline
6. Sobotka, R., McLean, S., Žuberová, M., Hunter, C. N., and Tichý, M. (2008) The C-terminal extension of ferrochelatase is critical for enzyme activity and for functioning of the tetrapyrrole pathway in *Synechocystis* strain PCC 6803. *J. Bacteriol.* **190,** 2086–2095 CrossRef Medline
7. Papenbrock, J., Mock, H. P., Tanaka, R., Kruse, E., and Grimm, B. (2000) Role of magnesium chelatase activity in the early steps of the tetrapyrrole biosynthetic pathway. *Plant Physiol.* **122,** 1161–1169 CrossRef Medline
8. Papenbrock, J., Pfündel, E., Mock, H. P., and Grimm, B. (2000) Decreased and increased expression of the subunit CHL I diminishes Mg chelatase activity and reduces chlorophyll synthesis in transgenic tobacco plants. *Plant J.* **22,** 155–164 CrossRef Medline
9. Crawford, T. S., Eaton-Rye, J. J., and Summerfield, T. C. (2016) Mutation of Gly195 of the ChlH subunit of Mg-chelatase reduces chlorophyll and further disrupts PS II assembly in a Ycf48-deficient strain of *Synechocystis* sp. PCC 6803. *Front. Plant Sci.* **7,** 1060 Medline
10. Xu, H., Vavilin, D., Funk, C., and Vermaas, W. (2002) Small Cab-like proteins regulating tetrapyrrole biosynthesis in the cyanobacterium *Synechocystis* sp. PCC 6803. *Plant Mol. Biol.* **49,** 149–160 CrossRef Medline
11. Sinha, R. K., Komenda, J., Knoppová, J., Sedlářová, M., and Pospíšil, P. (2012) Small CAB-like proteins prevent formation of singlet oxygen in the damaged photosystem II complex of the cyanobacterium *Synechocystis* sp PCC 6803. *Plant Cell Environ.* **35,** 806–818 CrossRef Medline
12. Hey, D., Rothbart, M., Herbst, J., Wang, P., Müller, J., Wittmann, D., Gruhl, K., and Grimm, B. (2017) LIL3, a light-harvesting complex protein, links terpenoid and tetrapyrrole biosynthesis in *Arabidopsis thaliana*. *Plant Physiol.* **174,** 1037–1050 CrossRef Medline
13. Zhou, F., Wang, C. Y., Gutensohn, M., Jiang, L., Zhang, P., Zhang, D., Dudareva, N., and Lu, S. (2017) A recruiting protein of geranylgeranyl diphosphate synthase controls metabolic flux toward chlorophyll biosynthesis in rice. *Proc. Natl. Acad. Sci. U.S.A.* **114,** 6866–6871 Medline
14. Hey, D., and Grimm, B. (2018) One-helix protein 2 (OHP2) is required for the stability of OHP1 and assembly factor HCF244 and is functionally linked to PSII biogenesis. *Plant Physiol.* **177,** 1453–1472 Medline
15. Myouga, F., Takahashi, K., Tanaka, R., Nagata, N., Kiss, A. Z., Funk, C., Nomura, Y., Nakagami, H., Jansson, S., and Shinozaki, K. (2018) Stable accumulation of photosystem II requires one-helix protein 1 (OHP1) of the light harvesting-like family. *Plant Physiol.* **176,** 2277–2291 CrossRef Medline
16. Engelken, J., Brinkmann, H., and Adamska, I. (2010) Taxonomic distribution and origins of the extended LHC (light-harvesting complex) antenna protein superfamily. *BMC Evol. Biol.* **10,** 233 CrossRef Medline
17. Engelken, J., Funk, C., and Adamska, I. (2012) The extended light-harvesting complex (LHC) protein superfamily: classification and evolutionary dynamics. In *Functional Genomics and Evolution of Photosynthetic Systems* (Burnap, R. L., and Vermaas, W. F. J., eds) pp. 265–284, Springer, New York
18. Heddad, M., Engelken, J., and Adamska, I. (2012) Light stress proteins in viruses, cyanobacteria and photosynthetic eukaryota. In *Photosynthesis: Plastid Biology, Energy Conversion and Carbon Assimilation* (Eaton-Rye, J. J., Tripathy, B. C., and Sharkey, T. D., eds) pp. 299–317, Springer, New York
19. Neilson, J. A., and Durnford, D. G. (2010) Evolutionary distribution of light-harvesting complex-like proteins in photosynthetic eukaryotes. *Genome* **53,** 68–78 CrossRef Medline
20. Jansson, S. (1999) A guide to the Lhc genes and their relatives in *Arabidopsis*. *Trends Plant Sci* **4,** 236–240 CrossRef Medline
21. Komenda, J., and Sobotka, R. (2016) Cyanobacterial high-light-inducible proteins: Protectors of chlorophyll-protein synthesis and assembly. *Biochim. Biophys. Acta* **1857,** 288–295 CrossRef Medline
22. Adamska, I., Roobol-Bóza, M., Lindahl, M., and Andersson, B. (1999) Isolation of pigment-binding early light-inducible proteins from pea. *Eur. J. Biochem.* **260,** 453–460 CrossRef Medline
23. Reisinger, V., Plöscher, M., and Eichacker, L. A. (2008) Lil3 assembles as chlorophyll-binding protein complex during deetiolation. *FEBS Lett.* **582,** 1547–1551 CrossRef Medline
24. Staleva, H., Komenda, J., Shukla, M. K., Šlouf, V., Kaňa, R., Polívka, T., and Sobotka, R. (2015) Mechanism of photoprotection in the cyanobacterial ancestor of plant antenna proteins. *Nat. Chem. Biol.* **11,** 287–291 CrossRef Medline
25. Shukla, M. K., Llansola-Portoles, M. J., Tichý, M., Pascal, A. A., Robert, B., and Sobotka, R. (2018) Binding of pigments to the cyanobacterial high-light-inducible protein HliC. *Photosyn. Res.* **137,** 29–39 CrossRef Medline
26. Standfuss, J., Terwisschavan Scheltinga, A. C., Lamborghini, M., and Kühlbrandt, W. (2005) Mechanisms of photoprotection and nonphotochemical quenching in pea light-harvesting complex at 2.5A resolution. *EMBO J.* **24,** 919–928 CrossRef Medline
27. Wei, X. P., Su, X., Cao, P., Liu, X., Chang, W., Li, M., Zhang, X., and Liu, Z. (2016) Structure of spinach photosystem II-LHCII supercomplex at 3.2 angstrom resolution. *Nature* **534,** 69–74 CrossRef Medline
28. Funk, C., and Vermaas, W. (1999) A cyanobacterial gene family coding for single-helix proteins resembling part of the light-harvesting proteins from higher plants. *Biochemistry* **38,** 9397–9404 CrossRef Medline
29. Sobotka, R., Tichý, M., Wilde, A., and Hunter, C. N. (2011) Functional assignments for the carboxyl-terminal domains of the ferrochelatase from *Synechocystis* PCC 6803: the CAB domain plays a regulatory role, and region II is essential for catalysis. *Plant Physiol.* **155,** 1735–1747 CrossRef Medline
30. Storm, P., Tibiletti, T., Hall, M., and Funk, C. (2013) Refolding and enzyme kinetic studies on the ferrochelatase of the cyanobacterium *Synechocystis* sp. PCC 6803. *PLoS One* **8,** e55569 CrossRef Medline
31. Sobotka, R., Komenda, J., Bumba, L., and Tichý, M. (2005) Photosystem II assembly in CP47 mutant of *Synechocystis* sp PCC 6803 is dependent on the level of chlorophyll precursors regulated by ferrochelatase. *J. Biol. Chem.* **280,** 31595–31602 CrossRef Medline
32. Shipovskov, S., Karlberg, T., Fodje, M., Hansson, M. D., Ferreira, G. C., Hansson, M., Reimann, C. T., and Al-Karadaghi, S. (2005) Metallation of the transition-state inhibitor N-methyl mesoporphyrin by ferrochelatase: Implications for the catalytic reaction mechanism. *J. Mol. Biol.* **352,** 1081–1090 CrossRef Medline
33. Liu, Z., Yan, H., Wang, K., Kuang, T., Zhang, J., Gui, L., An, X., and Chang, W. (2004) Crystal structure of spinach major light-harvesting complex at 2.72 A resolution. *Nature* **428,** 287–292 CrossRef Medline
34. Kořený, L., Sobotka, R., Janouškovec, J., Keeling, P. J., and Oborník, M. (2011) Tetrapyrrole synthesis of photosynthetic chromerids is likely homologous to the unusual pathway of apicomplexan parasites. *Plant Cell* **23,** 3454–3462 CrossRef Medline
35. Yang, J., Yan, R., Roy, A., Xu, D., Poisson, J., and Zhang, Y. (2015) The I-TASSER Suite: protein structure and function prediction. *Nat. Methods* **12,** 7–8 CrossRef Medline
36. Medlock, A., Swartz, L., Dailey, T. A., Dailey, H. A., and Lanzilotta, W. N. (2007) Substrate interactions with human ferrochelatase. *Proc. Natl. Acad. Sci. U.S.A.* **104,** 1789–1793 CrossRef Medline
37. Dailey, H. A., Wu, C. K., Horanyi, P., Medlock, A. E., Najahi-Missaoui, W., Burden, A. E., Dailey, T. A., and Rose, J. (2007) Altered orientation of

Downloaded from http://www.jbc.org/ at Institute of Physiology AS CR on July 24, 2019

active site residues in variants of human ferrochelatase: evidence for a hydrogen bond network involved in catalysis. *Biochemistry* **46,** 7973–7979 CrossRef Medline
38. Sánchez-Baracaldo, P., Raven, J. A., Pisani, D., and Knoll, A. H. (2017) Early photosynthetic eukaryotes inhabited low-salinity habitats. *Proc. Natl. Acad. Sci. U.S.A.* **114,** E7737–E7745 CrossRef Medline
39. Kilian, O., Steunou, A. S., Grossman, A. R., and Bhaya, D. (2008) A novel two domain-fusion protein in cyanobacteria with similarity to the CAB/ELIP/HLIP superfamily: evolutionary implications and regulation. *Mol. Plant* **1,** 155–166 CrossRef Medline
40. Rochaix, J. D., and Bassi, R. (2019) LHC-like proteins involved in stress responses and biogenesis/repair of the photosynthetic apparatus. *Biochem. J.* **476,** 581–593 CrossRef Medline
41. Niedzwiedzki, D. M., Tronina, T., Liu, H., Staleva, H., Komenda, J., Sobotka, R., Blankenship, R. E., and Polívka, T. (2016) Carotenoid-induced non-photochemical quenching in the cyanobacterial chlorophyll synthase–HliC/D complex. *Biochim. Biophys. Acta* **1857,** 1430–1439 CrossRef Medline
42. Rast, A., Heinz, S., and Nickelsen, J. (2015) Biogenesis of thylakoid membranes. *Biochim. Biophys. Acta* **1847,** 821–830 CrossRef Medline
43. Uniacke, J., and Zerges, W. (2007) Photosystem II assembly and repair are differentially localized in *Chlamydomonas*. *Plant Cell* **19,** 3640–3654 CrossRef Medline
44. Chidgey, J. W., Linhartová, M., Komenda, J., Jackson, P. J., Dickman, M. J., Canniffe, D. P., Koník, P., Pilný, J., Hunter, C. N., and Sobotka, R. (2014) A cyanobacterial chlorophyll synthase-HliD complex associates with the Ycf39 protein and the YidC/Alb3 insertase. *Plant Cell* **26,** 1267–1279 CrossRef Medline
45. Bučinská, L., Kiss, É., Koník, P., Knoppová, J., Komenda, J., and Sobotka, R. (2018) The ribosome-bound protein Pam68 promotes insertion of chlorophyll into the CP47 subunit of photosystem II. *Plant Physiol.* **176,** 2931–2942 Medline
46. Llansola-Portoles, M. J., Sobotka, R., Kish, E., Shukla, M. K., Pascal, A. A., Polívka, T., and Robert, B. (2017) Twisting a β-carotene, an adaptive trick from nature for dissipating energy during photoprotection. *J. Biol. Chem.* **292,** 1396–1403 CrossRef Medline
47. Hontani, Y., Kloz, M., Polívka, T., Shukla, M. K., Sobotka, R., and Kennis, J. T. M. (2018) Molecular origin of photoprotection in cyanobacteria probed by watermarked femtosecond stimulated Raman spectroscopy. *J. Phys. Chem. Lett.* **9,** 1788–1792 CrossRef Medline
48. Pan, X., Li, M., Wan, T., Wang, L., Jia, C., Hou, Z., Zhao, X., Zhang, J., and Chang, W. (2011) Structural insights into energy regulation of light-harvesting complex CP29 from spinach. *Nat. Struct. Mol. Biol.* **18,** 309–315 CrossRef Medline
49. Masoumi, A., Heinemann, I. U., Rohde, M., Koch, M., Jahn, M., and Jahn, D. (2008) Complex formation between protoporphyrinogen IX oxidase and ferrochelatase during haem biosynthesis in *Thermosynechococcus elongatus*. *Microbiology* **154,** 3707–3714 CrossRef Medline
50. Medlock, A. E., Shiferaw, M. T., Marcero, J. R., Vashisht, A. A., Wohlschlegel, J. A., Phillips, J. D., and Dailey, H. A. (2015) Identification of the mitochondrial heme metabolism complex. *PLoS One* **10,** e0135896 CrossRef Medline
51. Christodoulou, D., Link, H., Fuhrer, T., Kochanowski, K., Gerosa, L., and Sauer, U. (2018) Reserve flux capacity in the pentose phosphate pathway enables *Escherichia coli*'s rapid response to oxidative stress. *Cell Syst.* **6,** 569–578.e7 CrossRef Medline
52. Czarnecki, O., and Grimm, B. (2012) Post-translational control of tetrapyrrole biosynthesis in plants, algae, and cyanobacteria. *J. Exp. Bot.* **63,** 1675–1687 CrossRef Medline
53. Cornah, J. E., Terry, M. J., and Smith, A. G. (2003) Green or red: what stops the traffic in the tetrapyrrole pathway? *Trends Plant Sci.* **8,** 224–230 CrossRef Medline
54. Huang, L., and Castelfranco, P. A. (1990) Regulation of 5-aminolevulinic acid (ALA) synthesis in developing chloroplasts: evidence for functional-heterogeneity of the ALA pool. *Plant Physiol.* **92,** 172–178 CrossRef Medline
55. Terry, M. J., and Smith, A. G. (2013) A model for tetrapyrrole synthesis as the primary mechanism for plastid-to-nucleus signaling during chloroplast biogenesis. *Front. Plant Sci.* **4** CrossRef Medline
56. Scharfenberg, M., Mittermayr, L., von Roepenack-Lahaye, E., Schlicke, H., Grimm, B., Leister, D., and Kleine, T. (2015) Functional characterization of the two ferrochelatases in *Arabidopsis thaliana*. *Plant Cell Environ.* **38,** 280–298 CrossRef Medline
57. Sobotka, R. (2014) Making proteins green; biosynthesis of chlorophyll-binding proteins in cyanobacteria. *Photosyn. Res.* **119,** 223–232 CrossRef Medline
58. Kopečná, J., Cabeza de Vaca, I., Adams, N. B., Davison, P. A., Brindley, A. A., Hunter, C. N., Guallar, V., and Sobotka, R. (2015) Porphyrin binding to Gun4 protein, facilitated by a flexible loop, controls metabolite flow through the chlorophyll biosynthetic pathway. *J. Biol. Chem.* **290,** 28477–28488 CrossRef Medline
59. Schottkowski, M., Ratke, J., Oster, U., Nowaczyk, M., and Nickelsen, J. (2009) Pitt, a novel tetratricopeptide repeat protein involved in light-dependent chlorophyll biosynthesis and thylakoid membrane biogenesis in *Synechocystis* sp. PCC 6803. *Mol. Plant* **2,** 1289–1297 CrossRef Medline
60. Xiong, W., Shen, G., and Bryant, D. A. (2017) *Synechocystis* sp. PCC 6803 CruA (sll0147) encodes lycopene cyclase and requires bound chlorophyll a for activity. *Photosyn. Res.* **131,** 267–280 CrossRef Medline
61. Zhao, L., Cheng, D., Huang, X., Chen, M., Dall'Osto, L., Xing, J., Gao, L., Li, L., Wang, Y., Bassi, R., Peng, L., Wang, Y., Rochaix, J. D., and Huang, F. (2017) A light harvesting complex-like protein in maintenance of photosynthetic components in *Chlamydomonas*. *Plant Physiol.* **174,** 2419–2433 CrossRef Medline
62. Tanaka, R., Rothbart, M., Oka, S., Takabayashi, A., Takahashi, K., Shibata, M., Myouga, F., Motohashi, R., Shinozaki, K., Grimm, B., and Tanaka, A. (2010) LIL3, a light-harvesting-like protein, plays an essential role in chlorophyll and tocopherol biosynthesis. *Proc. Natl. Acad. Sci. U.S.A.* **107,** 16721–16725 CrossRef Medline
63. Takahashi, K., Takabayashi, A., Tanaka, A., and Tanaka, R. (2014) Functional analysis of light-harvesting-like protein 3 (LIL3) and its light-harvesting chlorophyll-binding motif in *Arabidopsis*. *J. Biol. Chem.* **289,** 987–999 CrossRef Medline
64. Lohscheider, J. N., Rojas-Stütz, M. C., Rothbart, M., Andersson, U., Funck, D., Mendgen, K., Grimm, B., and Adamska, I. (2015) Altered levels of LIL3 isoforms in *Arabidopsis* lead to disturbed pigment-protein assembly and chlorophyll synthesis, chlorotic phenotype and impaired photosynthetic performance. *Plant Cell Environ* **38,** 2115–2127 CrossRef Medline
65. Mork-Jansson, A., Bue, A. K., Gargano, D., Furnes, C., Reisinger, V., Arnold, J., Kmiec, K., and Eichacker, L. A. (2015) Lil3 assembles with proteins regulating chlorophyll synthesis in barley. *PLoS One* **10,** e0133145 CrossRef Medline
66. Tichý, M., Bečková, M., Kopečná, J., Noda, J., Sobotka, R., and Komenda, J. (2016) Strain of *Synechocystis* PCC 6803 with aberrant assembly of photosystem II contains tandem duplication of a large chromosomal region. *Front. Plant Sci.* **7,** 648 Medline
67. Schägger, H., and von Jagow, G. (1991) Blue native electrophoresis for isolation of membrane protein complexes in enzymatically active form. *Anal. Biochem.* **199,** 223–231 CrossRef Medline
68. Komenda, J., Lupínková, L., and Kopecký, J. (2002) Absence of the psbH gene product destabilizes photosystem II complex and bicarbonate binding on its acceptor side in *Synechocystis* PCC 6803. *Eur. J. Biochem.* **269,** 610–619 CrossRef Medline
69. Pilný, J., Kopečná, J., Noda, J., and Sobotka, R. (2015) Detection and quantification of heme and chlorophyll precursors using a high performance liquid chromatography (HPLC) system equipped with two fluorescence detectors. *Bio-protocol* **5,** e1390
70. Camacho, C., Coulouris, G., Avagyan, V., Ma, N., Papadopoulos, J., Bealer, K., and Madden, T. L. (2009) BLAST+: architecture and applications. *BMC Bioinformatics* **10,** 421 CrossRef Medline
71. Katoh, K., and Standley, D. M. (2013) MAFFT multiple sequence alignment software version 7: improvements in performance and usability. *Mol. Biol. Evol.* **30,** 772–780 CrossRef Medline
72. Shih, P. M., Wu, D., Latifi, A., Axen, S. D., Fewer, D. P., Talla, E., Calteau, A., Cai, F., Tandeau de Marsac, N., Rippka, R., Herdman, M., Sivonen, K.,

Downloaded from http://www.jbc.org/ at Institute of Physiology AS CR on July 24, 2019

Coursin, T., Laurent, T., Goodwin, L., *et al.* (2013) Improving the coverage of the cyanobacterial phylum using diversity-driven genome sequencing. *Proc. Natl. Acad. Sci. U.S.A.* **110,** 1053–1058 CrossRef Medline

73. Mareš, J. (2018) Multilocus and SSU rRNA gene phylogenetic analyses of available cyanobacterial genomes, and their relation to the current taxonomic system. *Hydrobiologia* **811,** 19–34 CrossRef
74. Stamatakis, A. (2014) RAxML version 8: a tool for phylogenetic analysis and post-analysis of large phylogenies. *Bioinformatics* **30,** 1312–1313 CrossRef Medline
75. Ronquist, F., Teslenko, M., van der Mark, P., Ayres, D. L., Darling, A., Höhna, S., Larget, B., Liu, L., Suchard, M. A., and Huelsenbeck, J. P. (2012) MrBayes 3.2: efficient Bayesian phylogenetic inference and model choice across a large model space. *Syst. Biol.* **61,** 539–542 CrossRef Medline
76. Miller, M. A., Schwartz, T., Pickett, B. E., He, S., Klem, E. B., Scheuermann, R. H., Passarotti, M., Kaufman, S., and O'Leary, M. A. (2015) A RESTful API for access to phylogenetic tools via the CIPRES science gateway. *Evol. Bioinform. Online* **11,** 43–48 Medline

Downloaded from http://www.jbc.org/ at Institute of Physiology AS CR on July 24, 2019